Full-scale ash deposition measurements at Avedøre Power Plant unit 2 during suspension-firing of wood with and without coal ash addition.

Wu, Hao; Shafique Bashir, Muhammad; Jensen, Peter Arendt

Publication date:
2012

Document Version
Publisher's PDF, also known as Version of record

Full-scale ash deposition measurements at Avedøre Power Plant unit 2 during suspension-firing of wood with and without coal ash addition

Hao Wu, Muhammad Shafique Bashir, Peter Arendt Jensen

July 2012

CHEC Research Centre

Department of Chemical and Biochemical Engineering

Technical University of Denmark

Søltofts Plads, Building 229, DK-2800, Lyngby, Denmark

CHEC Report NO.: R1204

Abstract

The formation of deposits during suspension-firing of wood at Avedøre Power Plant unit 2 (AVV2) was studied by using an advanced deposit probe system. The tests were conducted both with and without coal ash addition, and at two different locations with flue gas temperatures of 1250-1300 ^{o}C and 750-800 ^{o}C respectively. The deposit formation process was studied quantitatively though the mass uptake data from the load-cell of the probe, while camera pictures were used to qualitatively verify the obtained mass uptake data and to explain the deposit buildup/shedding mechanisms. The collected deposits along with the fly ash and bottom ash from the plant were characterized extensively by SEM-EDS, ICP-OES/IC and XRD. Based on the results from the present work, the deposit formation and shedding mechanisms under different operational conditions were proposed and discussed. The influence of coal ash addition on deposit formation during wood suspension-firing at AVV2 was evaluated. It was revealed that the addition of coal fly ash could significantly influence the ash deposition/shedding behaviors and the deposit properties. The effect was evident at both measurement locations. At the location with a high flue gas temperature of 1250-1300 ^{o}C, although the addition of coal fly ash increased the differential deposit formation rate (DDF-rate) and the ash deposition propensity, the deposit removal frequency were considerably increased and the major shedding mechanism was changed from soot-blowing induced shedding to natural shedding. This implied that the deposits at high temperatures were more easily removable when coal ash was added. Besides, the amount of K_2SO_4 in the high-temperature deposits was considerably reduced when coal ash was added, which was probably favorable in order to minimize corrosion. At the location with a low flue gas temperature of 750-800 ^{o}C, the addition of coal fly ash reduced the ash deposition propensity and caused the formed deposits being easily removable. Moreover, the KCl and KOH/K_2CO_3 found in the low-temperature deposits without coal ash addition disappeared when coal ash was added, which was also favorable from a corrosion point of view.

Table of contents

1. Introduction

The long-term goal for the Danish energy policy is to achieve 100% renewable energy supply by 2050. One of the milestones to secure this goal is to phase out coal from Danish power plants by 2030, mainly by replacing coal with biomass in CHP plants and by promoting wind power [1]. Due to the very different physical and chemical properties of biomass, a conversion from coal to biomass on existing suspension-firing power plants involves a range of major technical constraints for the boiler and the flue gas treatment units. Typical examples are the ash-related problems induced by the alkali metals and chlorine present in biomass, such as ash deposit formation, corrosion, deactivation of SCR catalyst, and dust emissions.

Wood is considered as one of the most feasible biomasses for replacing coal in suspension-firing power plants, primarily due to its relatively small alkali and chorine content. In order to facilitate the conversion from coal to wood on existing power plants, a systematic understanding of the ash deposit formation during suspension-firing of wood is required. However, research on ash deposit formation during full-scale suspension-firing of wood is scarce. To the authors' knowledge, the investigations carried out by Skrifvars et al. [2], Jensen et al. [3], and Bashir et al. [4,5] are the only full-scale data available on ash deposit formation during suspension-firing of wood. These studies have revealed some important features about ash deposit formation during wood suspension-firing. On the other hand, an extensive and detailed study on the transient formation of ash deposit at different locations of the boiler is still not available in literature, and this information is needed in order to facilitate the utilization of wood in suspension-firing plants.

The objective of the present work is to characterize and understand the formation of ash deposit during suspension-firing of wood at the Avedøre Power Plant unit 2 (AVV2), both with and without the addition of coal fly ash. The utilization of coal fly ash in AVV2 is proven to be effective in reducing the formation of ultrafine aerosols rich in alkali and chlorine [6], whereas its effect on the formation of ash deposit is not well-understood. In this work, the formation of ash deposit is studied by using an advanced and well-controlled deposit probe system. Two different boiler locations with significantly different flue gas temperature are selected in the tests. The formation of deposits at these two locations and at different operational conditions is compared, mainly with respect to the transient mass build-up/shedding of the deposits and the properties of the deposits.

2. Experimental

2.1 Boiler

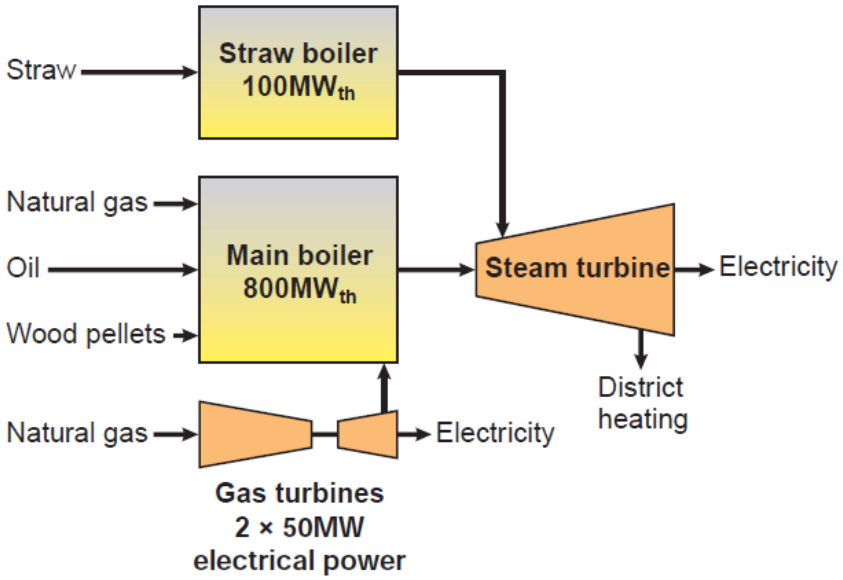

Figure 1 Simplified diagram of AVV2 [7].

As illustrated in Figure 1, the Avedøre Power Plant unit 2 (AVV2) consists of three types of combustors: a straw-fired grate boiler, a suspension-fired main boiler and two gas turbines. The main boiler of AVV2 is an ultra supercritical (USC), once through tower boiler of the Benson type. The boiler is a multi-fuel boiler that can apply wood, natural gas and heavy fuel oil as fuel, with a total thermal capacity of 800 MW_{th}. It has a total height of 80 m, and in the lower part is the combustion chamber with 16 tangential-fired burners in 4 levels. Three mills are used to pulverize the wood pellets, with one mill supplying to one burner level. During operation, the boiler can be in a pure condensing mode, a pure back pressure mode or any combination. When operating in pure condensing mode, a net electrical efficiency of 48% can be obtained at maximum biomass capacity. However, when operating in pure back pressure mode utilizing all the thermal energy in the condensed steam for district heating, the total energy efficiency is 94% [3].

2.2 Measurement locations

Figure 2 shows a schematic drawing of the main boiler of AVV2. In this work, two different locations were used for inserting the ash deposition probe. As illustrated in Figure 2, the first location (denoted as Location A in this report) is situated at a level of ~50m, which is just below the radiation shield of the boiler. This location has a very high flue gas temperature (~1250-1350 ^{o}C) when the boiler is close to full-load. The second location (denoted as Location B) is situated at a level of ~63m, which is in the superheater region of the boiler. The flue gas temperature at this location is about 750-800 ^{o}C when the boiler is close to full-load.

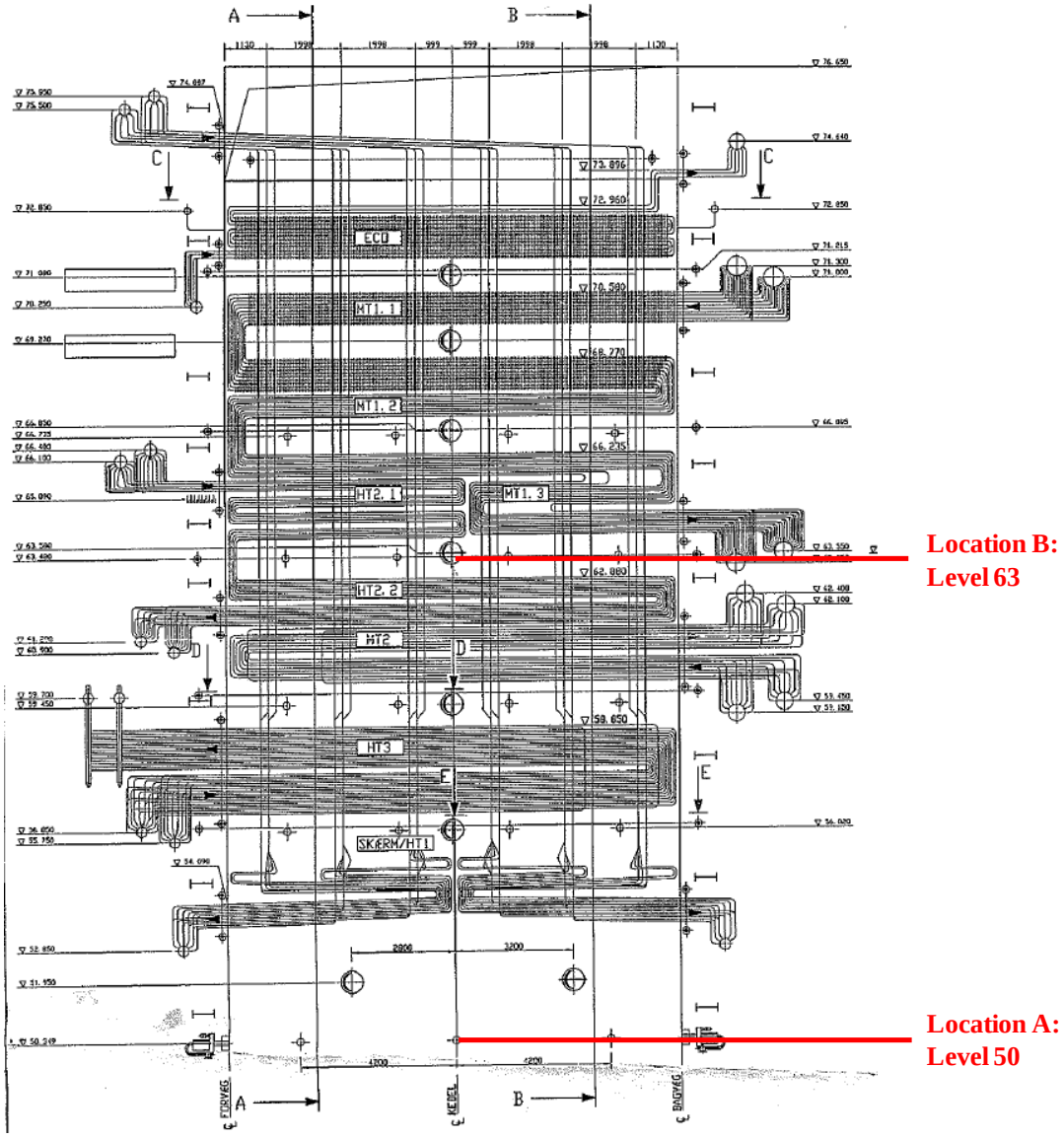

Figure 2 Schematic drawing of the main boiler of AVV2.

2.3 Ash deposition probe system

2.3.1 Probe system at Location A

Figure 3 illustrates the probe system used for the measurements at location A. The deposit probe is made of stainless steel, about 3 m long and having an outer diameter of 40.5 mm. A load cell was mounted to detect the force caused by the mass of deposit on the probe. The probe is cooled by water and air, whereby it is possible to determine the heat uptake by the probe and meanwhile keep a stable surface temperature. At this location, the probe is placed in an acoustic pyrometer port on the boiler wall. Due to the very high flue gas temperature, it was not possible to keep the probe surface temperature between 500 and 600 ^{o}C when the probe is fully inserted [8]. Therefore, a special port extension pipe was installed to keep the probe only 772 mm inside the boiler. In most cases, this solution appeared to work satisfactory towards controlling the surface temperature of the probe to be around 550 ^{o}C. In order to minimize the effect of soot blowing, the two nearest soot-blowers were shut off during the measurement period.

(a)

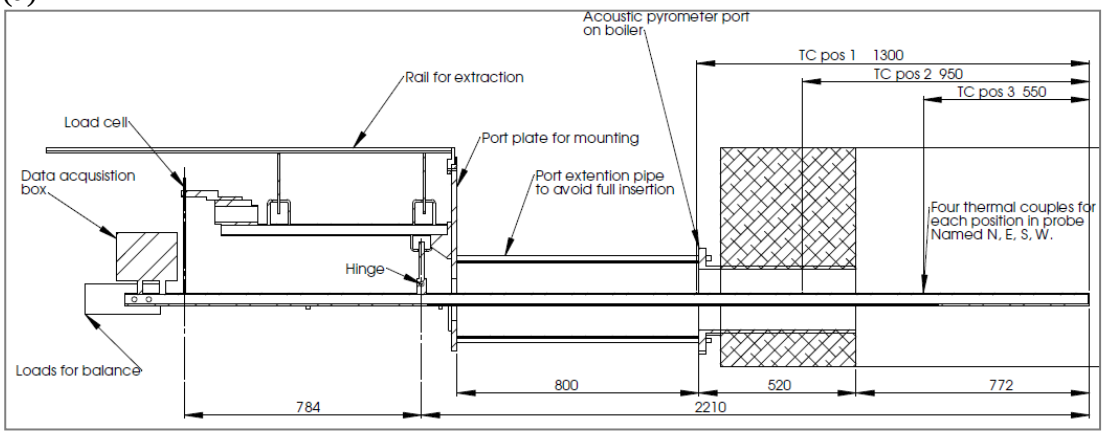

(b)

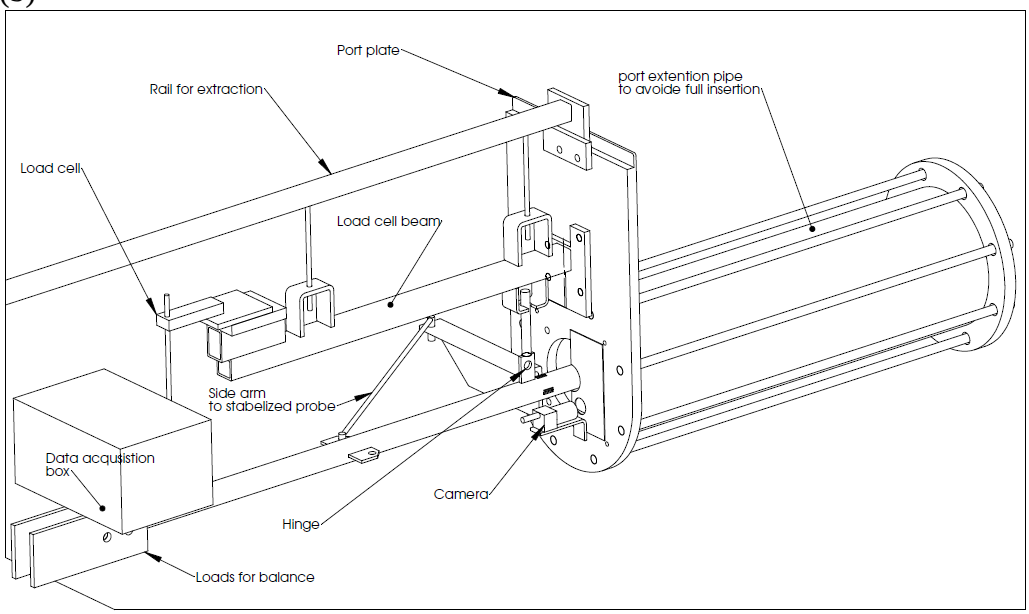

(c)

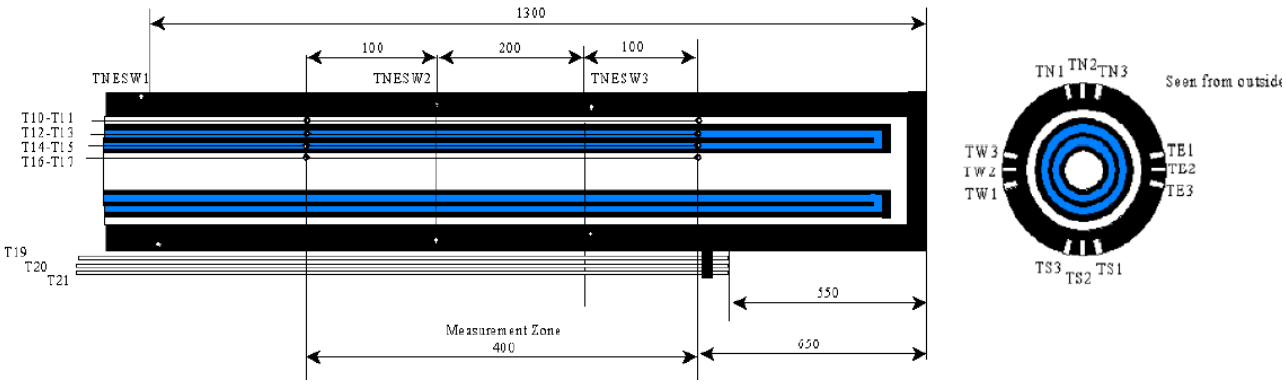

Figure 3 a) Schematic drawing of the probe with identified positions of temperature measurements, deposition area, port extension probe, port plate for mounting, hinge, load cell and rail for pulling out the probe, b) layout of the complete probe setup, c) cross-section view perpendicular to the probe axis and cross-sectional view along the axis of annuli.

As seen in Figure 3C, 12 thermocouples are placed inside the outer probe metal tube with four thermocouples at three different horizontal positions (TNESW1, TNESW2 and TNESW3). In each horizontal position, the thermocouples register temperature information from four positions (N, S, E and W) of the probe. However, due to the installation of the extension pipe, it was only possible to measure high temperature at horizontal position 3 (i.e. 750 mm from the tip of the probe), and the thermocouple S3 was used for controlling the temperature of the probe during the measurements.

The flue gas temperature near the probe was measured by using an S-type thermocouple placed in a ceramic protective shell. In addition, a suction pyrometer (International Flame Research Foundation model, IFRF [9]) was used for some periods to find the difference between the flue temperatures measured by the ceramic S-type thermocouple and the suction pyrometer. It has to be mentioned that due to the significantly high flue gas temperature at Location A, the formation of deposits on the ceramic thermocouple was quite fast and significant. A number of ceramic S-type thermocouples were destroyed during the measurement, resulting in some measurement periods without temperature information.

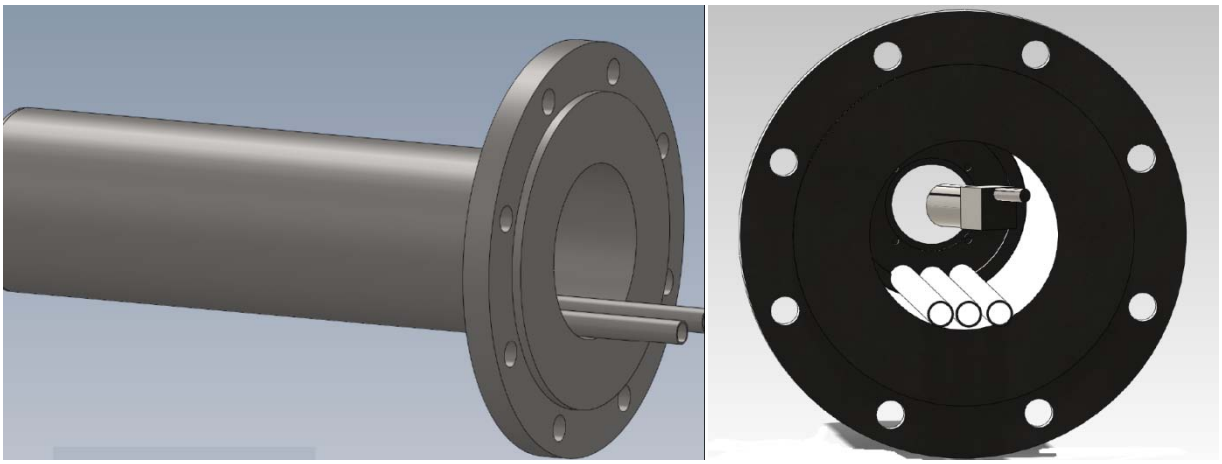

Figure 4 Schematic drawings of the camera port, with the left figure showing a side view and the right figure showing a front view.

A special port for video monitoring was mounted at the right wall of the probe measurement position. Schematic drawings of the probe are shown in Figure 4. The port was cooled both by water and air, and a CCD (charge-coupled device) camera was placed in the port to register the deposit formation and removal processes on the probe. The camera was coiled by water-cooled metal pipes, and cooling air was blown continuously towards it to ensure the camera temperature to be around 50 ^{o}C. Besides the camera on the right-wall, in some experiments, an additional camera was placed below the probe (as shown in Figure 3B), in order to obtain a better understanding of the ash formation and shedding processes.

2.3.2 Probe system at Location B

The probe system used at Location B is slightly different from that of Location A. The opening to the boiler at Location B only has an inner diameter of 80 mm, which is much smaller than that of Location A. Besides, the boiler wall at Location B vibrates significantly during the measurement. In order to minimize the effect of wall vibration, a special rig was made and installed on the floor, and the probe was mounted on the rig, instead of on the vibrating boiler wall. Since the flue gas temperature was relatively low at Location B, the probe was 1400 mm inside the boiler during the

measurement. In order to minimize the effect of soot blowing, the two nearest soot-blowers were shut off during the measurement period.

Flue gas temperature at Location B was measured at the wall opposite of the deposit probe, because there was no near-by opening available. The temperature measurement was carried out by using a K-type thermocouple placed in a metallic protective shell and a suction pyrometer that is mentioned above.

At Location B, video monitoring was not possible due to the small opening size and the limited availability of boiler openings.

2.4 Data treatment

2.4.1 Deposit mass uptake

The deposit mass uptake was calculated by using the following torque balance:

$$m_d = (m_{t0} - m_{t1})\frac{L_1}{L_2} \tag{1}$$

where m_d is the deposit mass (g), m_{t0} is the initial signal of the load cell (g), m_{t1} is the final signal of the load cell (g), while L_1 and L_2 are the distances (mm) from the hinge to the balance and to the mass center of the deposit, respectively.

2.4.2 Probe heat uptake

The water and air flow to the probe was measured by the flow meters at the inlets of the probe. The inlet and outlet temperatures of the water and air were also measured by four thermocouples. With the information above, the probe heat uptake can be calculated by using:

$$Q = \frac{\dot{m}_w C_{p,w}(T_{w,out} - T_{w,in}) + \dot{m}_a C_{p,a}(T_{a,out} - T_{a,in})}{s} \tag{2}$$

where Q is the heat uptake (W/m^2), $\dot{m}$ is the flow rate (kg/s), C_p is the average heat capacity (J/kg/K), T is the temperature (K), s is the effective probe surface area (m^2), while in subscript w and a represents water and air, respectively.

2.4.3 Ash deposition rate and propensity

With the information of deposit mass uptake, surface area of the probe exposed to flue gas and the corresponding exposure time, the ash deposition rate (g/m^2/h) can be calculated. In this work the differential deposit formation rate (DDF-rate) is used to characterize the deposit formation. The DDF-rate is calculated by taking the time derivative of the deposit mass uptake in-between two major shedding events. Therefore, the DDF-rate represents a “true” deposit formation rate, which is an averaging of the time derivative over periods that do not include major shedding events, but do include some minor shedding events in addition to noise [4]. A detailed description of the calculation procedures of DDF is given in Appendix A.

With the calculated DDF-rate, the ash deposition propensity can be determined by using:

$$Ash\,deposition\,propensity = \frac{DDF-rate}{Ash\ flux} \tag{3}$$

$$Ash\ flux\ (g/m^2/h) = \frac{m_f X_a}{A_r} + \frac{ash_{coal}}{A_r} \tag{4}$$

where m_f is the wood flue flow to the boiler (g/h), X_a represents wood ash fraction, ash_{coal} is the coal ash flow (g/h) and A_r is the cross-sectional area of the boiler at the probe measuring position.

2.5 Fuel properties

During the measurements, the fuels used in the AVV2 boiler were wood and natural gas. In addition, coal fly ash was added to the boiler during some periods. Sampling of wood and coal fly ash was carried out by Ramboll Denmark A/S. The analysis of wood was conducted, with the average values of different days shown in Table 1. The properties of coal fly ash and natural gas are not available, thus the properties from a previous test [3] are used in this work. This may introduce slight uncertainties for the interpretation of results in this work. From the fuel analyses, it can be seen that the ash content of the wood is very low, only about 1 wt%. The major ash forming elements in wood are Si, Ca and K. The Cl and S content in wood is much lower than the K content. Different from the wood, the coal ash is characterized by a large content of Si and Al.

Table 1 Properties of the fuels and coal fly ash. The data of wood is the average values of the samples collected in different days, while the data of coal fly ash and natural gas are based on [3].

Properties	Wood	Coal ash	Parameter	Natural gas
Ash contents (wt% ar), assumed	0.99	--	--	--
Moisture (wt%)	6.76	--	--	--
Higher Heating Value (MJ/kg db)	17.51	--	Heating value (MJ/kg)	48.07
S (wt% db)	0.017	0.26	CH_4 (mol%)	89.06
Cl (wt% db)	0.0069	0	C_2H_6 (mol%)	6.08
Al (wt% db)	0.024	14	C_3H_8 (mol%)	2.47
Ca (wt% db)	0.208	5.2	iC_4H_{10} (mol%)	0.39
Fe (wt% db)	0.020	2.3	nC_4H_{10} (mol%)	0.54
K (wt% db)	0.091	0.45	C_5H_{12} (mol%)	0.11
Mg (wt% db)	0.034	0.91	nC_5 (mol%)	0.08
Na (wt% db)	0.007	0.11	C_{5+} (mol%)	0.05
P (wt% db)	0.012	0.81	N_2 (mol%)	0.29
Si (wt% db)	0.17	20	CO_2 (mol%)	0.91

2.6 Boiler operation data

In order to explain the obtained ash deposit formation results, a number of boiler operation data were obtained after the measurements. A list of the collected data is given in Table 2. These results are shown together with the ash deposition data and are used in the calculation of ash deposition propensities.

Table 2 List of collected boiler data.

No.	Boiler data	unit	code
1	Wood flow from mill 30	kg/s	52 HFB30FF001
2	Wood flow from mill 20	kg/s	52 HFB20FF001
3	Wood flow from mill 10	kg/s	52 HFB10FF001
4	Total air flow to the boiler	kg/s	52 HHL90CF901
5	Total oil flow to the boiler	kg/s	52 HHF55FF901
6	Total natural gas flow	kg/s	52HHY01FF901
7	Boiler load	%	52 HHY01FF902
8	Steam temperature	^{o}C	52 LBA20CT003
9	NOx in flue gas before DeNOx	ppm	52HSA16CQ001
10	CO in flue gas at exit of boiler	ppm	52HSA10CQ010
11	O_2 in flue gas at exit of boiler	%	52 HSA10CQ901
12	SO_2 in flue gas at exit of boiler (before FGD)	ppm	52 HTA10CQ002
13	Flow of fly ash	ton/h	52_ETK10AF000R
14	Temp. of backwall at level 50 (peak means sootblower is active)	^{o}C	52_HCB51CT001

2.7 Experimental matrix

An overview of the performed experiments is shown in Table 3. It can be seen that experiments were carried out at two locations, both with and without coal additions. In all of the experiments, the target deposit probe surface temperature (S3) was 550 ^{o}C.

Table 3 Matrix of the experiments performed in winter 2011.

Test	Probe Location	Start date	Duration (h)	Boiler load (%)	Biomass load (%)	Coal ash addition (ton/h)	Target probe temp. (^{o}C)
1	A	21-Nov	100.8	92.1	83.1	-	550
2	A	25-Nov	66.1	78.8	76.7	-	550
3	B	30-Nov	40.3	80.5	71.8	-	550
4	B	5-Dec	23.6	96.3	86.7	6.0	550
5	A	9-Dec	25.5	93.4	78.2	5.8	550
6	A	12-Dec	18.0	85.7	78.9	6.0	550
7	A	13-Dec	25.1	82.8	73.2	5.7	550
8	A	14-Dec	20.2	88.8	81.0	6.0	550

It has to be noted that a number of problems have occurred during the experiments. Most of them were difficult to predict and detect. These problems and their possible consequences to the measurement results are listed in Table 4.

Table 4 List of the difficulties/problems in different experiment.

Test	Experimental difficulties/problems
1	Mass uptake influenced by water condensation/evaporation in the probe. This was caused by a leak of water between the cooling water channel and cooling air channel of the probe.
2	Mass uptake influenced by water condensation/evaporation in the probe - probe repaired afterwards
3	Mass uptake influenced by boiler wall movement at low boiler load (night). The boiler wall moved upwards and touched the probe when the boiler load was lowered during night.
4	-
5	Mass uptake data only available for the initial 1.5 hours - load cell was not functional afterwards
6	Heat uptake data not available due to a broken thermocouple, and part of boiler data not available
7	Results influenced by an unexpected cooling-water shut-off during the measurement
8	Probe temperature at south much larger than other directions - probe may be bended

3. Results and discussion

3.1 Experimental conditions

Table 5 shows a summary of the experimental conditions during the tests. The data presented are average values with standard deviations. The detailed transient data are available in Appendix B. It can be seen that the average boiler load is generally kept at a high level (~79-96%) during the tests. Wood pellet is the dominant fuel, which usually corresponds to more than 90% of the total load. The first three tests were carried out without coal ash addition, whereas the remaining five tests were conducted with the addition of about 1.6 kg/s coal fly ash. Compared to the tests without coal ash addition, the ash flux in the flue gas is increased by 5-6 times when coal fly ash is added. The compositions of flue gas are analyzed and recorded during the tests. It can be seen that the O_2 level in the flue gas is quite consistent (~3.0-3.2%) during different tests, indicating that the tests are carried out at similar excess air ratio conditions. The NO_x concentrations are normally in the range of 120-180 (ppm). However, no clear tendency can be found between the average NO_x concentration and the average boiler/biomass load. The average CO concentrations are relatively small (10-90 ppm), implying a high level of burnout in these tests. On the other hand, the standard deviations of the CO concentration are quite significant, suggesting that the combustion conditions may not be very stable. An interesting tendency is observed for the SO_2 concentration. Without the addition of coal fly ash, the concentration of SO_2 is negligible in the flue gas. This implies that the sulfur in wood may be mostly converted to sulfates. This hypothesis is supported by the significant amount of alkali sulfates found in the aerosols from wood combustion in the same boiler [6]. However, with the addition of coal fly ash, the concentration of SO_2 is increased to a level of ~ 10-15 (ppm). This clearly indicates that reactions may have taken place between the alkali sulfates and the added coal fly ash, which may generate alkali aluminosilicates and release SO_2 to the flue gas [6].

Besides the parameters obtained from the boiler operation data, the flue gas temperature at the measurement locations and the probe surface temperatures during the tests are also shown in Table 5. It can be seen that the flue gas temperature at Location A is generally in a range of 1250-1350 ^oC, whereas the temperature at Location B is around 770-800 ^oC. Although the flue gas temperature differs significantly at these two locations, the probe surface temperatures are controlled to be similar, especially for the temperatures of the S3 thermocouple. For tests 1-4 and 6, the average probe temperatures (average of N3, E3, S3 and W3) are similar. However, for test 5, the average probe temperature is considerably higher than that of tests1-4 and 6. This is probably related to the characteristics of deposit formation at test 5, which will be discussed in detail later. For test 7, the average probe temperature is the highest and the standard deviation is very significant. This is mainly because of the occurrence of cooling water shut-off during this test, which leads to a significant increase of the probe surface temperature. The average probe surface temperature during test 8 is much lower than that of other tests. A plausible explanation is that the probe may be bended after being exposed to high temperature during test 7. Thus, the cooling at S-direction of the probe may become less efficient, and the cooling at other directions may be promoted. This would result in a decrease of the average probe surface temperature when the thermocouple at S-direction of the probe is used to control the probe surface temperature.

Table 5 Summary of the detailed conditions in different experiment.

Conditions	Test 1	Test 2	Test 3	Test 4	Test 5	Test 6	Test 7	Test 8
Location	A	A	B	B	A	A	A	A
Duration (h)	100.8	66.1	40.3	23.6	25.5	18.0	25.1	20.2
Bioiler load (%)	92.1±9.8	78.8±5.7	80.5±11.4	96.3±4.0	93.4±3.4	85.7±1.7	82.8±5.2	88.8±5.8
Biomass load (%) [a]	83.1±7.4	76.7±5.6	71.8±9.0	86.7±3.5	78.2±9.3	78.9±1.8	73.2±21.4	81.0±4.3
Natrual gas flow (kg/s)	1.4±1.4	0.2±0.4	1.3±0.7	1.4±0.2	1.5±1.7	0	1.5±3.3	1.1±0.5
Coal ash flow (kg/s)	-	-	-	1.66±0.02	1.62±0.10	1.66±0.02	1.57±0.23	1.66±0.03
Coal ash to wood ash ratio	-	-	-	4.1±0.2	4.4±0.3	4.5±0.1	- [c]	4.4±0-2
Ash flux ($g/m^2/h$)	11296±1026	10422±765	9756±1234	59689±714	57277±4003	58600±459	55150±9534	58663±1295
NO_x (ppm)	134±27	144±23	128±18	184±10	170±11	147±18	125±12	121±11
CO (ppm)	86±81	60±58	40±52	7±13	18±28	37±62	29±53	32±54
O_2 (%)	3.0±0.3	3.2±0.2	3.0±0.3	3.0±0.2	3.0±0.3	3.1±0.4	3.1±0.4	3.1±0.2
SO_2 (ppm)	-2.3±0.7	-2.4±0.8	-2.4±0.7	14.5±2.8	12.7±2.5	14.7±2.1	15.5±3.8	11.6±2.0
Flue gas temperature (thermocouple, ^oC)	1084±39	1038±29	717±17	732±7	-	-	1122±10	-
Corrected flue gas temperature (^oC) [b]	1275±39	1258±29	783±17	768±7	1269±22	1260±30	-	1319±32
Probe surface temperature (N3, ^oC)	533±30	514±10	505±23	514±6	576±38	524±15	580±106	379±25
Probe surface temperature (E3, ^oC)	509±37	486±7	521±23	531±6	561±39	498±16	566±122	464±23
Probe surface temperature (S3, ^oC)	550±5	550±3	530±24	546±7	551±11	559±14	551±8 [d]	568±25
Probe surface temperature (W3, ^oC)	544±31	528±9	504±23	516±6	582±30	537±15	588±125	462±22
Average probe temperature (^oC)	534±33	520±24	515±26	527±14	568±34	530±27	575±108	468±71

[a] Biomass load is calculated by assuming the higher heating value of wood is 17 MJ/kg (db) and the boiler maximum load is 800 MW.

[b] Temperature measured by thermocouple (S/K type) is corrected by the average difference found between the thermocouple and suction pyrometer measurement. When temperature measured by thermocouple is not available, the average temperature measured by the suction pyrometer is used.

[c] The boiler was operating without wood for some periods during this test, thus the average coal ash to wood ash ratio was not calculable.

[d] During test 7, the cooling water of the probe was stopped for some period and destroyed the S3 thermocouple. Thus only the data obtained before the stop of cooling water is shown for S3. For other temperatures (N3, S3, W3), both the data before and after the stop of cooling water are presented.

3.2 Formation and removal of deposits

In this work, the deposit formation process was studied quantitatively though the mass uptake data from the load-cell of the probe, while camera pictures were used to qualitatively confirm the obtained mass uptake data and to explain the deposit build-up/shedding mechanisms. However, due to the problems listed in Table 4, the mass uptake data of several tests are influence by different factors. In test 1 and 2, the water condensation/evaporation inside the probe may have greatly influenced the mass uptake data, and the effect would be particularly pronounced for test 2 since a significant water leakage was observed shortly after the test. In test 3, only part of the mass uptake data is usable due to influence of moving boiler wall. In test 5, the mass uptake data is only available for the initial 1.5 hours. In test 7, only part of results is obtained under controlled probe temperature conditions, due to the cooling water shut-off in the middle of the test. For test 8, the results are considered not to be reliable since the probe temperature at the south direction is significantly higher than that of other directions. Overall, considering the problems mentioned above, only the results from test 1, 3, 4, 5, 6 and 7 are included and discussed in this section.

3.2.1 Deposit mass uptake

The deposit mass uptake results of different tests are summarized in Figure 5. Before starting to analyze the results, it should be noted that the results of Test 1 are influenced by water condensation/evaporation in the probe, thus they are not representative for the deposit mass uptake at Location A without coal ash addition. The results of Test 3-7 are more reliable and representative, although the probe temperature is not well-controlled in Test 7 (after 20 h) and part of the mass uptake data is neglected in Test 3 because the probe has touched the boiler wall (after 30 h).

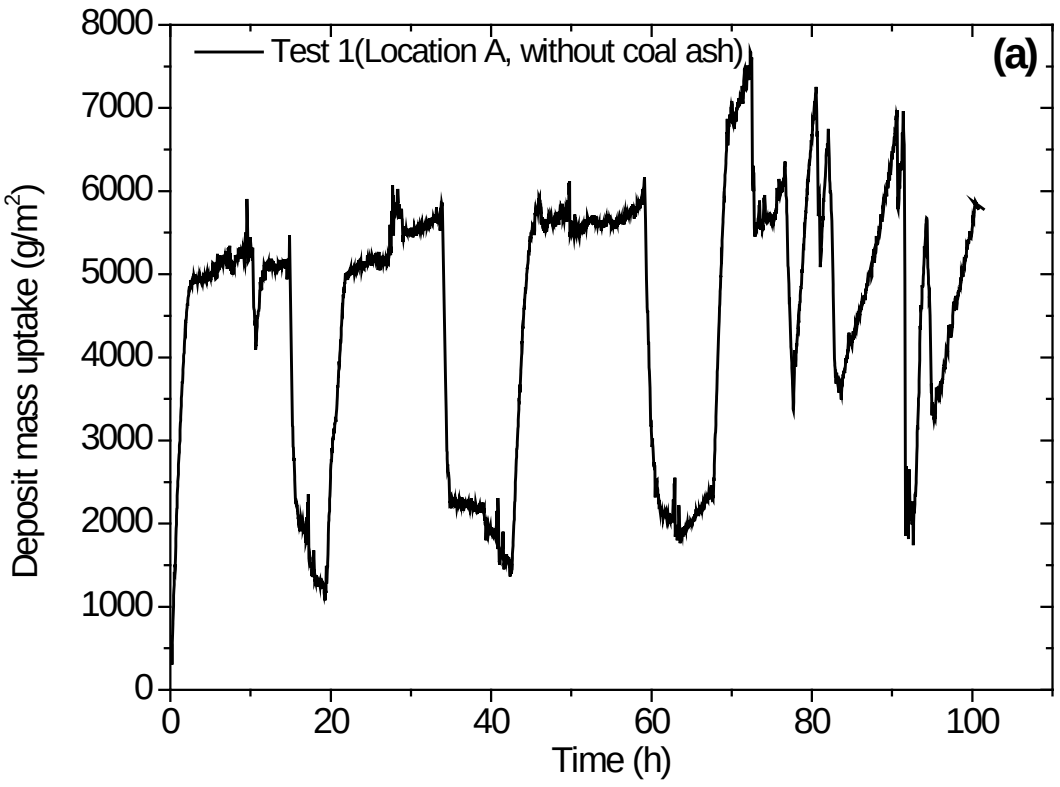

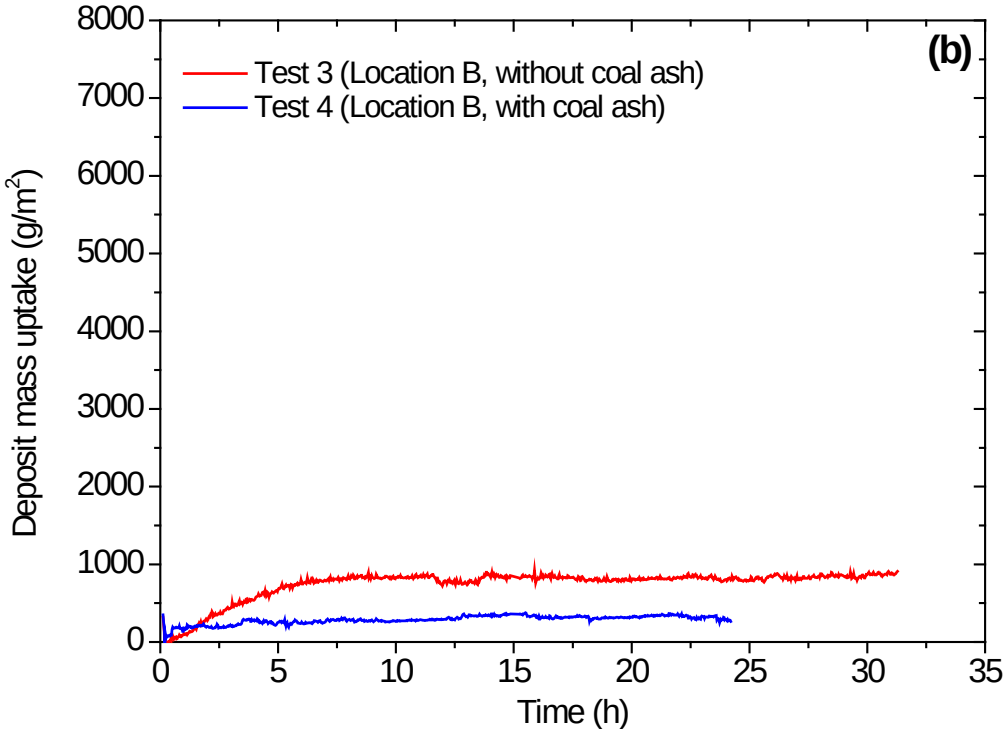

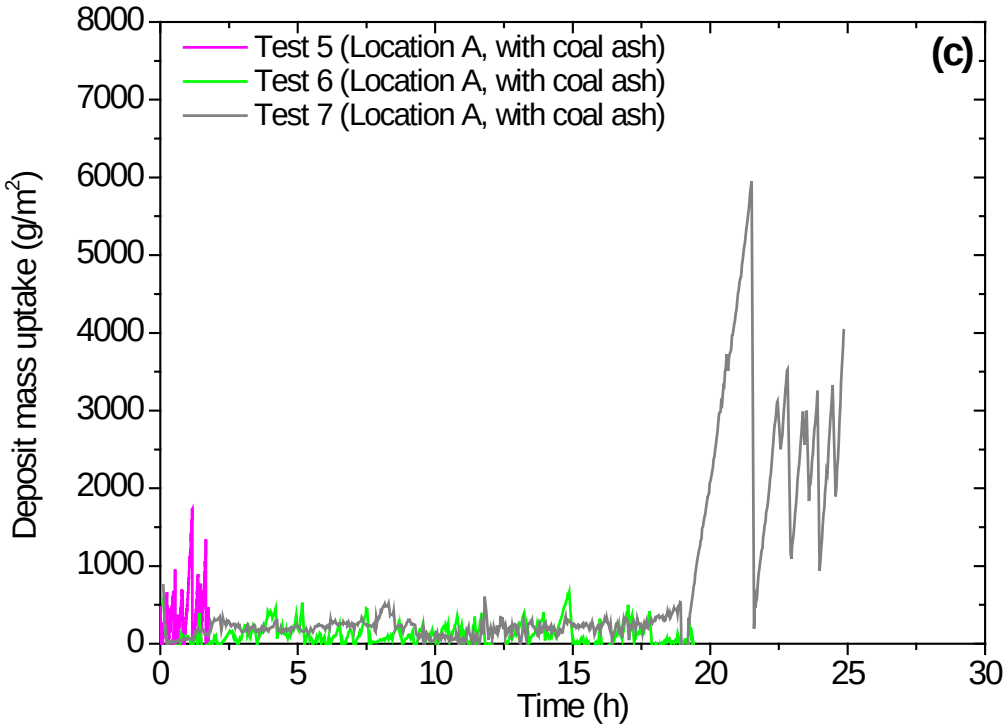

Figure 5 Summarized deposit mass uptake during different tests: (a) test conducted at Location A without coal ash addition (Test 1); (b) tests conducted at Location B with (Test 4) and without (Test 3) coal ash addition; (c) tests conducted at Location A with coal ash addition (Test 5-7).

According to Figure 5b, the deposit mass build-up at Location B shows similar tendencies for the test with and without coal ash addition (Test 4 and Test 3). In general, the deposit mass build-up is

relatively slow at this location, and the mass-uptake of the deposit probe becomes almost constant after a few hours, implying that the deposit build-up and shedding are close to equilibrium. Compared with the test without coal ash addition (Test 3), the stabilized deposit mass-uptake appears to be smaller when coal ash is added (Test 4).

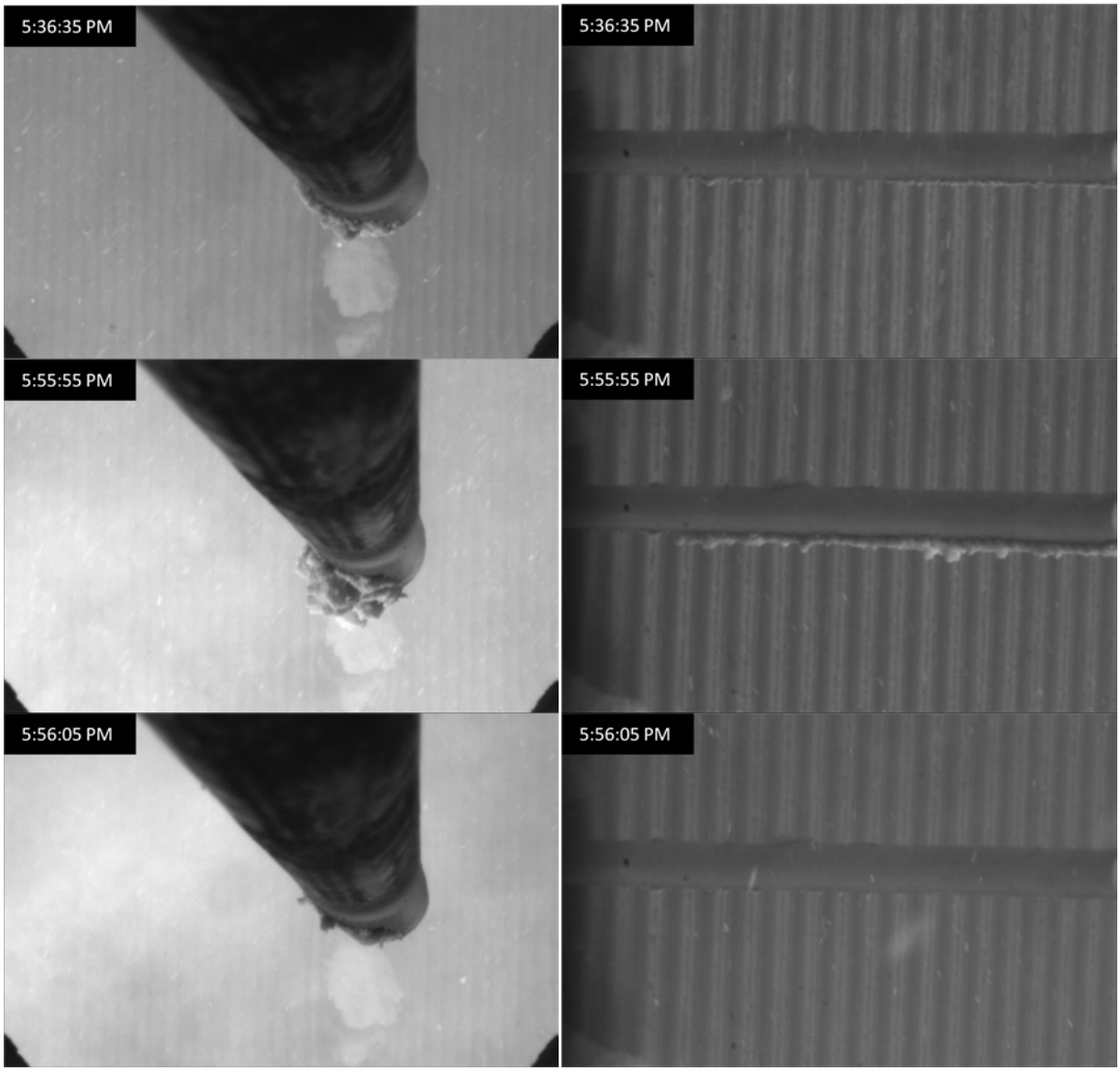

Figure 6 Typical examples of the deposit formation and shedding during the addition of coal fly ash. The pictures are obtained from Test 5. The left pictures are from the camera placed below the probe, while the right pictures are from the camera placed on the right side of the probe.

During the addition of coal ash, the characteristics of deposit mass build-up at Location A (Test 5-7) is quite different from that of Location B (Test 4). As shown in Figure 5c, the deposit formation at Location A is characterized by a relatively fast build-up, followed by a sudden shedding of deposits. The deposit buildup and shedding are evidently recorded by the two cameras placed below and on the right side of the probe. A typical example is shown in Figure 6. It can be seen that a layer of deposits is formed after about 20 minutes of exposure time during Test 5. Then these deposits are almost completely removed within 10 seconds. These results are clearly demonstrated in both cameras, and a combination of the pictures from both cameras provides a good overview of the

deposit formation and shedding processes. The frequency of deposit shedding during Test 5-7 is considerably higher that of soot-blower (see the detailed frequency in Appendix B). Thus it is most likely that the shedding of deposits during Test 5-7 is mainly caused by natural shedding, rather than soot-blowing. With the addition of coal fly ash, the level of deposit mass-uptake seems to be similar at Location A and Location B (see Figure 5b and Figure 5c). An exceptional case is in Test 7, where the level of deposit mass-uptake is increased significantly after 20 hours. This is most likely related to the significant increase of probe surface temperature (by about 250 ^{o}C) caused by cooling-water shut off. Such a large increase of probe surface temperature may result in a much higher deposit surface/front temperature, which may increase the stickiness of the deposit front and promote deposit formation.

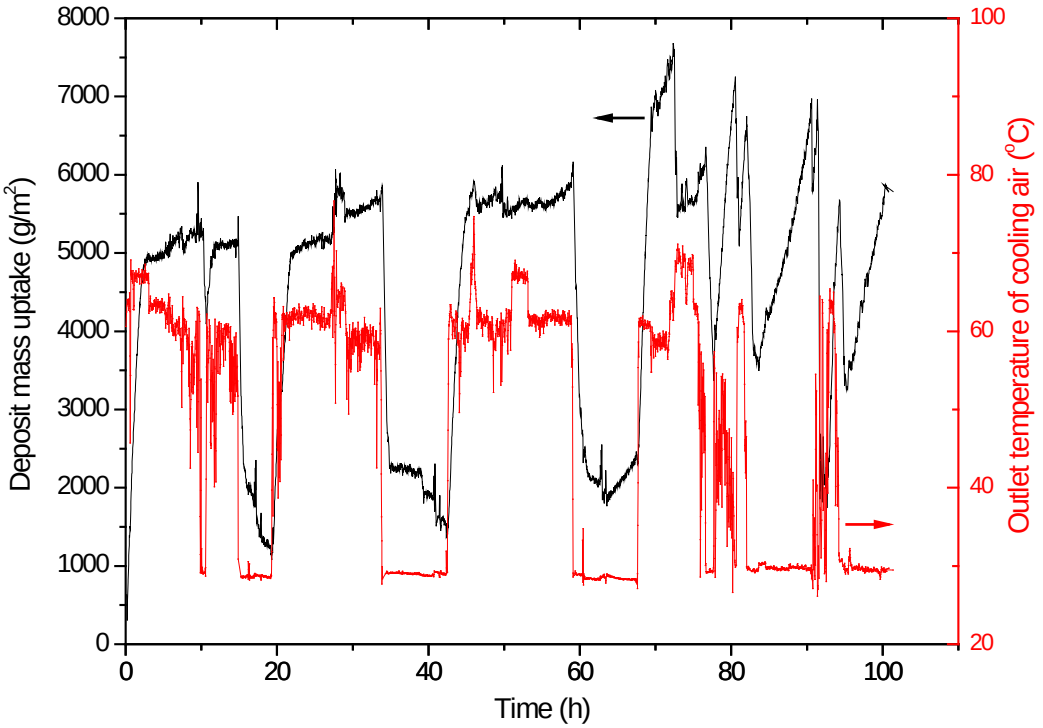

Figure 7 Deposit mass uptake and outlet temperature of cooling air during test 1.

It is difficult to analyze the deposit mass uptake results of test 1 (Location A, without coal ash addition), since they may have been greatly influenced by water condensation and evaporation in the probe. This happened because there was a small leak (the leak was not detected until the end of Test 2) between the cooling water channel and the cooling air channel. Therefore, when the pressure of the cooling air is lower than that of cooling water, cooling water may go into the cooling air channel, which can quickly decrease the temperature of the cooling air and cause water condensation. Since the outlet of the cooling air contains some isolation materials (used as sound damper) which can absorb a significant amount of water, the mass at the left side of the probe would increase when water condensation happens. According to Eq. (1), this mass increase will be read as shedding of deposits in Figure 5a. On the other hand, when the pressure of the cooling air is increased (this happens when more air is needed in order to control the surface temperature of probe), the cooling water will not be able to enter the cool air channel and the air temperature will increase considerably. The high-temperature air will evaporate the water absorbed by the isolation materials and cause a mass decrease on the left side of the probe. This would result in an increase of deposit mass uptake shown in Figure 5a.

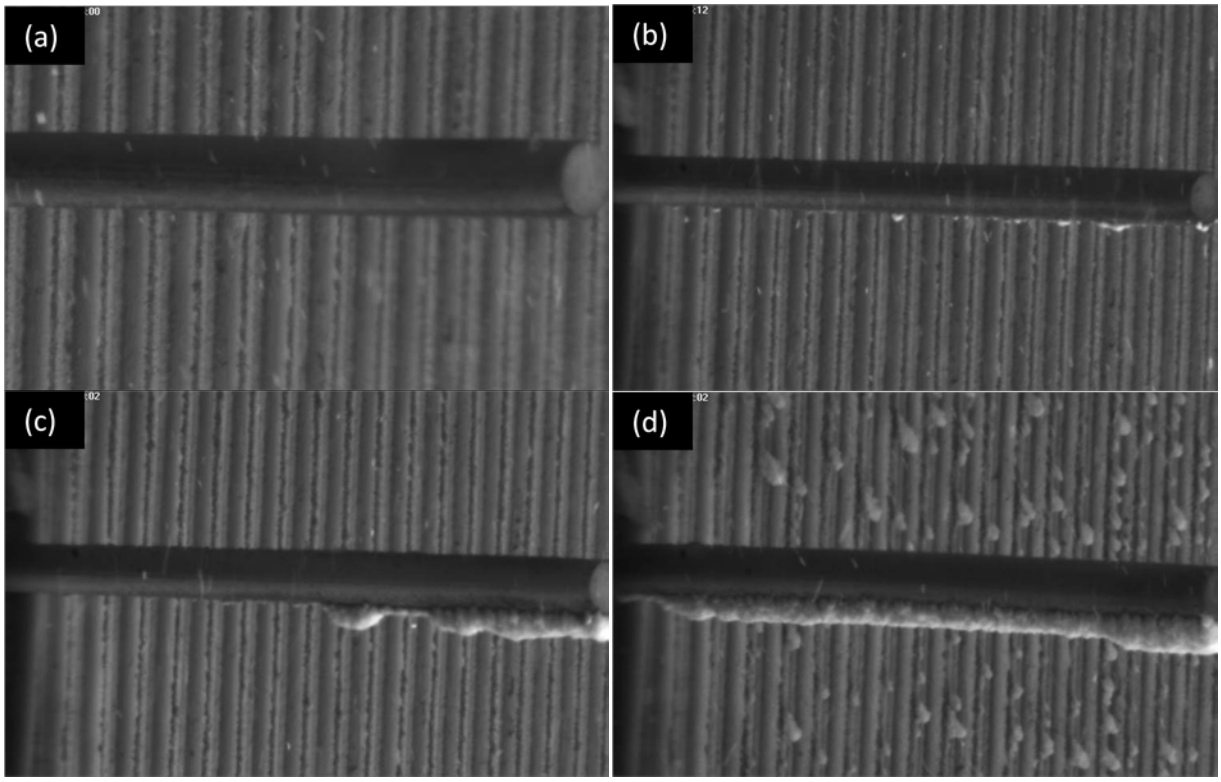

Figure 8 Typical examples of the deposit formation on the horizontal probe during test 1, with the flue gas coming from the bottom of the pictures: (a) picture obtained at around 5 h with a lens focusing on a relatively small area; (b) picture obtained at around 53 h with a lens focusing on the entire probe inside the boiler; c) picture obtained at around 72 h, (d) picture obtained at around 90 h.

Because the occurrence of water condensation would significantly decrease the outlet temperature of cooling air, it is possible to evaluate whether water condensation happens by examining the cooling air temperature. As illustrated in Figure 7, the outlet temperature of the cooling air is only about 30 ^{o}C during some periods, indicating that water condensation may happen in these periods and may result in a decrease of deposit mass uptake. Such tendency has been confirmed by the recorded deposit mass uptake as shown in Figure 7. On the other hand, when the temperature is increased from 30 ^{o}C to about 60 ^{o}C, a significant increase of the deposit mass uptake is often observed, suggesting that the condensed water is re-evaporated. Based on the results shown in Figure 7, it can be concluded that the decrease and increase of deposit mass uptake during about 10-11 h, 15-22 h, 34-45 h, and 59-70 h are probably caused by water condensation and re-evaporation in the probe. The initial increase of mass uptake during 0-2.5 h may also be a result of water re-evaporation in the probe, since the air pressure was kept low before the start of test and almost no deposit is observed by the camera placed on the right side of the probe during this period. According to the pictures recorded by the camera, the formation of deposits is generally not significant in the period of about 0-65 h. Typical examples of the deposit probe during this period are shown in Figure 8a and Figure 8b. During the period of 65-100 h, the formation of deposits appears to be more significant and faster. This tendency is evident in the camera pictures, with two typical examples shown in Figure 8c and Figure 8d. In consistent with the camera pictures, the deposit mass uptake results also suggest that the deposit formation is more significant during this period. As an example, during 84-90 h, a significant increase of the deposit mass uptake is seen when the outlet temperature of cooling air is kept at around 30 ^{o}C. This indicates that the increase of mass uptake in this period is caused by the formation of deposits on the probe, rather than re-

evaporation of water. Besides deposit formation, deposit shedding is also observed during the period of 65-100 h. According to the camera pictures, the deposits are mainly removed through debonding, i.e. a large layer of deposit is detached from the probe. A typical example is given in Figure 9, where two consecutive pictures with an interval of 10 seconds are seen. The debonding of deposits is clearly seen in the pictures from both cameras. The occurrence of deposit shedding seems to be closely related to the operation of nearby soot-blowers. During the period of 65-100 h, the major shedding events are observed from the cameras in the periods of 70-73 h and 90.5-91.8 h. These two periods almost coincide with the operation periods of nearby soot-blowers (see Figure B1 in Appendix B). This indicates that although the nearest two soot-blowers are closed, the shedding of deposits during Test 1 is still primarily induced by the operation of other soot-blowers nearby.

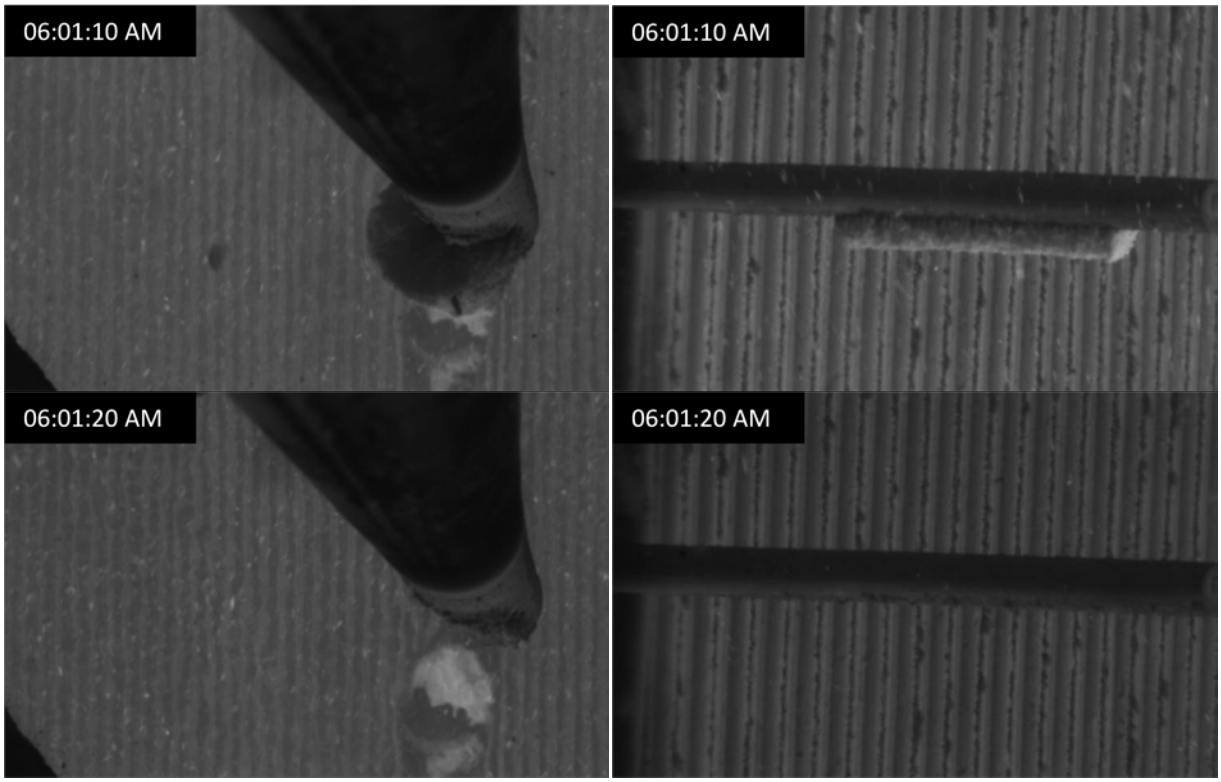

Figure 9 Typical examples of the deposit shedding during test 1. The pictures are obtained on 25-11-11 (around 91.8 h). The left pictures are from the camera placed below the probe, while the right pictures are from the camera placed on the right side of the probe.

Based on the discussions above, it can be concluded that the formation of deposits during Test 1 is insignificant during the period of 0-65 h. However, the formation of deposits becomes more pronounced during the period of 65-100 h, particularly after 80 h. It is difficult to find out the exact reasons for the increased deposit formation. According to the detailed transient measurement data shown in Appendix B, the flue gas temperature after 80 h/65 h is not higher than before. Thus the increased deposit formation cannot be explained by a change of the flue gas temperature. A phenomenon which may be related to the increased deposit formation after 80 h is that the boiler is almost operate at pure wood mode during this period and an increase of NO_x emission is observed. This indicates that the flame pattern/ignition of the wood burner may have been changed and may have influenced the release and transformation of ash species. Another possible explanation could be the variation of fuel properties after around 80 h. This hypothesis may be confirmed by the fuel sampling and analysis carried out simultaneously with the deposition measurement. In comparison

with the tests with coal ash addition under similar conditions (Test 5-7), the results from Test 1 have the following characteristics: 1) depending on the operational conditions, the formation of deposits (i.e. the amount of deposits sitting on the probe) can be either more significant or less; 2) the deposit build-up and shedding cycle observed from the cameras is longer (the cycle during test 1 is often more than 10 h, while in test 5-7 it is often less than 1 h; 3) the shedding of deposits is primary induced by nearby soot-blowers during Test 1 whereas the shedding in Test 5-7 is caused by natural shedding. A more detailed comparison of the deposit formation rate, ash deposition propensity and deposit removal frequencies during different tests will be given in the following sections.

3.2.2 Observation on boiler walls

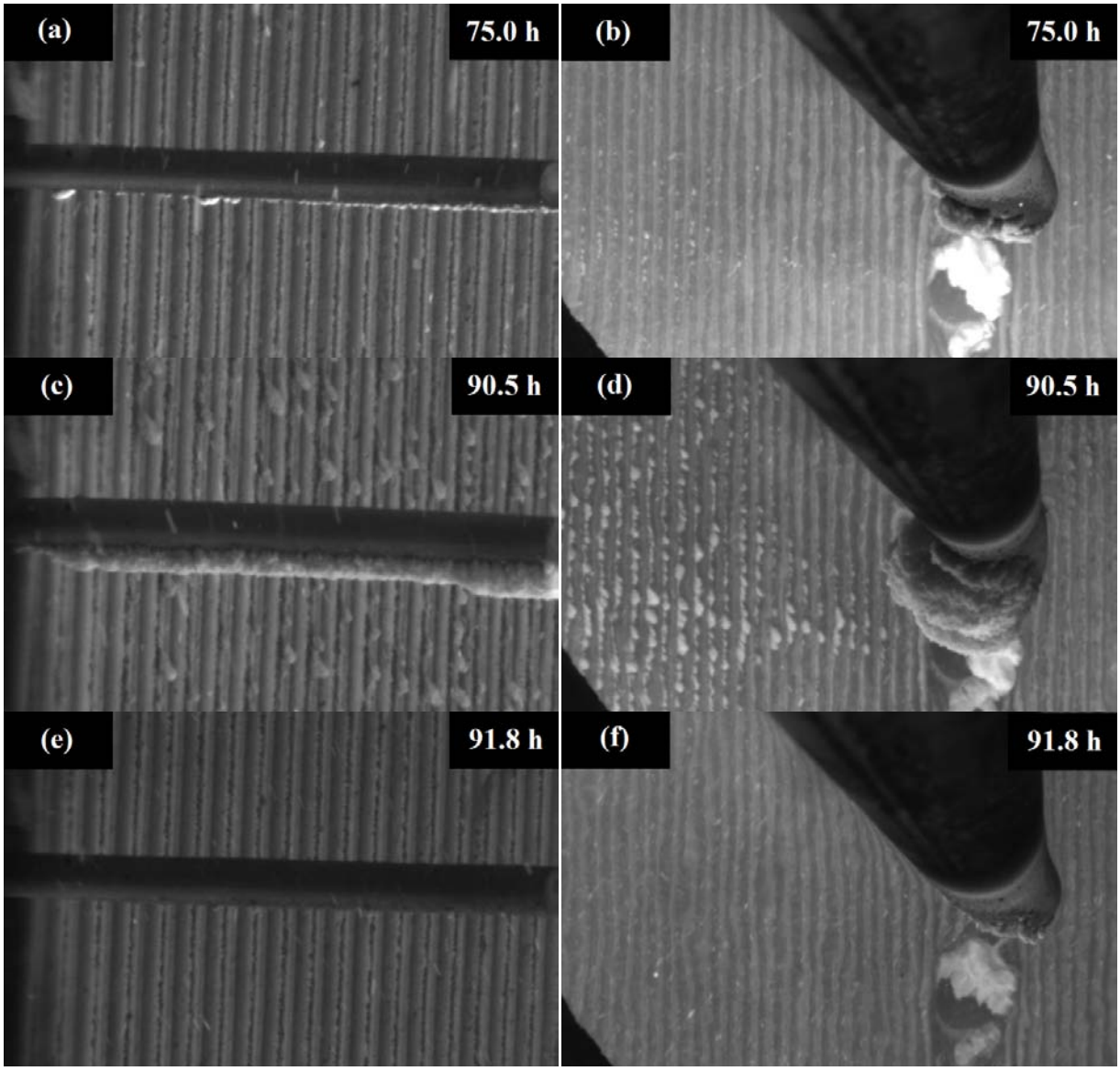

Figure 10 Typical examples of the wall deposits during Test 1. The left pictures are from the camera placed on the right side of the probe, while the right pictures are from the camera placed below the probe.

Besides the deposit formation on the probe, the formation of deposits on the boiler walls can be also seen by the cameras. It is generally observed that the formation of deposits on the boiler walls near

Location A is not significant during the tests with coal ash addition (Test 5-7), whereas a considerable amount of wall deposits can be seen in some periods during the test without coal ash addition (Test 1).

Through a detailed analysis of the camera pictures from Test 1, it is found that the formation of wall deposits is not significant before ~80 h. A typical example of the boiler wall in this period is shown in Figure 10a and Figure 10b. During the period of ~80-90.5 h, a considerable amount of deposits is formed on the boiler walls (see Figure 10c and Figure 10d). However, these deposits are almost completely removed in the period of 90.5-91.8 h. After 91.8 h, the formation of wall deposits is not very significant until the end of measurement (see an example in Figure 10e and Figure 10f).

The tendency of deposit formation on the boiler walls seems to be in agreement with that of probe deposit formation. Thus the considerable increase of wall deposits during the period of ~80-90.5 h in Test 1 may be related to a variation of fuel properties and/or a stop of natural gas supply which may change the ignition and ash release behaviors of wood particles. The complete removal of probe and wall deposits in the period of 90.5-91.8 is mostly likely induced by the operation of nearby soot-blowers during this period.

3.2.3 DDF-rate and deposition propensity

A summary of the average DDF-rate and ash deposition propensity during different tests are given in Table 6. It should be noted that for Test 1, only the time periods that are believed not significantly influenced by water condensation/evaporation are considered. For Test 3, only the time period before the moving of boiler wall (<30 h) is taken into account. For Test 7, the results are separated into two parts, i.e. before and after the cooling water shut-off.

It is shown in Table 6 that both the DDF-rate and the ash deposition propensity vary significantly during Test 1. No clear correlation is observed between the DDF-rate/deposition propensity and the flue gas temperature. On the other hand, the average probe temperature seems to be somewhat higher during 83.7-90.6 h and 95.3-100 h in Test 1. This is mostly like because the formation of deposits (especially at S-direction) is more significant during these periods. Thus less cooling capacity is needed in order to control the probe temperature at the S-direction, resulting in an increase of probe temperature at the other directions. The influence of boiler load on DDF-rate/deposition propensity is also not obvious during test 1. As discussed in previous sections, the different DDF-rate/deposition propensity observed during of Test 1 is probably related to the variation of the wood properties. In addition, the boiler is almost operated on pure wood mode after about 80 h, which may also affect the ash deposition behavior.

Compared to Test 1, the DDF-rate and ash deposition propensity during Test 3 is generally lower, which is most likely because of the lower flue gas temperature at Location B. The results from Test 4 are similar to Test 3 with respect to the DDF rate. However, the ash deposition propensity is slightly higher during Test 3.

Compared to Test 4, the DDF-rate and the ash deposition propensity during Test 5-7 are considerably higher, probably linked to the higher flue gas temperature at Location B. On the other hand, significantly different DDF-rates/deposition propensities are observed during Test 5-7. The discrepancies between Test 5 and Test 6 are difficult to explain, since both tests are carried out at similar temperature and load conditions. According to the pictures recorded by the cameras, the

major shedding mechanism during Test 5 is debonding (see Figure 6 as an example), meaning that a large layer of deposits is formed and then detached from the probe. However, during Test 6, the formation of a large layer of deposits is generally not observed. Instead, small pieces of deposits are shed before a large layer is formed. Since the calculation of DDF-rate neglects the major shedding events but includes the smalls, the different shedding behaviors during Test 5 and Test 6 could be an explanation to the different DDF-rate and ash deposition propensity obtained. On the other hand, the different shedding behaviors as well as the DDF-rates obtained during Test 5 and Test 6 are most likely related to a variation of fuel properties. However, detailed analysis data on fuel properties are needed in order to better explain the discrepancies obtained in Test 5 and Test 6.

In comparison with Test 6, the first period of Test 7 shows similar DDF-rate and deposition propensity, while the second period of Test 7 has significantly larger DDF-rate and deposition propensity. This is probably because the cooling-water to the probe was shut-off during this period and the probe was operated at very high temperature (~780 ^{o}C).

3.2.4 Quantification of deposit removal

During the calculation of DDF-rate, a cut off level of -3800 g/m^2/h was selected to determine the major shedding events. This cut off level strikes a balance between including larger shedding events in the analysis and preventing deposit mass signal noise from being counted on a shedding event [4,10]. The selected minimum magnitude of a shedding event included in the analysis was -105 g/m^2. This magnitude was calculated from the following equation, based on a sampling interval of 100 s:

$$\text{minimum shedding event manitude} = \text{slope cut off level} \times \text{sampling interval} = -3800 \frac{\text{g}}{\text{m}^2\text{h}} \frac{\text{h}}{3600\ \text{s}} \times 100\ \text{s} = -105 \frac{\text{g}}{\text{m}^2} \quad (5)$$

According to the equation above, the number of shedding events during a certain time period can be obtained, and the deposit removal frequency (hr^{-1}) can be calculated from dividing the number of shedding events by the time period (hr). In addition, the mean deposit drop (g/m^2) of the shedding events during the time period can also be calculated.

The deposit removal frequency and the mean deposit drop during different tests are summarized in Table 6. It can be seen that the deposit removal frequency is zero for the tests at Location B, both with and without coal ash addition. This suggests that shedding of deposits almost does not happen at Location B, which is consistent with the mass uptake profiles shown in Figure 5b. For the tests at Location A, shedding of deposits is seen both for the cases with and without coal ash addition. For Test 1, it can be seen that the mean deposit drop is increased considerably after ~70h, whereas no clear tendency is seen from the deposit removal frequency. For Test 5-7, it is seen that the deposit removal frequency and mean deposit drop vary considerably. A significant increase of mean deposit drop is observed during the second period of Test 7 (18.8-25.1 h), which is probably linked to the high probe temperature in this period. A detailed comparison of the probe removal frequency and mean deposit drop will be conducted in the following section, by including the results from a previous test in the same boiler under similar conditions [8].

Table 6 Summary of the DDF rate and ash deposition propensity in different experiment.

Test NO.	Probe Locati	Coal ash (kg/s)	Exposure time (h)	Boiler load (%)	Biomass load (%)	Flue gas T. (^oC)	Average Probe T. (^oC)	DDF rate ($g/m^2/h$)	Ash Flux ($g/m^2/h$)	Deposition propensity (%)	Deposit removal frequency (hr^{-1})	Mean deposit drop (g/m^2)
1	A	-	2.5-10.3	99.1	80.3	1294	529	227	10914	2.1	1.15	142
1	A	-	12.0-14.7	91.5	90.4	1230	522	16	12285	0.1	0.37	194
1	A	-	21.9-33.8	99.5	82.9	1279	524	177	11269	1.6	0.25	145
1	A	-	44.9-58.9	99.8	88.5	1310	527	104	12011	0.9	0.36	126
1	A	-	69.4-76.6	101.0	88.6	1305	524	384	12026	3.2	1.53	354
1	A	-	83.7-90.6	83.4	82.4	1285	587	471	11643	4.0	0.29	652
1	A	-	95.3-100	80.6	79.6	1244	596	497	10818	4.6	0.21	160
3	B	-	0-30	83.7	74.7	776	523	86	10157	0.8	0.00	0
4	B	1.66	0-23.6	96.3	86.7	768[a]	527	86	59689	0.1	0.00	0
5	A	1.62	0-1.3	89.5	83.3	1269[a]	541	6197	59396	10.4	4.62	568
6[b]	A	1.66	0-18	85.7	78.9	1260[a]	530	543	58600	0.9	1.83	256
7	A	1.57	0-18.8	82.7	70.3	1319	524	323	54027	0.6	0.64	162
7	A	1.57	18.8-25.1	83.2	82.2	1319	780[c]	3963	58703	6.8	1.11	2010

[a] Average value from the measurement is used.
[b] Only part of boiler data is available and is used in calculations.
[c] High probe surface temperature caused by unexpected shut-off of cooling water to the probe

3.2.5 Comparison with previous tests

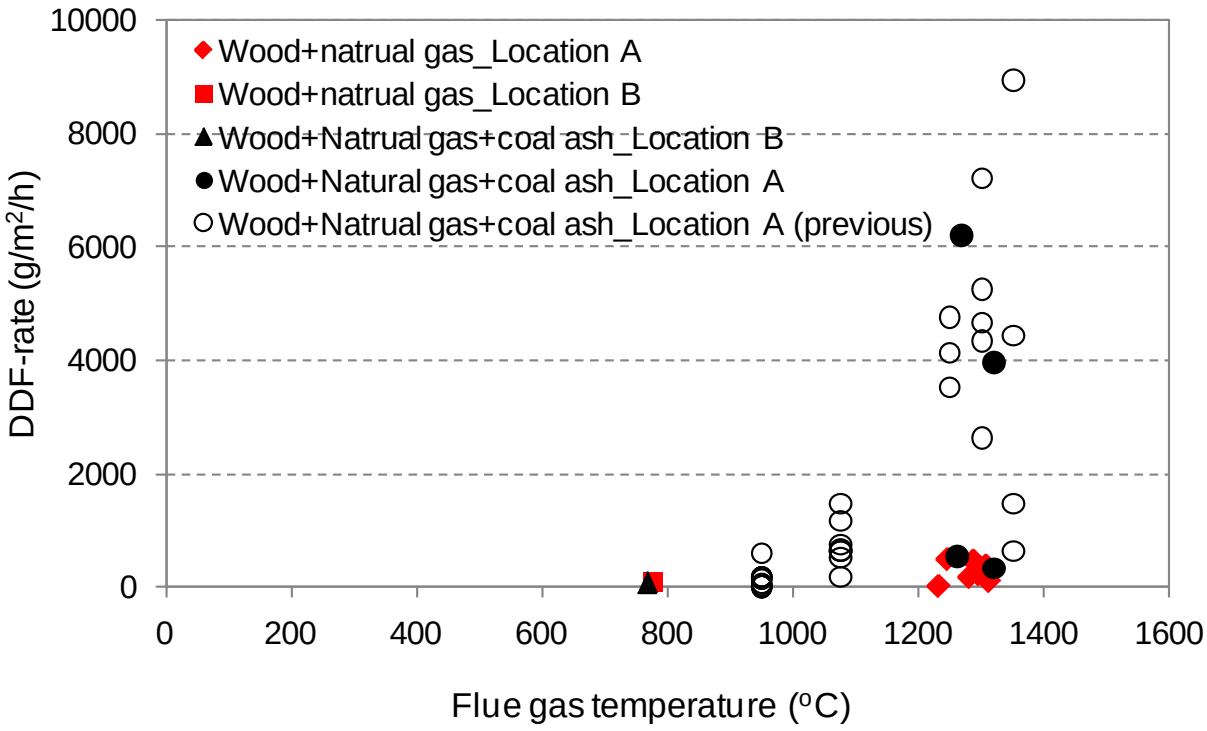

Figure 11 DDF-rate (g/m^2/h) versus flue gas temperature (^{o}C) at different tests. The solid symbols denote the results from this work; the hollow symbols denote the results from previous work [8].

Ash deposition tests similar to this work have been carried out at the same boiler at Location A by Bashir et al. [8]. Their tests were conducted when the plant was operated with coal fly ash addition. Comparisons of the results from this study and the previous tests are performed, as shown in Figure 11-Figure 14. In these figures, the DDF-rate, the ash deposition propensity, the deposit removal frequency and the mean deposit drop are plotted against the flue gas temperature. The flue gas temperature is chosen here because it is an important parameter for ash deposition and it can reflect the effect of measurement location and boiler load. It should be noted that the results of previous work are mostly from an average data over a period of 6 h [8].

From Figure 11, it can be seen that at temperatures above 1200 ^{o}C, the tests with coal ash addition generally show higher DDF-rate than those without coal ash addition. This is primarily related to the significant larger ash flux during coal ash addition, as illustrated in Table 6.

The deposition propensity of fly ash also plays a role here, which will be discussed in detail later. With decreasing flue gas temperature, the DDF-rate also decreases. At a flue gas temperature around 800 ^{o}C, very low DDF-rate is observed both for the tests with and without coal ash.

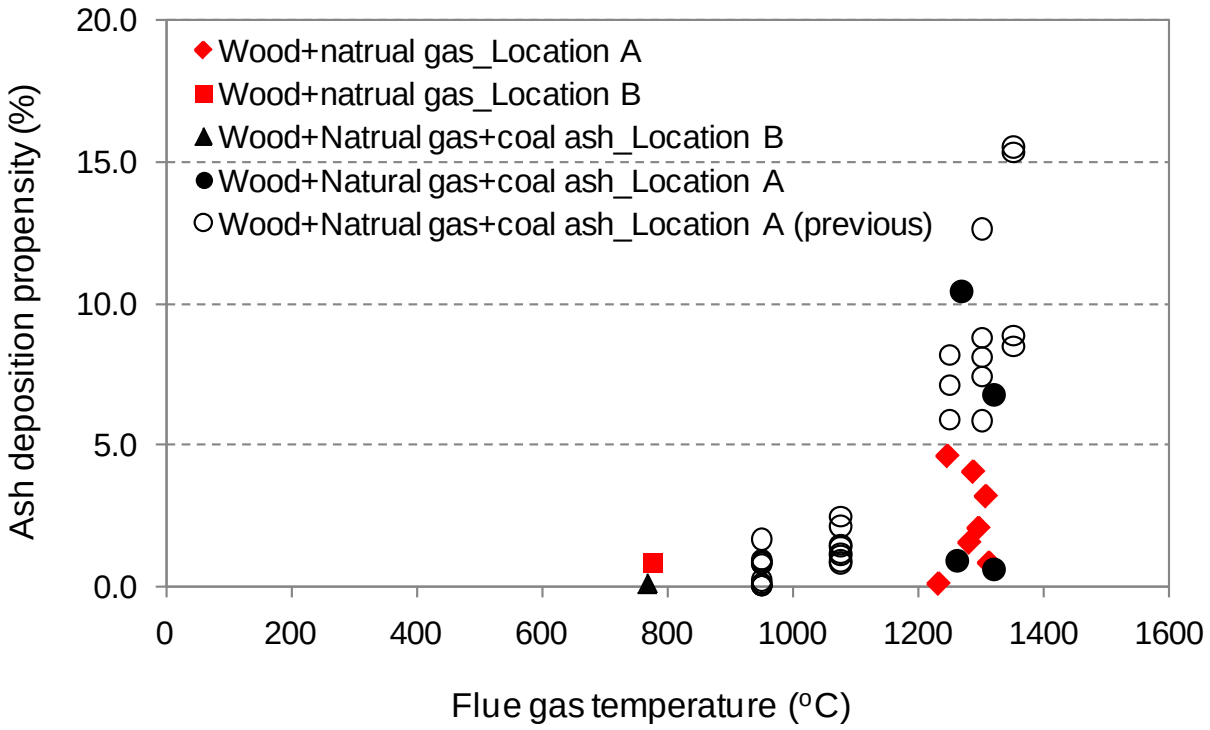

Figure 12 Ash deposition propensity (%) versus flue gas temperature (^{o}C) at different tests. The solid symbols denote the results from this work; the hollow symbols denote the results from previous work [8].

Figure 12 depicts the ash deposition propensity obtained at different tests. It is seen that at temperatures above 1200 ^{o}C, the tests with coal ash addition generally show higher ash deposition propensities than those without coal ash addition. This difference is probably linked to the physical and chemical properties of the fly ash. According to the camera pictures as well as the mass of deposits collected after the measurement, it is evident that the majority of the deposits formed on the probe are through inertial impaction. The formation of deposits through this mechanism is mainly dependent on the impaction and capture efficiency of fly ash particles, which are influenced by many factors such as ash particle size distribution, density, morphology, and melting behavior of fly ash. A systematical analysis of these factors is needed in order to understand the different ash deposition propensities observed, which is outside the scope of this work.

When the flue gas temperature becomes lower than 1200 ^{o}C, it can be seen that the ash deposition propensity is decreased, both for the tests with and without coal ash addition. The ash deposition propensity becomes very small at flue gas temperature around 800 ^{o}C. However, under this condition, it seems that the ash deposition propensity is slightly lower during coal ash addition. This may be related to a shift of major deposition mechanism under this condition. At Location B, more deposits are found at the leeward of the probe than at the windward. Due to the low flue gas temperature, it is believed that the formation of deposits through inertial impaction becomes insignificant at Location B. Alternatively, condensation may become a more important deposit formation mechanism at this location. Thus, the lower ash deposition propensity observed during the test with coal ash addition is probably linked to a decrease of the condensable species at this temperature (e.g. KCl). The influence of coal ash addition on the compositions of fly ash and deposit will be discussed in the following sections.

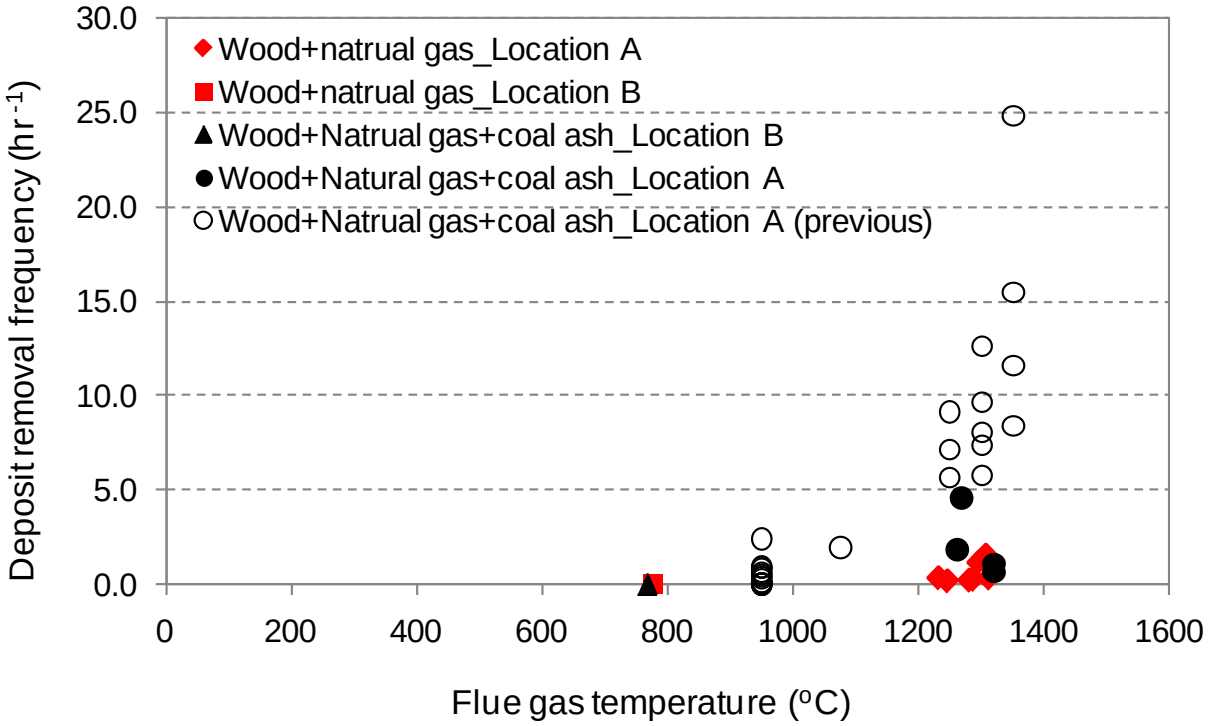

Figure 13 Deposit removal frequency (hr^{-1}) versus flue gas temperature (^oC) at different tests. The solid symbols denote the results from this work; the hollow symbols denote the results from previous work [8].

The deposit removal frequencies (hr^{-1}) obtained from different tests are shown in Figure 13. At high flue gas temperatures above 1200 ^oC, it is seen that the deposit removal frequencies are generally much higher when coal ash is added. This tendency is in agreement with the observations by the cameras at Location A. When the flue gas temperature is decreased, the deposit removal frequency appears to be decreased. At about 800 ^oC, the deposit removal frequency becomes zero, indicating that there is no major shedding event occurring at this location, both for the cases with and without coal ash addition.

Figure 14 illustrates the mean deposit mass drop (g/m^2) calculated during different tests. It is seen that at high flue gas temperatures above 1200 ^oC, the mean deposit drop is generally larger when coal ash is added. For the high-temperature test without coal ash addition (Test 1), the mean deposit drop is mostly below 200 (g/m^2) according to Table 6.Such small mass drops are generally not seen obviously by the cameras, indicating that they may be partly related to the analysis noise of the probe caused by the turbulence conditions of the boiler. However, for the two cases during Test 1 (see Table 6) where the mean deposit drop is larger than 300 (g/m^2), deposit shedding is clearly seen from the cameras. For the high flue gas temperature tests with coal ash addition (Test 5-7 in Table 6), the identified deposit drops generally correlate well with the camera observations. For example, the camera pictures show that the deposit layer dropped during Test 5 is usually much larger than that of Test 6. This is clearly reflected by the mean deposit mass drop calculated in these two tests.

The temperature dependency of the mean deposit mass drop is also reflected at Figure 14. A general tendency is that the mean deposit mass drop decreases with decreasing flue gas temperature. At

temperatures about 800 °C, the mean deposit mass drop becomes zero since no major deposit removal happens at this temperature, both with and without coal ash addition.

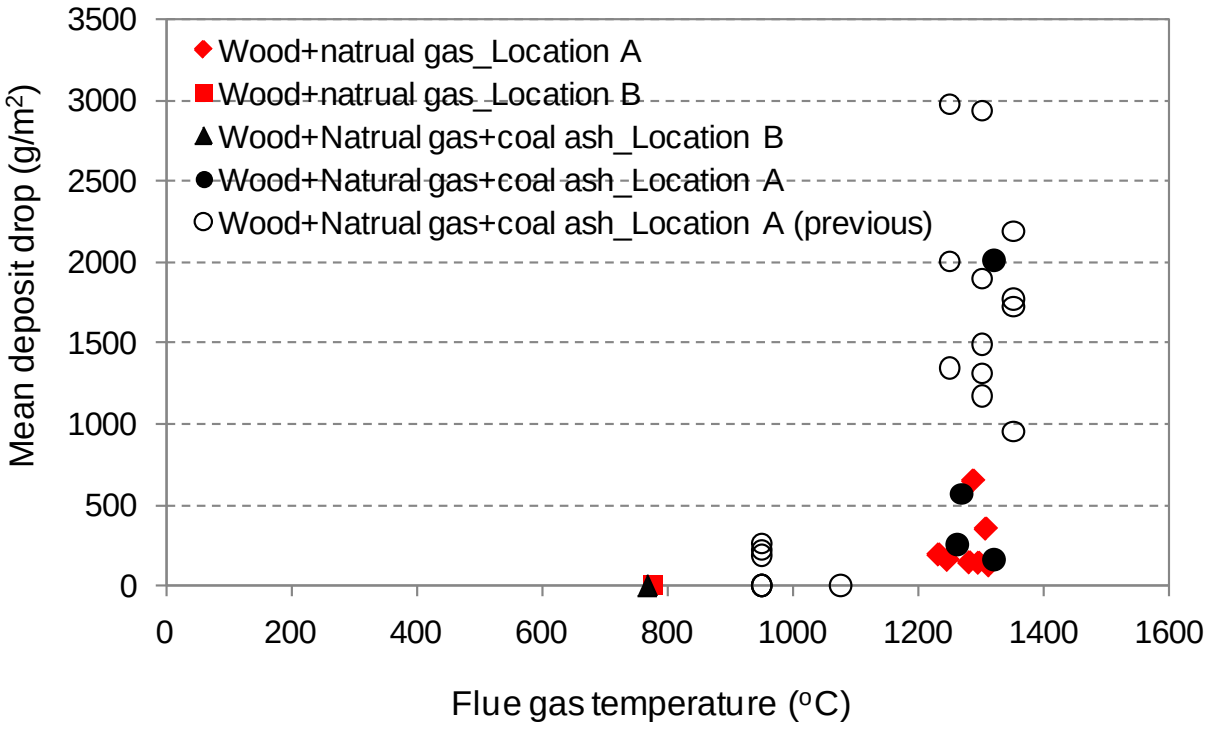

Figure 14 Mean deposit drop (g/m^2) versus flue gas temperature (°C) at different tests. The solid symbols denote the results from this work; the hollow symbols denote the results from previous work [8].

3.3 Fly ash and bottom ash properties

The fly ash and bottom ash during the tests without coal ash addition are collected and analyzed by SEM-EDS. In addition, the fly ashes from the normal operation conditions of the boiler (i.e. with coal ash addition) are also received and analyzed. Although the fly ashes from the normal boiler operation conditions are not exactly from the measurement period of this work, they are still considered to be representative in chemical and physical properties. The SEM-EDS analyses were conducted at DTU Mechanical Engineering. Prior to analyses, the samples were coated with a layer of about 20-50 nm carbon, in order to avoid charging of samples and to improve the analysis quality. Besides the SEM-EDS analyses, the fly ashes with and without coal addition were analyzed by ICP-OES (Inductively Coupled Plasma Optical Emission Spectroscopy) or IC (Ion Chromatography) for the bulk/water soluble inorganic compositions. XRD (X-ray Diffraction) analyses were conducted to identify the crystalline phases in the fly ashes. In addition, With the purpose of identifying the alkali and earth alkaline species present in the fly ash without coal ash addition, 2g of the fly ash is dissolved in 100 ml water and the pH value of the solution is measured by a pH meter.

3.3.1 Fly ash without coal ash addition

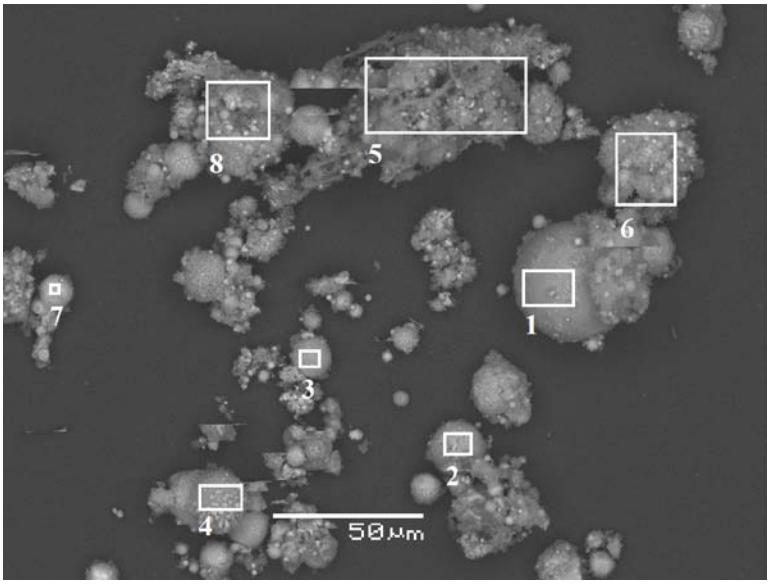

Element (mol%)	Spectrum 1	2	3	4	5	6	7	8
O	50	47	44	49	50	50	12	46
Na	-	-	2	-	-	2	-	2
Mg	3	8	4	-	2	-	-	2
Al	8	-	7	7	-	-	-	2
Si	24	5	16	24	3	2	14	7
P	-	2	-	-	-	-	7	-
S	-	-	2	-	4	5	-	4
Cl	-	-	1	-	2	2	-	4
K	8	4	15	14	21	25	6	23
Ca	3	30	6	2	13	9	53	9
Fe	3	-	2	-	-	-	3	-

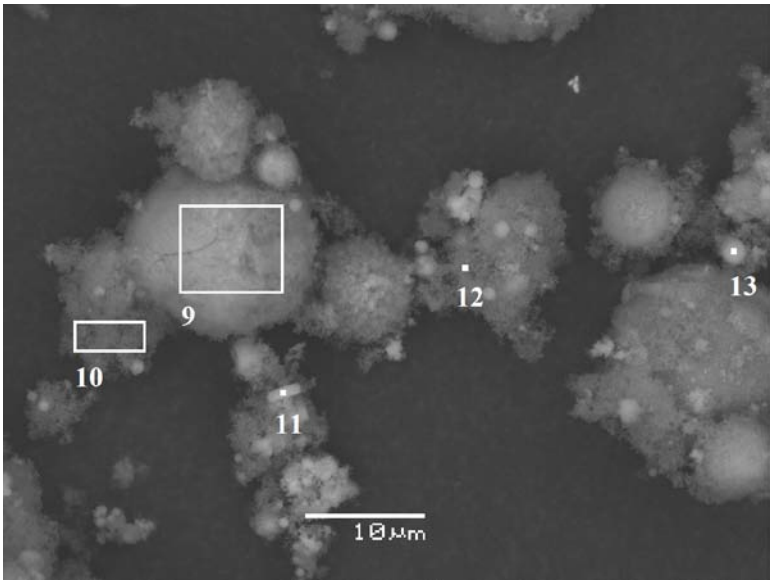

Element (mol%)	Spectrum 9	10	11	12	13
O	27	52	41	44	45
Na	2	3	2	3	-
Mg	2	-	-	-	2
Al	-	-	-	-	5
Si	2	-	-	-	9
P	3	-	-	-	4
S	4	7	3	8	-
Cl	14	2	15	3	-
K	30	28	28	30	4
Ca	14	4	6	6	27
Fe	-	-	-	-	2

Figure 15 Typical SEM-EDS results of the fly ash from the test without coal ash addition (only the elements above 2 mol% are shown).

The fly ash collected during the tests without coal ash addition primarily consists of ash particles with spherical appearance (see Figure 15). EDS analyses reveal that these particles are generally dominated by Ca, Si and K. The size of the spherical particles varies significantly, from large particles with diameter around 50 μm to small ones with diameter about 1 μm. Some extremely fine particles (smaller than 1 μm) rich in K, S, and Cl are also observed. These fine particles either attach to the surface of large particles (e.g. Spectrum 9) or present as clusters themselves (e.g. Spectrum 10 and 12). The morphology of these fine particles suggests that they are most likely generated from homogeneous nucleation of K, S and Cl rich species, such as KCl and K_2SO_4. The results are consistent with the aerosol measurements carried out at the same plant, showing that the submicron ash particles are dominated by K, S and Cl when coal ash is not added [6]. The molar

ratio of K/(2S+Cl) in Spectrum 9-12 is generally greater than 1, indicating that other form of K species (e.g. K_2CO_3 and KOH) may also present.

Table 7 Bulk (total) compositions of the fuel ash (wood), and bulk and water soluble elemental compositions of the fly ash collected with and without coal ash addition.

	Fuel ash (wood)	Fly ash without coal ash addition		Fly ash with coal ash addition
	Bulk	Bulk	Water soluble	Water soluble
Al (wt%, dry basis)	2.45	2.13		
Ca (wt%, dry basis)	21.05	20.80		
Cl (wt%, dry basis)	0.70	0.20	0.23	0.01
Fe (wt%, dry basis)	2.00	1.73		
K (wt%, dry basis)	9.19	6.26	4.41	0.11
Mg (wt%, dry basis)	3.40	3.22		
Na (wt%, dry basis)	0.68	0.43	0.19	0.02
P (wt%, dry basis)	1.19	1.09	0.00	0.00
S (wt%, dry basis)	1.70	1.08	0.86	0.09
Si (wt%, dry basis)	17.61	17.70		
Zn (wt%, dry basis)	-	0.17		

In order to accurately quantify the compositions, the fly ash collected during the tests without coal ash addition was analyzed by ICP-OES. In addition, the content of water soluble K, Na, S, Cl and P in the fly ash was obtained by leaching the ash in hot water (120 ^oC) for one hour and by analyzing the solution with ICP-OES (for K, Na and P) and IC (for Cl and S). The resulted bulk and water soluble elemental compositions of the fly ash are shown in Table 7, along with the bulk compositions of the fuel ash calculated from the wood properties in Table 1. It can be seen that the fly ash without coal ash addition primarily consists of Ca, Si and K. The Cl and S content in the fly ash is about 0.2 wt.% and 1.1 wt.% respectively. Compared to the fuel ash, it appears that the contents of Cl, K and S are considerably smaller in the fly ash collected without coal ash addition. This is probably because a large fraction of KCl and K_2SO_4 present in the flue gas has been deposited in the boiler during the tests without coal ash addition.

Through a comparison of the water soluble composition with the bulk compositions of fly ash, it appears that the Cl in fly ash is totally water soluble. For S, K and Na, the water soluble fraction in fly ash is about 80%, 70% and 43% respectively, whereas the P in fly ash is almost insoluble in water. The molar ratio of water soluble K/(Cl+2S) in the fly ash without coal ash addition is about 1.9, indicating that only about 50% of the water soluble K may exist as KCl and K_2SO_4. The remaining water soluble K is likely KOH or K_2CO_3. By dissolving 2 g of the fly ash in 100 ml water, the pH value is measured to be 12.04. This base solution is probably resulted from the KOH, K_2CO_3, CaO and other possible base components presented in the fly ash.

XRD analysis has been carried out to identify the crystalline phase present in the fly ash, and the results are shown in Figure 16. It can be seen that the main crystalline components found in the fly ash are SiO_2 and CaO. Besides, KCl, K_2SO_4, MgO, $CaCO_3$, KOH and K_2CO_3 are also observed. The results suggest that the water soluble K species in the fly ash is probably a mixture of KCl, K_2SO_4, KOH and K_2CO_3. It also indicates that most of the K-Ca-Si rich particles observed in SEM-EDS analysis (see Figure 15) are probably in an amorphous phase, since almost no K-Ca-Si rich crystalline phase is found in the XRD analysis.

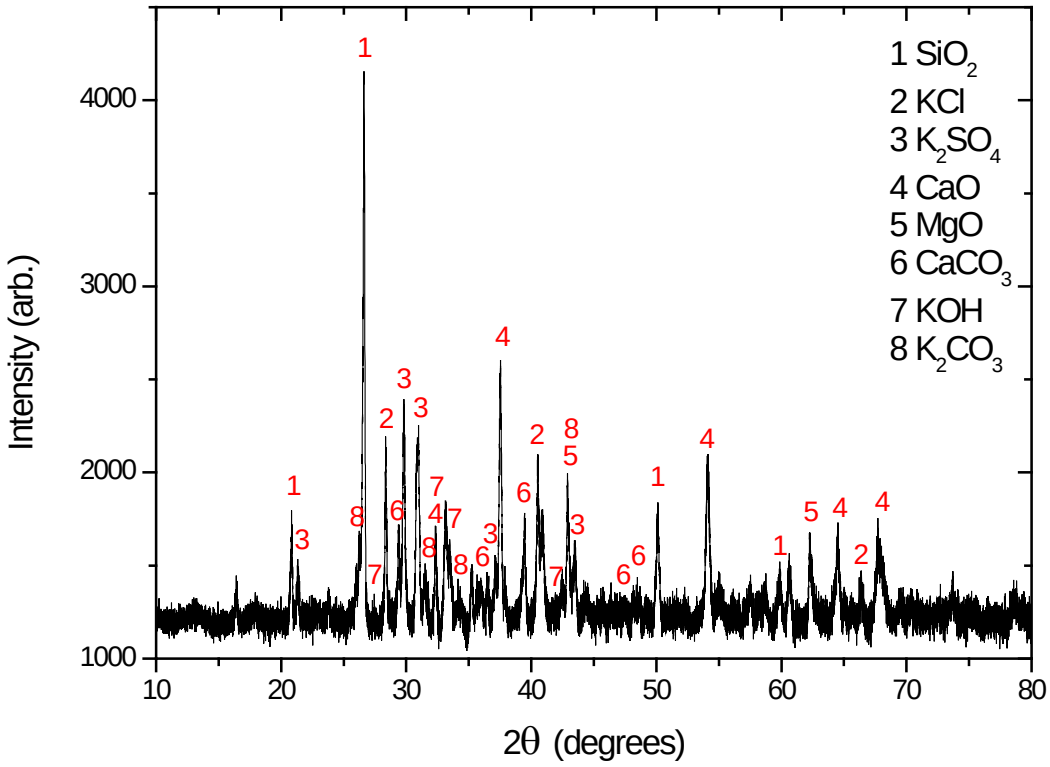

Figure 16 XRD patterns of the fly ash without coal ash addition.

3.3.2 Fly ash with coal ash addition

With the addition of coal fly ash, the fly ash collected from the ESP (electrostatic precipitator) of the plant is dominated by the added coal fly ash particles. This is evident in Figure 17, where a lot of spherical ash particles with large Si and Al content are seen. The presence of S and Cl is generally not observed in the fly ash collected during coal ash addition. This is supported by the analysis of water soluble Cl, S, K and Na in the fly ash (see Table 7). Compared to the fly ash collected without coal addition, the fly ash collected with coal ash addition has remarkably smaller (~10–40 times) water soluble Cl, S and K content. The decreased water soluble Cl, S and K content is clearly beyond the dilution effect caused by the added coal ash (see the coal ash to wood ash ratio given in Table 5). This clearly indicates that the coal ash has reacted with the water soluble Cl, S and K formed during wood combustion.

The XRD patterns of the fly ash collected during the tests with coal ash addition are shown in Figure 18. It can be seen that the major crystalline phases present in the fly ash are SiO_2 and mullite ($3Al_2O_3 \cdot 2SiO_2$). Besides, CaO and MgO are also observed. However, the KCl, K_2SO_4, KOH and K_2CO_3 observed in Figure 16 do not appear in Figure 18. This further supports that the added coal ash has reacted with the KCl, K_2SO_4, KOH and K_2CO_3 generated/released from wood combustion. The reaction products are probably K-aluminosilicates, K-silicates and gaseous species such as HCl and SO_2. Since no crystalline phase containing K-Al-Si or K-Si is observed in Figure 18, it is most likely the generated K-aluminosilicates or K-silicates is in amorphous phase.

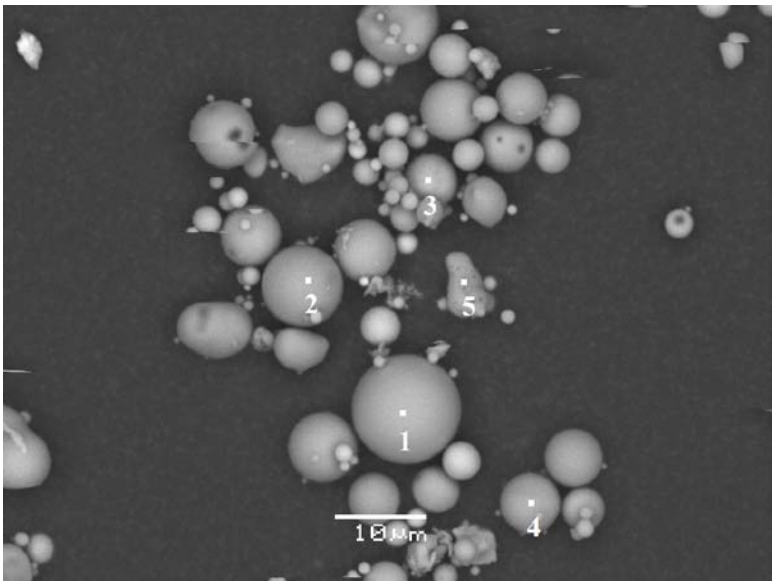

Element (mol%)	Spectrum 1	2	3	4	5
O	49	44	47	50	47
Na	-	-	-	-	-
Mg	-	-	-	-	-
Al	10	17	12	9	23
Si	26	29	29	32	25
P	-	-	-	-	-
S	-	-	-	-	-
Cl	-	-	-	-	-
K	-	5	5	6	3
Ca	11	-	4	-	-
Fe	2	2	-	-	-

Figure 17 Typical SEM-EDS results of the fly ash from the test with coal ash addition (only the elements above 2 mol% are shown).

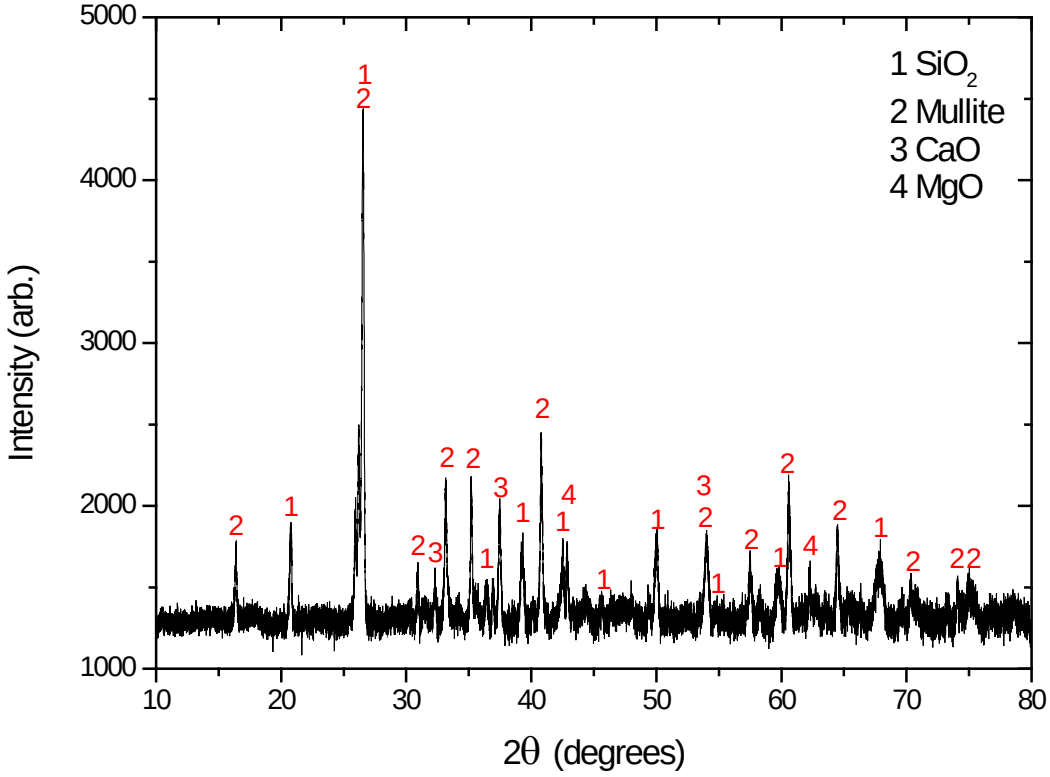

Figure 18 XRD patterns of the fly ash with coal ash addition.

3.3.3 Bottom ash properties

Typical results of the bottom ash from the tests without coal ash addition are shown in Figure 19. It can be seen that the bottom ash mainly contains some very large inorganic particles (> 100 μm) with high Si contents (see Spectrum 1 and 2). These particles might originate from the sand in the wood pellets or large inorganic particles present in the wood structure. On the other hand, some large unburnt char particles are also observed in the bottom ash (see Spectrum 3 and 4). It should be noted that carbon content is usually neglected in the SEM-EDS results due to the low analysis accuracy on carbon, the influence of carbon coating, and the general low carbon content in most of the ash particles. However, for the Spectrum 3 and 4 in Figure 19, the quantitative results of carbon are included, since the carbon is found to be the dominant element in this sample. The presence of inorganic elements is negligible in Spectrum 3 and 4.

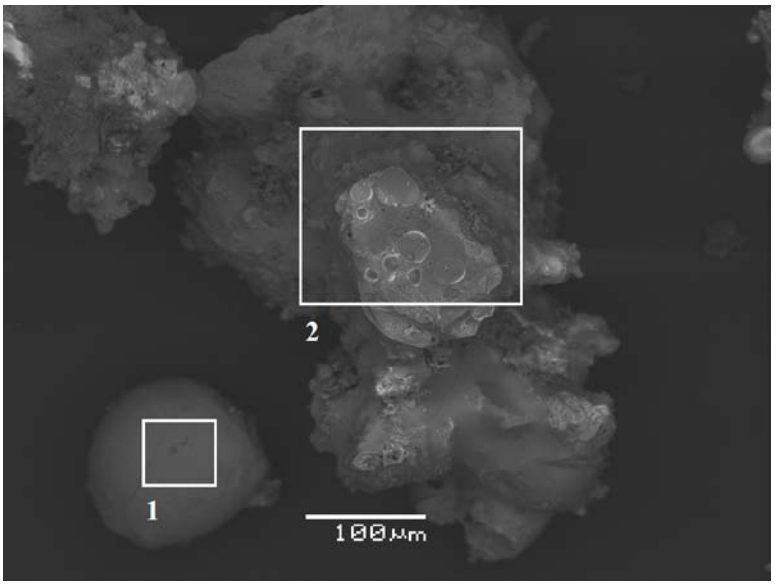

Element (mol%)	Spectrum 1	2
O	49	55
Na	-	2
Mg	3	3
Al	2	5
Si	26	23
P	-	-
S	-	-
Cl	-	-
K	5	4
Ca	12	8
Fe	-	-

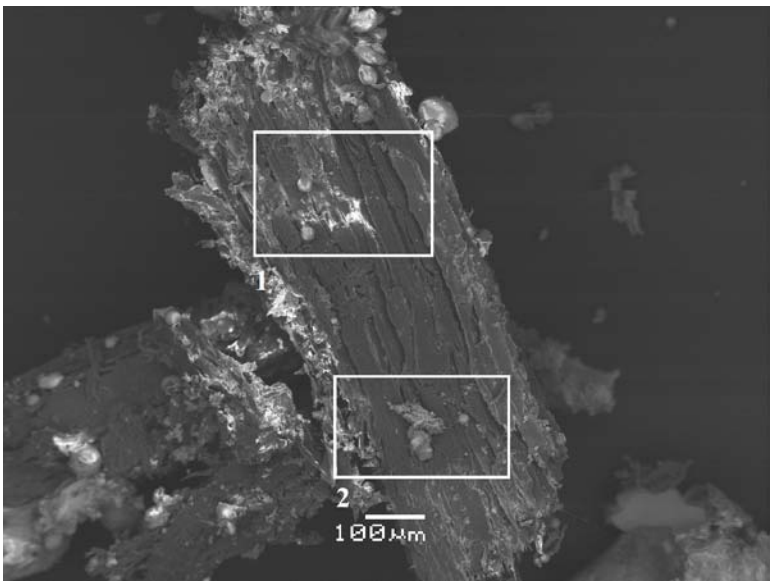

Element (mol%)	Spectrum 1	2
C	61	62
O	36	34
Na	-	-
Mg	-	-
Al	-	-
Si	-	-
P	-	-
S	-	-
Cl	-	-
K	-	-
Ca	-	3
Fe	-	-

Figure 19 Typical SEM-EDS results of the bottom ash from the test without coal ash addition (only the elements above 2 mol% are shown).

3.4 Deposit properties

At the end of each test, the deposit probe was taken out of the boiler and the deposits were collected carefully. At Location A, the collected deposits are divided into three parts, namely outer-layer windward deposits, inner-layer windward deposits, and leeward deposits. In this work, it is assumed that the flue gas is blown from the bottom of the boiler and the deposits collected on the half-circle facing the bottom of boiler are denoted as windward deposits. The outer-layer deposits are large pieces of deposits (see Figure 8d as a typical example) which can be easily removed by using a glass stick. On the other hand, the inner-layer deposits or the leeward deposits contain some condensed species which are generally more difficult to remove. Therefore, a metal brush is used to collect the inner-layer windward deposits and leeward deposits.

At Location B, the collected deposits are simply divided into windward deposits and leeward deposits, since the formation of a large outer layer of deposits was not observed at this location. It is worthwhile to mention that the deposits from the tests without coal ash addition seem to be more difficult to remove at this location, compared with the deposits collected during coal ash addition. This is mostly likely related to the chemical compositions of the deposits, which will be discussed in detail in the following sections.

3.4.1 Deposits at Location A without coal ash addition

Deposits collected during Test 1 were analyzed by SEM-EDS. Figure 20 illustrates the typical outer-layer windward deposits collected during Test 1. It can be seen that the deposits are mainly comprised of ash particles with large Si, K and Ca content. Majority of these particles are relatively large spherical particles with diameters mainly varying from ~5-100 μm (e.g. Spectrum 1, 7, 8, 9, 10 and 14). However, some of the particles appear to be partially melted and glued other particles together (e.g. Spectrum 4, 5, 6, 11, 12 and 16). Compared with the spherical particles, these partially melted particles seem to have larger Si and K content, and smaller Al content. The presence of these partially melted particles is probably important for the deposit build-up/sintering at high flue gas temperatures during suspension-firing of wood. According to the SEM-EDS results, the presence of Cl is found to be negligible in the outer-layer deposits. Some S species (most likely potassium sulfate) are detected in the outer-layer deposits, but the amount is not significant.

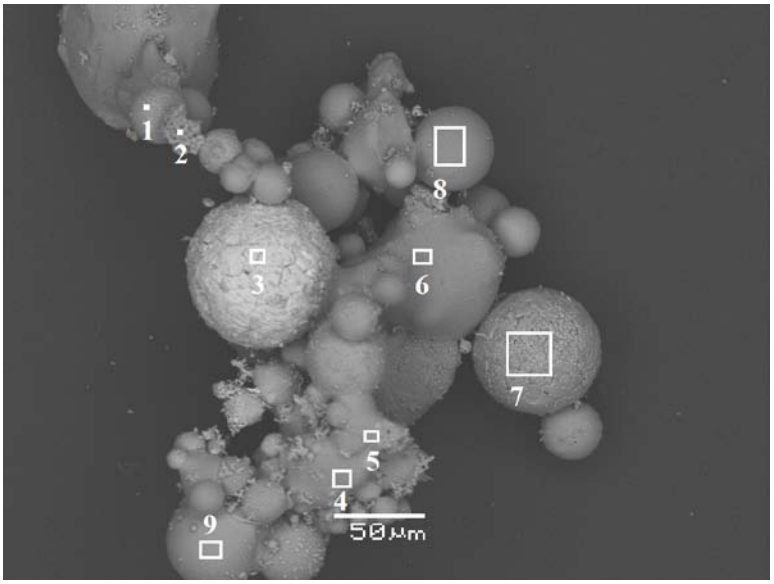

Element (mol%)	Spectrum 1	2	3	4	5	6	7	8	9
O	43	48	43	44	39	26	38	45	45
Na	3	-	-	4	4	-	-	3	-
Mg	4	-	-	-	-	5	8	-	4
Al	10	-	-	-	-	3	3	19	4
Si	22	-	-	33	37	14	12	19	23
P	-	-	-	-	-	-	-	-	-
S	-	2	-	-	-	3	-	-	-
Cl	-	-	-	-	-	-	-	-	-
K	12	2	-	12	13	14	-	10	5
Ca	-	45	-	2	4	27	36	-	13
Fe	5	-	55	-	-	5	-	-	2

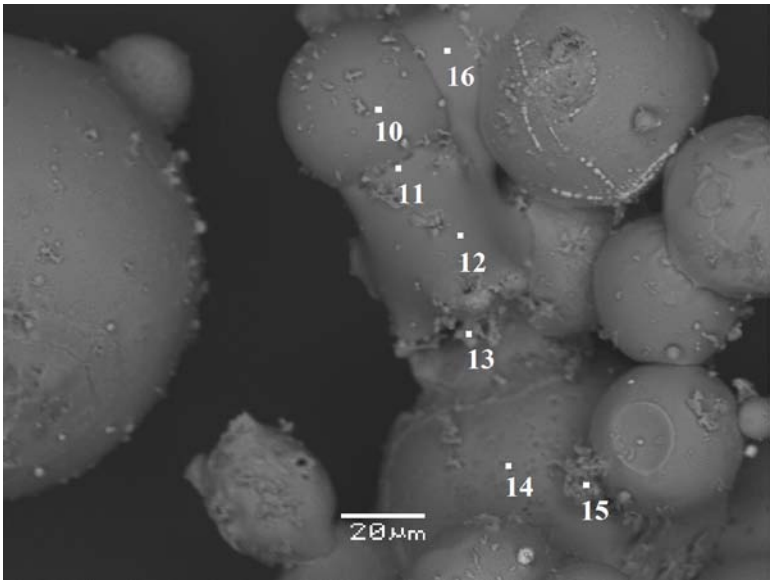

Element (mol%)	Spectrum 10	11	12	13	14	15	16
O	31	46	46	35	49	43	39
Na	2	4	5	-	-	-	4
Mg	-	-	-	6	5	14	-
Al	11	-	-	3	3	3	-
Si	31	33	33	15	19	7	38
P	-	-	-	2	2	5	-
S	-	-	-	2	-	2	-
Cl	-	-	-	-	-	-	-
K	14	11	12	5	3	2	15
Ca	11	3	2	28	17	18	4
Mn	-	-	-	-	-	2	-
Fe	-	-	-	2	-	3	-

Figure 20 Typical SEM-EDS results of the outer-layer windward deposits collected at Location A without coal ash addition (Test 1).

The bulk and water soluble elemental compositions of the outer layer windward deposits collected during Test 1 were analyzed by ICP-OES/IC. The results are given in Table 8, along with the bulk compositions of the fuel ash calculated from the wood properties in Table 1. It is seen that the outer layer windward deposits primarily consist of Ca and Si, supplemented by a small amount of Al, Fe, K, and Mg. In agreement with the SEM-EDS results, S and Cl are found to be negligible in the outer layer windward deposits. The analysis of the water soluble element indicates that the majority of the K (> 98%) in the outer layer windward deposits is not soluble in water. According to SEM-EDS analyses (Figure 20), these water insoluble K species are probably present as K-silicates, K-Al-silicates or K-Ca-silicates.

Table 8 Bulk compositions of the fuel ash, and bulk and water soluble elemental compositions of the deposits collected without coal ash addition at Location A (Test 1).

	Fuel ash (wood)	Windward deposits - outer layer		Windward deposits - inner layer		Leeward deposits	
	Bulk	Bulk	Water soluble	Bulk	Water soluble	Bulk	Water soluble
Al (wt%, dry basis)	2.45	4.80		4.30		2.19	
Ca (wt%, dry basis)	21.05	25.30		20.20		14.75	
Cl (wt%, dry basis)	0.70	<0.09	0.00	<0.09	0.10	0.21	0.20
Fe (wt%, dry basis)	2.00	2.62		3.22		2.04	
K (wt%, dry basis)	9.19	3.04	0.04	6.05	3.76	17.60	17.10
Mg (wt%, dry basis)	3.40	3.40		4.69		2.77	
Na (wt%, dry basis)	0.68	0.78	0.01	0.89	0.37	2.25	1.64
P (wt%, dry basis)	1.19	0.82	0.00	1.37	0.00	0.95	
S (wt%, dry basis)	1.70	0.07	0.04	1.91	1.74	6.39	6.07
Si (wt%, dry basis)	17.61	24.90		14.00		7.37	
Zn (wt%, dry basis)	-	0.04		0.21		0.54	

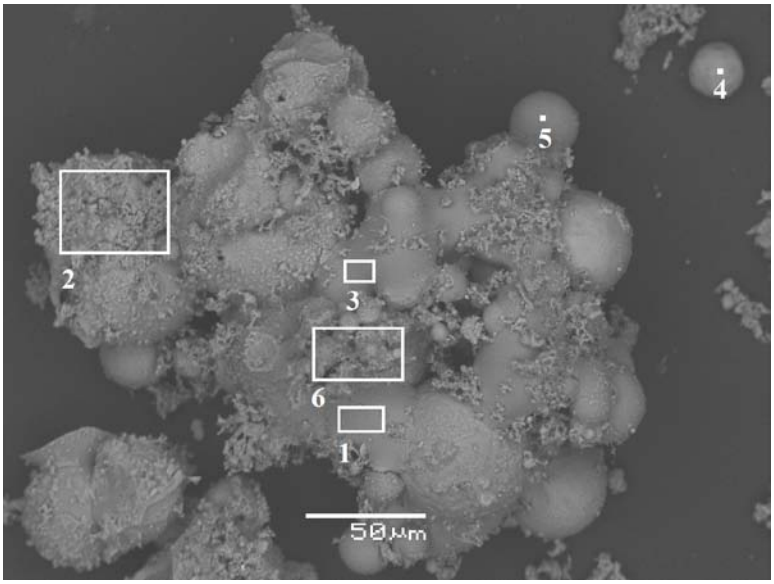

Element (mol%)	Spectrum 1	2	3	4	5	6
O	42	47	54	42	47	48
Na	2	2	4	-	2	-
Mg	2	9	-	3	-	5
Al	-	2	-	6	9	3
Si	21	4	27	12	27	6
P	-	2	-	4	-	-
S	-	5	-	-	-	4
Cl	-	-	-	-	-	-
K	10	10	11	0	11	9
Ca	19	17	3	29	3	20
Fe	-	-	-	-	-	-

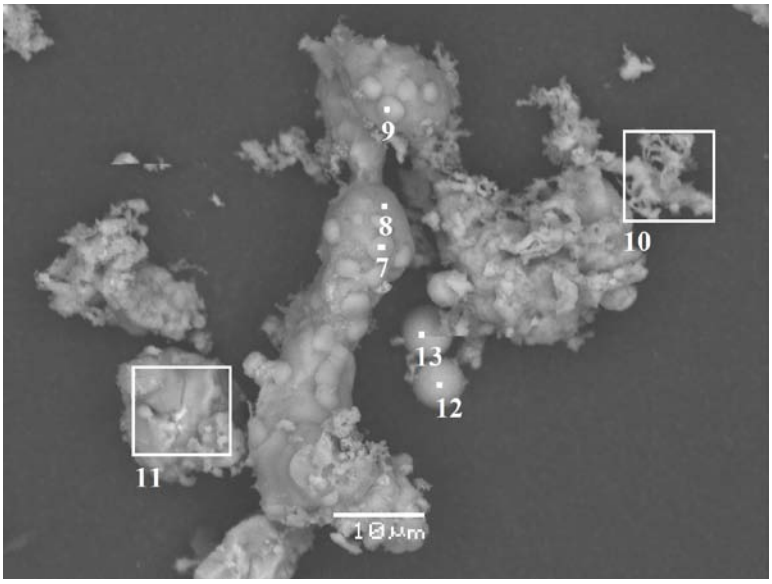

Element (mol%)	Spectrum 7	8	9	10	11	12	13
O	36	41	53	55	42	-	-
Na	5	-	6	-	3	-	-
Mg	2	4	2	9	3	5	-
Al	6	14	2	-	-	6	7
Si	7	18	3	2	2	13	9
P	-	-	1	3	-	-	-
S	14	-	9	-	13	2	-
Cl	-	-	-	-	-	-	-
K	27	18	13	-	20	6	7
Ca	3	3	8	24	13	45	68
Ti	-	-	-	-	-	8	-
Mn	-	-	4	-	-	3	3
Fe	-	-	-	-	3	11	7

Figure 21 Typical SEM-EDS results of the inner-layer windward deposits collected at Location A without coal ash addition (Test 1). EDS results of Spectrum 12 and 13 may not be very reliable due to the very low counts number in these analyses.

Figure 21 shows the typical morphology and elemental compositions of the inner-layer windward deposits collected from Test 1. Similar to the outer-layer deposits, spherical particles rich in Si, K, Ca and Al are found in the inner-layer deposits (see Spectrum 4 and 5). The diameter of these spherical particles is typically ~5-100 µm. Besides, partially melted particles with high Si and K content and low Al content are also observed (see Spectrum 1 and 3). However, compared to the outer-layer deposits, the inner-layer deposits seem to contain more sulfur species. These sulfur species can either be very small submicron particles attached to the surface of large particles (e.g. Spectrum 2 and 4), or relatively large crystalline/molten supermicron particles (e.g. Spectrum 7, 9 and 11). Although sulfur species is observed, chorine is still not found in the inner-layer deposits.

The bulk and water soluble elemental compositions of the inner layer windward deposits are also shown in Table 8. It is seen that the inner layer deposits are also dominated by Ca and Si. Compared with the outer layer deposits, the content of K and S is considerable larger in the inner layer deposits. A significant fraction (~40%) of the K in the inner layer deposits is water soluble. The molar ratio of the water soluble (K+Na)/(Cl+2S) is about 1.01, indicating that the water soluble alkalis in the inner layer deposits are probably alkali chlorides and sulphates. The molar ratio of the water soluble S/Cl in the deposits is about 20, implying that the majority of the water soluble alkalis are sulphates.

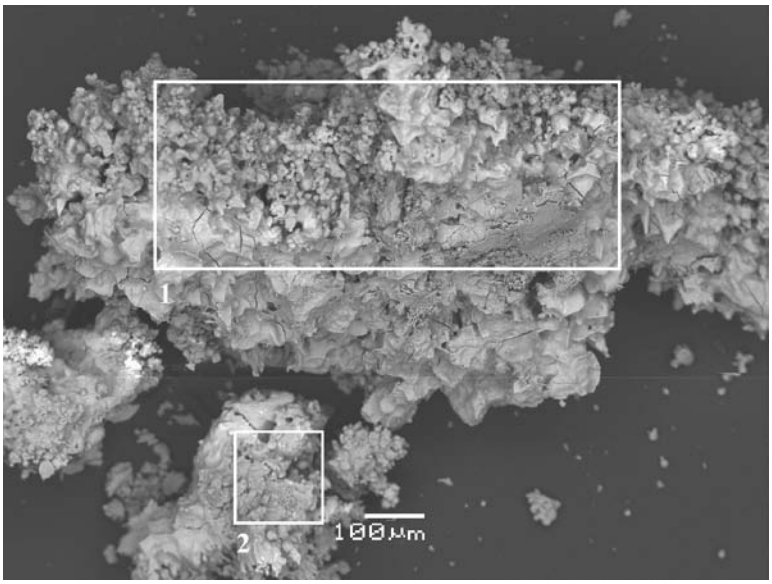

Element (mol%)	Spectrum 1	2
O	42	41
Na	3	4
Mg	-	-
Al	-	-
Si	3	-
P	-	-
S	13	17
Cl	-	-
K	32	33
Ca	4	3
Fe	-	-

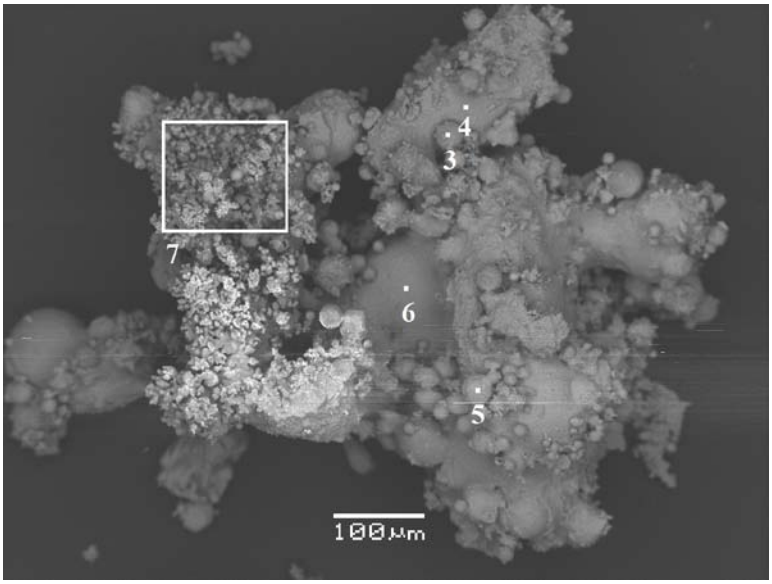

Element (mol%)	Spectrum 3	4	5	6	7
O	51	42	43	48	41
Na	-	-	2	2	3
Mg	-	-	-	7	-
Al	-	-	8	4	-
Si	4	35	19	8	3
P	-	-	-	-	-
S	-	-	5	7	14
Cl	-	-	-	-	-
K	-	7	21	12	27
Ca	41	12	-	8	8
Fe	-	-	-	2	-

Figure 22 Typical SEM-EDS results of the leeward deposits collected at Location A without coal ash addition (Test 1).

The typical SEM-EDS results of the leeward deposits collected from Test 1 are shown in Figure 22. It is seen that the deposits contain a lot of sulfur species (Spectrum 1, 2 and 7). These sulfur species are most likely K_2SO_4 since a large amount of K and S are both found in the spectrums. The morphology of these sulfur species indicates that they are partially melted (Spectrum 1 and 2). On

the other hand, some small submicron particles rich in K and S are also seen (Spectrum 7). Besides the sulfur species, some relatively large (e.g. >10 μm) K, Si and Ca rich spherical particles and molten appearance K and Si rich particles are also observed in the leeward deposits (Spectrum 4-6).

The bulk and water soluble elemental compositions of the leeward deposits are shown in Table 8. Different from the windward deposits, the leeward deposits are dominated by Ca and K. Besides, a considerable amount of S and Si is also observed. The Cl content of the leeward deposits is about 0.2 wt.%, which is slightly higher than that of the windward deposits. The analyses of water soluble elemental compositions reveal that the majority (>95%) of the S, K and Cl present in the leeward deposits are water soluble. The major ratio of water soluble (K+Na)/(Cl+2S) is about 1.36, suggesting that the water soluble alkalis in the leeward deposits are not only sulphates and chlorides, but may also contain other water soluble species (e.g. hydroxides or carbonates). The molar ratio of S/Cl in the leeward deposits is about 34, indicating that alkali sulphates are dominant over chlorides. Through a comparison with the fuel ash composition, it can be seen that the leeward deposits are enriched in K and S, whereas depleted in Ca and Si. This indicates that the leeward deposits are primarily formed by the condensation of K_2SO_4 and/or the condensation of KCl/KOH followed by heterogeneous sulfation. The formation mechanisms will be discussed in detail in Section 3.4.5.

3.4.2 Deposits at Location B without coal ash addition

Figure 23 shows the typical morphologies and elemental compositions of the windward deposits collected at Location B during the test without coal ash addition (Test 3). The general compositions of the deposits can be seen from Spectrum 1 and 2, showing that the windward deposits are dominated by K, Ca, S and Cl. In these two spectrums, the molar ratio of K/(2S+Cl) is greater than 1, suggesting that besides KCl and K_2SO_4, other forms of potassium (e.g. KOH or K_2CO_3) may also be present in the deposits. The morphology of the deposits indicates that they are mostly clusters of small submicron particles. Large fly ash particles rich in Si, Ca and K are generally not seen in the collected windward deposits.

The bulk and water soluble elemental compositions of the winward deposits are presented in Table 9, along with the bulk compositions of the fuel ash calculated from the wood properties in Table 1. It is seen that the major inorganic elements in the windward deposits collected at Location B without coal ash addition are Ca and K, supplemented by a relatively smaller amount of Cl, Fe, S and Si. Compared to the windward deposits collected at Location A under the similar conditions (Table 8), the windward deposits collected at Location B are characterized by a significantly larger K, S and Cl content, and a much smaller Si content. The majority of the K (~88%) in the windward deposits is water soluble. The molar ratio of the water soluble (K+Na)/(Cl+2S) is about 2.44, indicating that a large fraction (~60%) of the water soluble alkalis in the deposits may be hydroxide or carbonate. The molar ratio of water soluble S/Cl is about 0.94, suggesting that the amount of the alkali sulphates and alkali chlorides is equal in the windward deposits.

By comparing the compositions of winward deposits with that of fuel ash, it is revealed that the windward deposits are significantly enriched in K, Cl and S. This implies that the condensation of KCl and K_2SO_4 is probably an important mechanism for the winward deposit formation at Location B without coal ash addition.

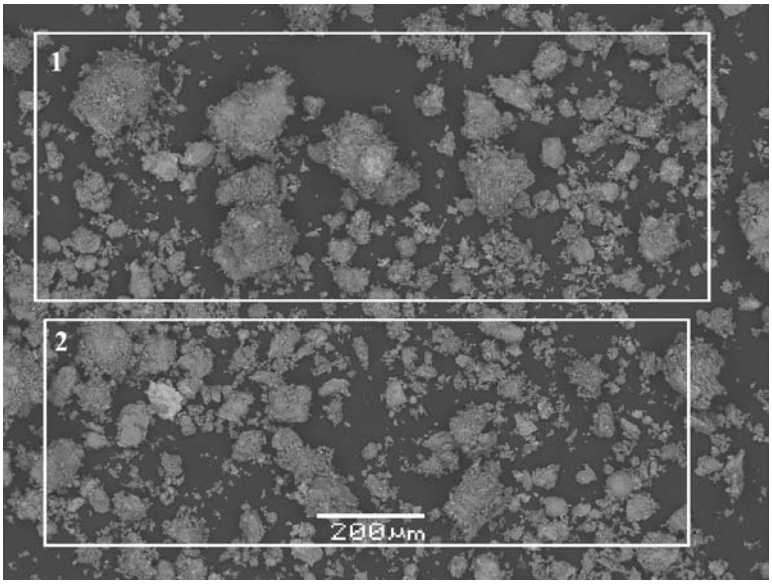

Element (mol%)	Spectrum 1	Spectrum 2
O	46	51
Na	-	-
Mg	2	-
Al	-	-
Si	-	-
P	-	-
S	6	4
Cl	5	4
K	30	28
Ca	8	8
Fe	-	-

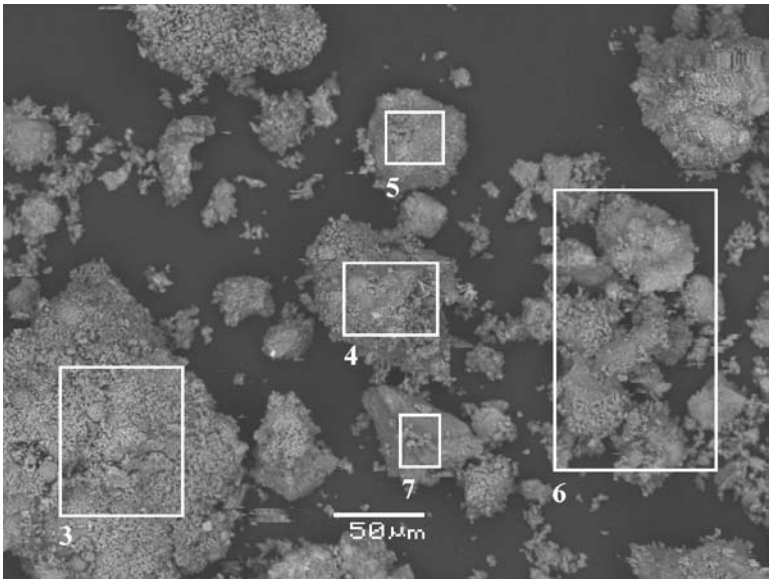

Element (mol%)	Spectrum 3	Spectrum 4	Spectrum 5	Spectrum 6	Spectrum 7
O	46	44	37	41	48
Na	-	-	-	-	-
Mg	4	4	-	-	2
Al	-	-	-	-	-
Si	-	-	-	-	-
P	-	-	-	-	-
S	2	2	5	6	4
Cl	-	6	9	4	3
K	16	24	36	33	29
Ca	28	17	8	10	10
Fe	-	-	-	-	-

Figure 23 Typical SEM-EDS results of the windward deposits collected at Location B without coal ash addition (Test 3).

The general compositions of the leeward deposits collected under this condition (see Spectrum 1 and 2 in Figure 24) are quite similar to those of the windward deposits. The morphology of the leeward deposits (see Spectrum 6 and 7) also suggests that they are dominated by clusters of submicron particles rich in K, Cl, S and Ca. However, different from the windward deposits, some relatively large ash particles (e.g. >10 µm) rich in Si and Ca are observed in the leeward deposits (see Spectrum 3 and 4).

Table 9 Bulk compositions of the fuel ash, and bulk and water soluble elemental compositions of the deposits collected without coal ash addition at Location B (Test 3).

	Fuel ash (wood)	Windward deposits		Leeward deposits	
	Bulk	Bulk	Water soluble	Bulk	Water soluble
Al (wt%, dry basis)	2.45	0.86		1.16	
Ca (wt%, dry basis)	21.05	15.80		13.95	
Cl (wt%, dry basis)	0.70	3.19	2.97	3.41	3.19
Fe (wt%, dry basis)	2.00	3.33		5.41	
K (wt%, dry basis)	9.19	24.75	21.85	21.00	21.15
Mg (wt%, dry basis)	3.40	2.41		2.24	
Na (wt%, dry basis)	0.68	0.79	0.65	0.84	0.65
P (wt%, dry basis)	1.19	1.01	0.00	1.00	0.00
S (wt%, dry basis)	1.70	3.09	2.52	4.25	3.81
Si (wt%, dry basis)	17.61	3.44		3.66	
Zn (wt%, dry basis)	-	0.50		0.54	

The bulk and water soluble element compositions of the leeward deposits are also similar to that of windward deposits (see Table 9). The leeward deposits are also dominated by K and Ca, and almost all of the K is found to be water soluble. Compared to the fuel ash, the enrichment of K, Cl and S in the leeward deposits suggest that the condensation of KCl and K_2SO_4 is probably an important mechanism for the leeward deposit formation at Location B without coal ash addition. The major ratio of the water soluble (K+Na)/(Cl+2S) is about 1.74, suggesting that a certain fraction (~40%) of water soluble alkalis is probably present as hydroxide or carbonate in the leeward deposits. The molar ratio of water soluble S/Cl is about 1.33, indicating that amount alkali sulphates and alkali chlorides is comparable in the leeward deposits.

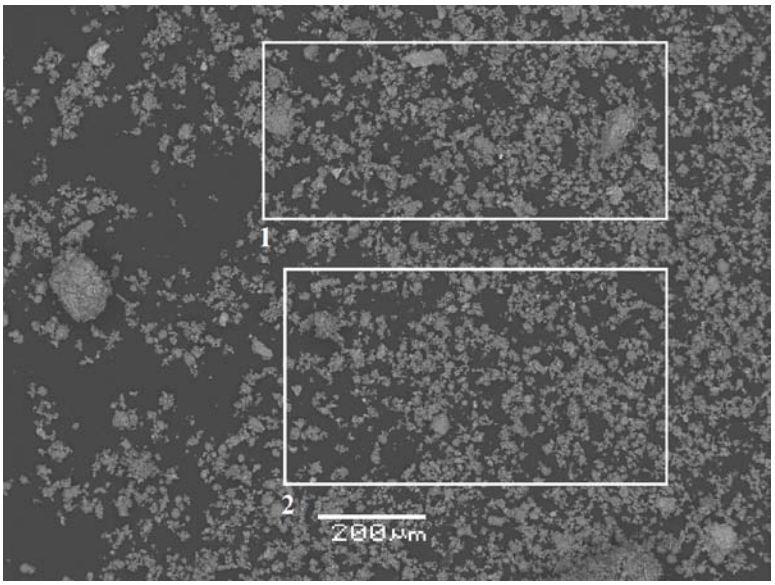

Element (mol%)	Spectrum 1	2
O	47	52
Na	2	-
Mg	-	-
Al	-	-
Si	2	2
P	-	-
S	7	6
Cl	7	5
K	26	24
Ca	7	7
Fe	-	-

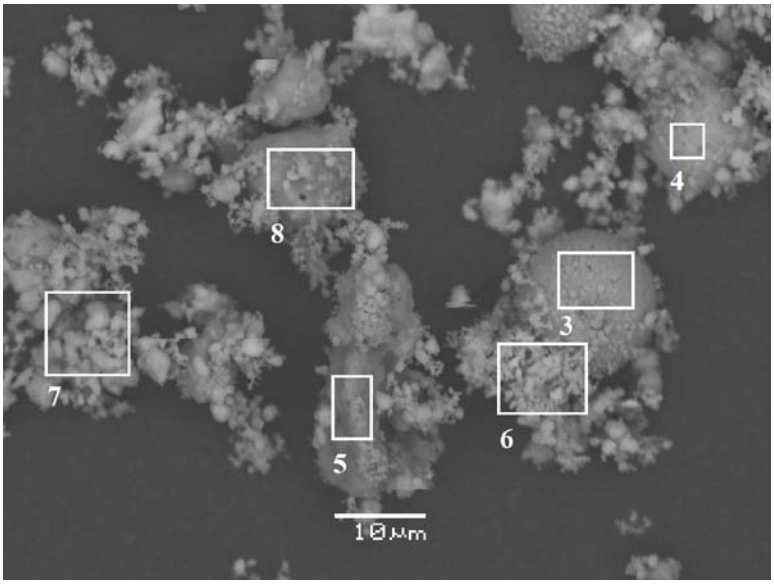

Element (mol%)	Spectrum 3	4	5	6	7	8
O	42	44	49	17	32	44
Na	-	-	2	-	-	2
Mg	4	9	9	-	-	-
Al	2	3	-	-	-	-
Si	14	11	-	3	-	-
P	-	2	-	-	-	-
S	-	-	2	8	7	3
Cl	-	-	2	17	16	-
K	5	2	19	44	37	32
Ca	27	27	16	8	5	16
Fe	-	-	-	-	-	-

Figure 24 Typical SEM-EDS results of the leeward deposits collected at Location B without coal ash addition (Test 3).

3.4.3 Deposits at Location B with coal ash addition

The windward deposits collected at Location B during the test with coal ash addition (Test 4) are illustrated in Figure 25. The general compositions (e.g. Spectrum 1-3) of the windward deposits suggest that they are dominated by K, Si, S, Al and Ca. More detailed analyses suggest that the deposits are partly comprised of agglomerated small particles (around or below 1 µm) with large K and S content (e.g. Spectrum 4, 8 and 9). The molar ratio of K and S in Spectrum 4 indicates they are most likely K_2SO_4. On the other hand, the windward deposits also contain some spherical ash particles with large Si, Al and K content (e.g. Spectrum 5-7). These spherical ash particles often have a size of about 2-3 µm. Based on the general compositions of the deposits, it is most likely both type of particles have important contributions to the formation of windward deposits. Different from the windward deposits shown in Figure 23, no chlorine is found in the windward deposits at Location B when coal fly ash is added.

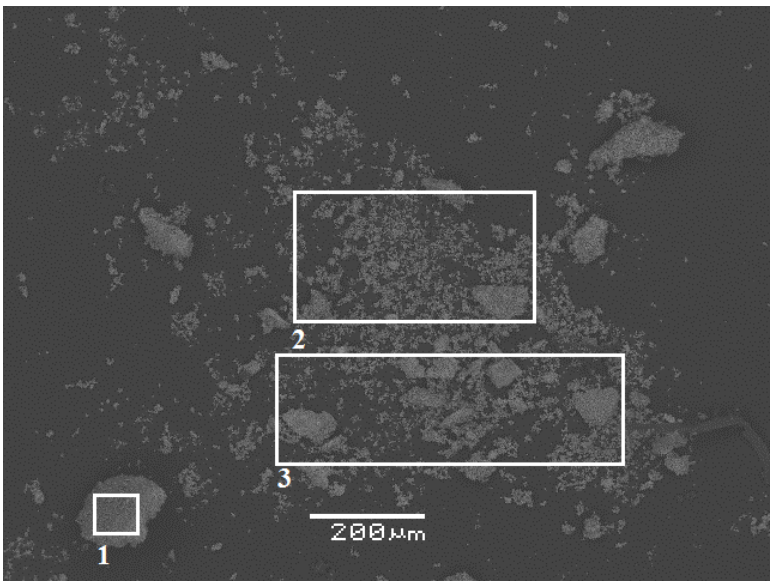

Element (mol%)	Spectrum 1	2	3
O	53	54	53
Na	-	-	-
Mg	-	-	-
Al	9	5	5
Si	14	9	9
P	2	-	2
S	5	9	9
Cl	-	-	-
K	8	14	14
Ca	5	4	4
Fe	-	-	-

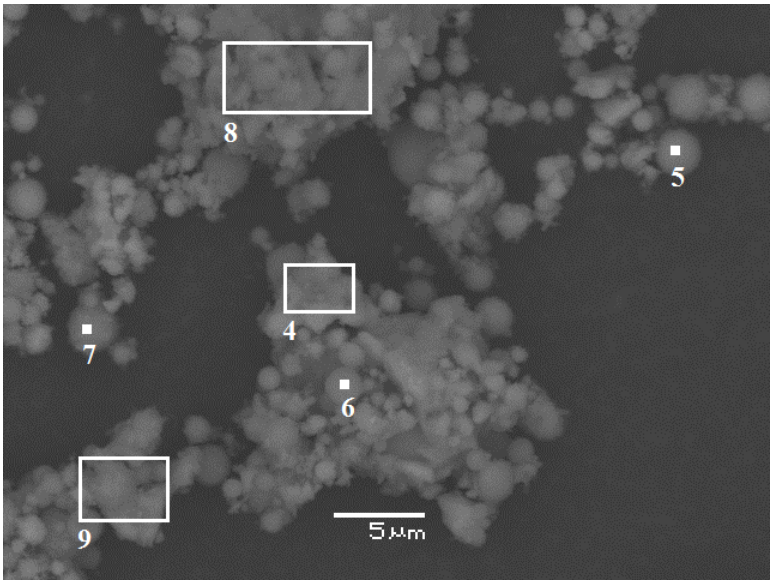

Element (mol%)	Spectrum 4	5	6	7	8	9
O	51	47	53	49	45	47
Na	-	-	-	-	-	-
Mg	-	-	-	-	-	-
Al	-	16	8	3	4	6
Si	2	24	24	37	6	8
P	-	-	-	-	-	2
S	14	-	2	-	14	11
Cl	-	-	-	-	-	-
K	27	7	9	5	24	15
Ca	-	-	-	-	3	7
Fe	-	2	-	-	-	-

Figure 25 Typical SEM-EDS results of the windward deposits collected at Location B with coal ash addition (Test 4).

Compared to the windward deposits, the morphology and compositions of the leeward deposits are quite different. As shown in Figure 26, the leeward deposits from Test 4 are dominated by relatively large spherical particles with large Si, Al and K content (see Spectrum 2, 3 and 6-11). These particles typically have a size of ~2-20 μm and are most likely originated from the added coal fly ash. Some small ash particles with relatively large K and S content are also observed in the leeward deposits (see Spectrum 12), but their contribution is insignificant for the formation of leeward deposits. Similar to the windward deposits, chlorine is still not found in the leeward deposits at Location B during coal ash addition. It should be noted that the leeward deposits formed during coal ash addition appears to be quite loose, which is more easily removable than the leeward deposits from the case without coal ash addition.

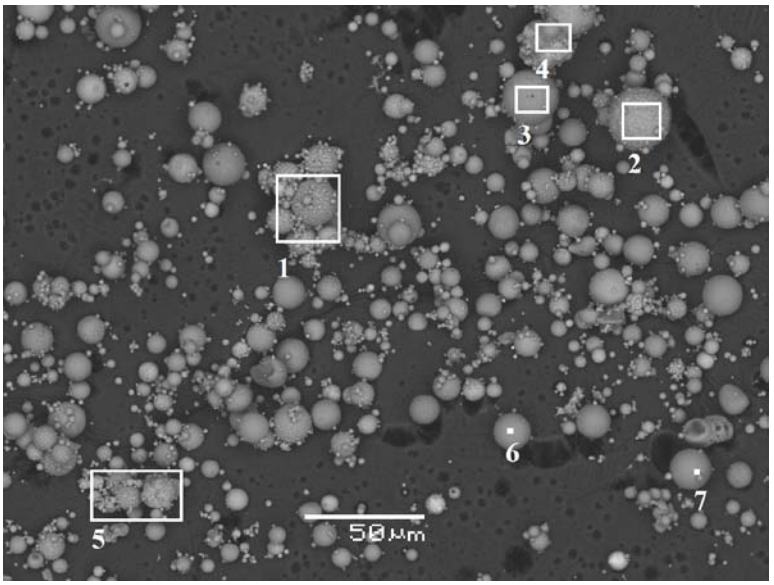

Element (mol%)	Spectrum 1	2	3	4	5	6	7
O	43	49	44	40	50	46	34
Na	-	-	-	2	-	-	-
Mg	-	4	-	-	-	4	-
Al	9	2	15	7	6	10	14
Si	15	4	23	15	11	25	32
P	-	3	-	2	-	-	-
S	7	7	-	8	7	-	-
Cl	-	-	-	-	-	-	-
K	15	-	8	15	9	2	11
Ca	6	28	-	8	13	9	3
Fe	2	-	5	2	-	2	2

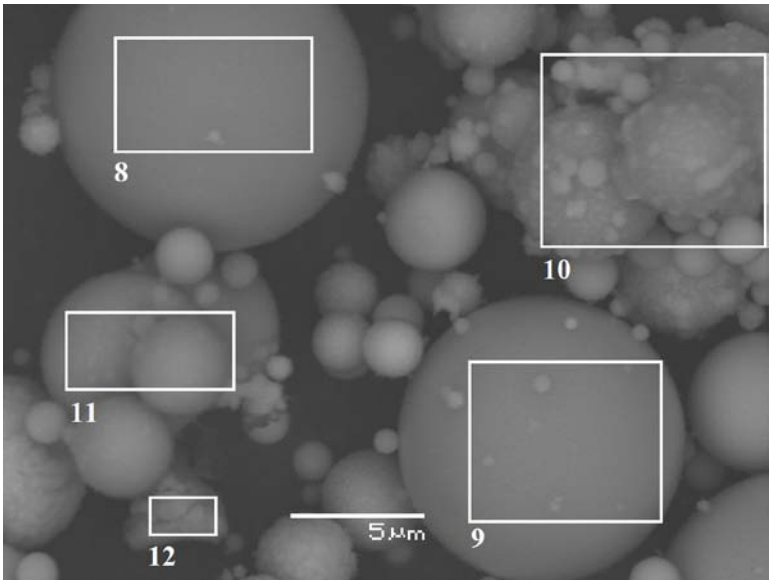

Element (mol%)	Spectrum 8	9	10	11	12
O	46	45	48	49	13
Na	-	-	-	-	-
Mg	-	-	-	-	-
Al	11	12	10	11	2
Si	31	29	22	25	6
P	-	-	-	-	-
S	-	-	2	-	15
Cl	-	-	-	-	-
K	8	4	11	8	49
Ca	-	5	2	2	10
Fe	-	-	2	2	2

Figure 26 Typical SEM-EDS results of the leeward deposits collected at Location B with coal ash addition (Test 4).

The water soluble Cl, K, Na, P and S in the deposits collected during Test 4 were analyzed by ICP-OES and IC, and the results are presented in Table 10. It can be seen that the water soluble K and S content is considerably large in the windward deposits, whereas the content of water soluble Cl is extremely small. The molar ratio of water soluble K/2S is about 1.7, suggesting that not all of the water soluble K is K_2SO_4. Since the water soluble Cl content is very small, it is most likely that the remaining water soluble K is KOH or K_2CO_3. The water soluble compositions of the leeward deposits are quite different. Compared to the windward deposits, the content of water soluble K and S in the leeward deposits is significantly (20-7 times) lower. The molar ratio of water soluble K/2S in the leeward deposits is about 0.6. This suggests that besides K_2SO_4, there is other form of water soluble sulfur present in the leeward deposits.

Table 10 Water soluble elemental compositions of the deposits collected with coal ash addition at Location B (Test 4).

Water soluble element	Windward deposits	Leeward deposits
Cl (wt%, dry basis)	0.056	0.004
K (wt%, dry basis)	25.00	1.195
Na (wt%, dry basis)	0.784	0.062
P (wt%, dry basis)	<0.003	<0.003
S (wt%, dry basis)	6.170	0.858

3.4.4 Deposits at Location A with coal ash addition

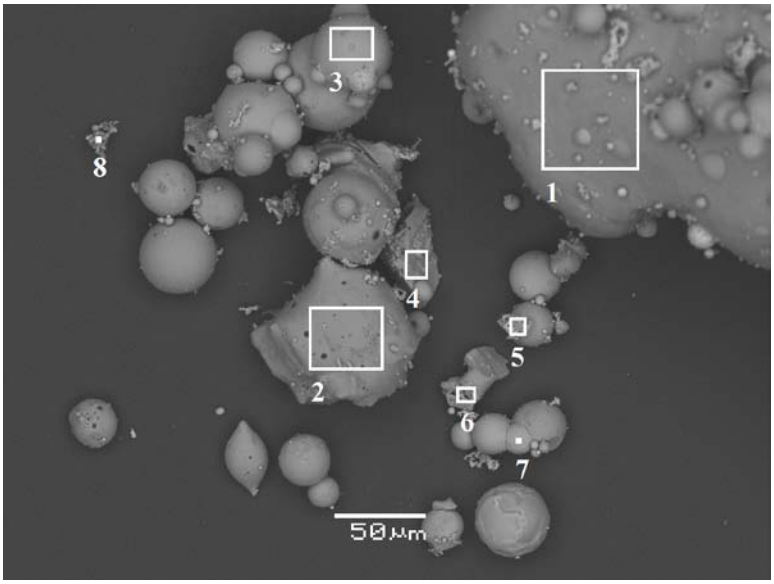

Element (mol%)	Spectrum 1	2	3	4	5	6	7	8
O	51	49	49	58	56	42	36	48
Na	-	-	-	-	-	-	-	-
Mg	-	-	3	2	5	2	12	-
Al	-	8	12	7	2	3	4	19
Si	45	35	20	19	4	17	19	25
P	-	-	-	-	-	-	-	-
S	-	-	-	-	3	-	-	-
Cl	-	-	-	-	-	-	-	-
K	-	3	2	-	-	6	-	4
Ca	-	3	8	11	27	6	24	-
Ti	-	-	2	-	-	3	-	-
Fe	-	-	2	-	-	18	3	-

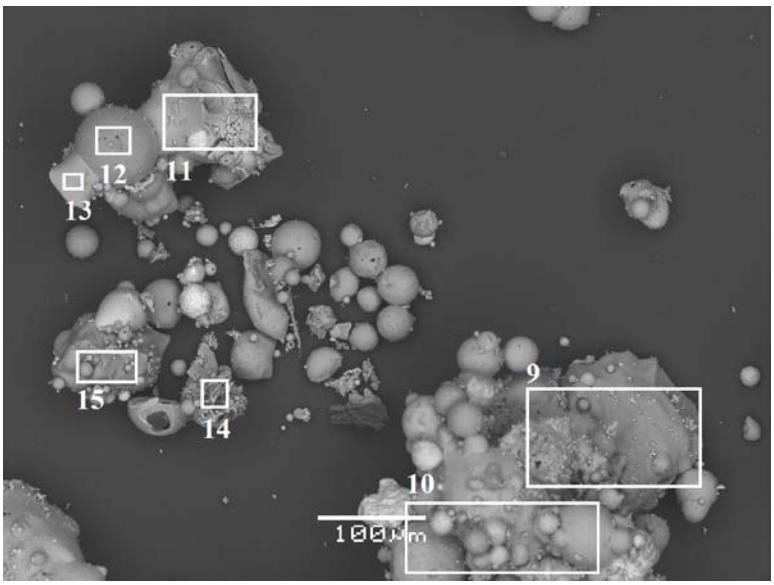

Element (mol%)	Spectrum 9	10	11	12	13	14	15
O	47	46	47	49	47	47	48
Na	-	-	-	-	-	-	-
Mg	-	2	4	-	4	-	-
Al	5	11	8	19	11	19	7
Si	38	20	17	26	27	27	36
P	-	-	-	-	-	-	-
S	-	-	-	-	-	-	-
Cl	-	-	-	-	-	-	-
K	2	2	2	2	-	4	3
Ca	3	12	15	-	7	2	4
Ti	-	-	-	-	-	-	-
Fe	2	2	5	-	2	-	-

Figure 27 Typical SEM-EDS results of the outer-layer windward deposits collected at Location A with coal ash addition (Test 5).

Figure 27 shows the morphology and elemental compositions of the outer-layer windward deposits collected at Location A during coal ash addition (Test 5). It can be seen that the deposits are dominated by ash particles with large Si and Al content. These particles are typically in a size range of ~5-100 μm. The compositions of these particles are consistent with the fly ash particles obtained during coal ash addition (see Figure 17), suggesting that the outer-layer windward deposits are predominantly formed by the added coal fly ash. Besides, another obvious tendency in Figure 27 is that S and Cl are almost not present in the outer-layer deposits.

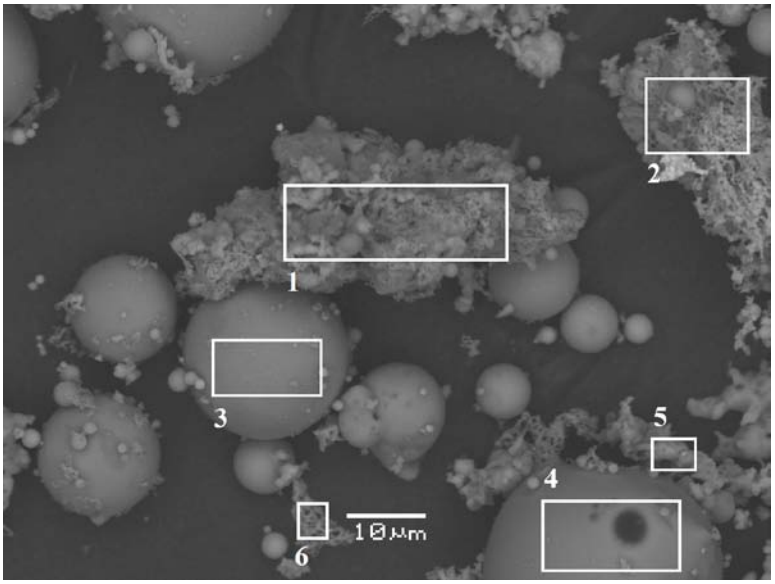

Element (mol%)	Spectrum 1	2	3	4	5	6
O	56	58	45	48	47	55
Na	-	-	-	-	-	-
Mg	3	-	-	-	4	5
Al	-	3	10	13	3	-
Si	4	4	27	27	8	3
P	2	-	-	-	6	-
S	2	2	-	-	7	13
Cl	-	-	-	-	-	-
K	-	2	9	3	2	-
Ca	31	29	3	4	22	19
Fe	-	-	2	2	-	-

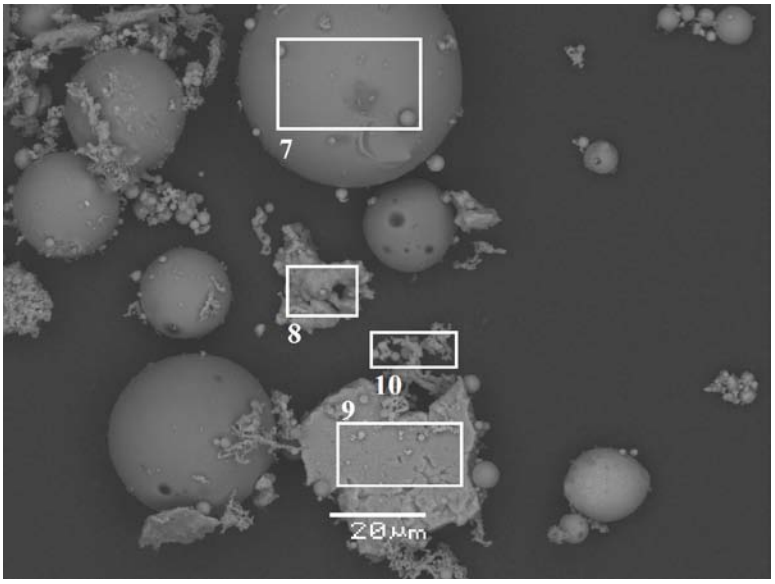

Element (mol%)	Spectrum 7	8	9	10
O	42	34	41	47
Na	-	-	2	-
Mg	3	2	-	3
Al	8	2	-	5
Si	31	3	-	7
P	-	-	-	-
S	-	11	19	12
Cl	-	-	-	-
K	3	-	27	5
Ca	7	45	7	19
Fe	5	-	-	-

Figure 28 Typical SEM-EDS results of the inner-layer windward deposits collected at Location A with coal ash addition (Test 5).

The morphology and compositions of the inner-layer windward deposits from Test 5 are illustrated in Figure 28. Similar to the outer-.layer deposits, spherical ash particles rich in Si and Al are also found in the inner-layer deposits (e.g. Spectrum 3, 4 and 7). Most of these particles are in a size range of ~5-100 μm. In addition, some Ca rich particles with similar size are observed (e.g. Spectrum 1, 2, 5, 6, 8 and 10). Different from the spherical Si and Al rich particles, most of these Ca rich particles seem to have more irregular and porous appearance, indicating they are not highly melted during combustion. Some of these Ca rich particles also have a relatively large S content (e.g. Spectrum 6, 8 and 10), suggesting that $CaSO_4$ may be present in these particles. A few particles with large K and S content are seen in the inner-layer deposits (e.g. Spectrum 9), implying that the inner-layer deposits may contain a small amount of K_2SO_4.

The leeward deposits collected at Location A during coal ash addition are illustrated in Figure 29. The deposits contain a large number of ash particles rich in Si, Al, K and Ca (e.g. Spectrum 2-6).

Majority of these ash particles have spherical appearances and are attached with other particles. The typical size of these particles is between 5 and 100 μm. A few particles with relatively large S content are observed in the deposits (e.g. Spectrum 1 and 7-9). These particles are generally clusters of submicron particles. The compositions of these particles (e.g. Spectrum 8 and 9) suggest that K_2SO_4 may be present, but other species such as $CaSO_4$ or K-silicates may also exist.

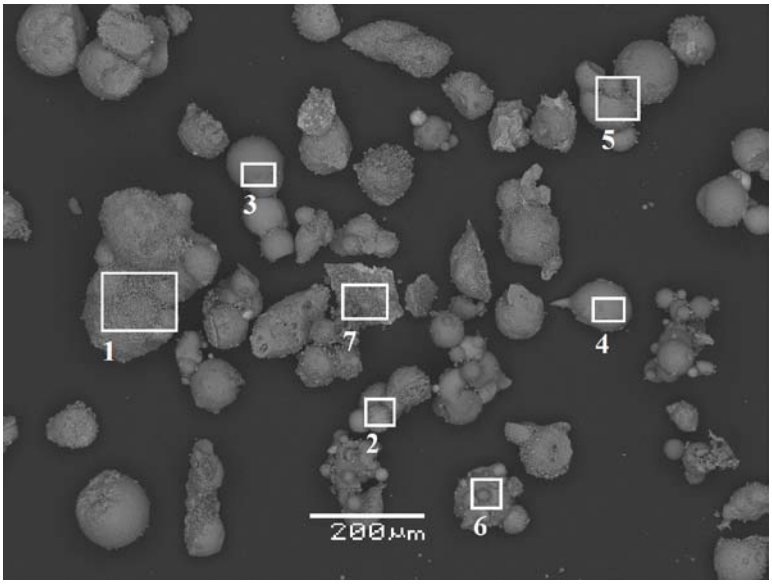

Element (mol%)	Spectrum 1	2	3	4	5	6	7
O	42	47	43	44	44	47	43
Na	-	-	-	-	-	-	2
Mg	2	3	3	4	5	4	2
Al	5	8	16	5	6	7	6
Si	9	17	25	13	13	15	10
P	2	-	-	2	2	-	2
S	11	2	-	4	4	3	8
Cl	-	-	-	-	-	-	-
K	14	2	4	5	3	2	14
Ca	11	13	3	19	21	17	7
Mn	-	-	-	-	-	-	2
Fe	2	5	4	-	-	3	3

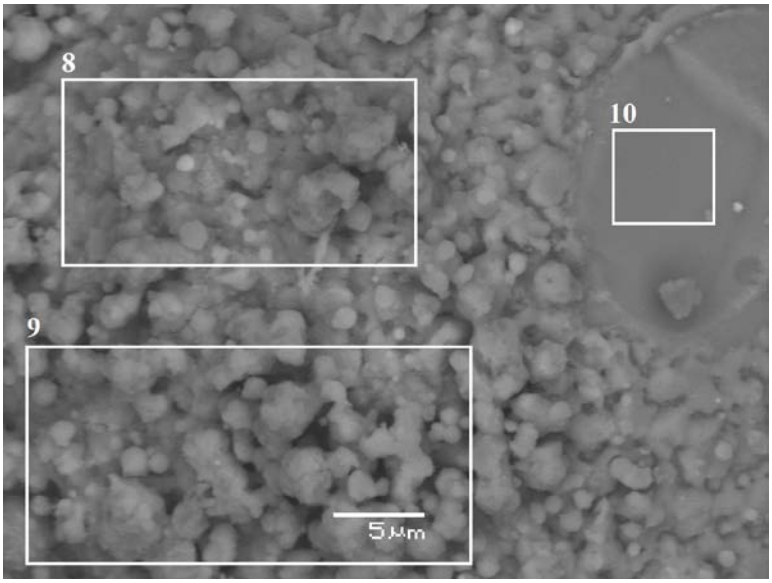

Element (mol%)	Spectrum 8	9	10
O	48	44	32
Na	2	2	-
Mg	-	-	6
Al	2	3	2
Si	6	6	22
P	2	2	3
S	11	13	-
Cl	-	-	-
K	19	23	-
Ca	7	6	33
Mn	-	-	-
Fe	-	-	-

Figure 29 Typical SEM-EDS results of the leeward deposits collected at Location A with coal ash addition (Test 5).

Table 11 shows the water soluble element compositions of the deposits collected during Test 5. It is seen that the water soluble element compositions are generally very low in the outer layer windward deposits. Compared to the outer layer windward deposits, the content of water soluble Cl, K, Na and S is a little increased in the windward deposits, and a slight further increase is observed in the leeward deposits. In general, compared to the deposits collected without coal ash addition (see Table 8), the content of water soluble element is considerable decreased with the addition of coal ash, particularly for the leeward deposits.

Table 11 Water soluble elemental compositions of the deposits collected with coal ash addition at Location A (Test 5).

Water soluble element	Outer layer windward deposits	Inner layer windward deposits	Leeward deposits
Cl (wt%, dry basis)	<0.0012	0.002	0.007
K (wt%, dry basis)	0.070	0.696	1.155
Na (wt%, dry basis)	0.005	0.036	0.057
P (wt%, dry basis)	<0.003	<0.003	<0.003
S (wt%, dry basis)	0.058	0.544	0.872

3.4.5 Comparison and discussions of deposit properties

The deposit properties obtained under different conditions are summarized in Figure 30. From the figure, it is evident that the deposit properties are both greatly affected by the addition of coal fly ash and the location of the measurement.

Without the addition of coal fly ash, the deposits at Location A are dominated by Ca, Si and K. According to SEM-EDS analysis, the deposits are primarily comprised of K-Ca-Si rich spherical particles, K-Si rich partially melted particles, Ca rich spherical particles, and K_2SO_4 clusters. The K-Ca-Si rich, K-Si rich and Ca rich particles are probably originated from the residual ash (ash that is not vaporizable during combustion) in wood pellets. During combustion, the residual ash would undergo fragmentation, melting and coalescences, and result in the formation of spherical/molten fly ash particles typically in a range of ~5-100 μm. At Location A, the major deposition mechanism for these fly ash particles would be inertial impaction since the majority of these particles are found at the windward of the probe. Besides, these fly ash particles may also form deposits through thermophoresis (primarily for small ash particles rich in Ca), this may be an explanation to the spherical ash particles found at the leeward of the probe. The K_2SO_4 clusters found on the deposits may be formed by three different mechanisms. According to the aerosol measurements carried out at the same plant [6], both KCl and K_2SO_4 aerosols are collected when coal fly ash is not added, suggesting that both KCl and K_2SO_4 would be present in the flue gas from wood combustion. At Location A, the KCl and K_2SO_4 (if present) in the flue gas are probably in a vapor phase, due to the high flue gas temperature. Therefore, condensation may be an important deposition mechanism for the KCl and K_2SO_4, even though the high flue gas temperature may limit the extent of KCl condensation on the probe. The condensed KCl may be further converted to K_2SO_4 through the heterogeneous reactions with gaseous SO_2. Such reactions are found to be significant at temperatures higher than 750 ^oC [11]. This temperature is probably achievable in the deposits due to the significant temperature gradient between the probe surface and the flue gas. The long measurement time is another favorable condition for the heterogeneous sulfation reactions. Besides condensation and chemical reaction, thermophoresis could also be a mechanism for the deposition of K_2SO_4. This is mainly because that the temperature difference between the probe surface and the flue gas is significant. When the gaseous K_2SO_4 is diffuse from bulk flue gas to the probe surface, submicron K_2SO_4 aerosols may be generated and form deposits through thermophoresis. All of the three mechanisms mentioned above are more favorable towards cold surfaces. This explains why most of the K_2SO_4 is found in the inner-layer of windward deposits and the leeward deposits. On the other hand, the analysis of leeside deposits suggests that KOH/K_2CO_3 may also present in the deposits. At high temperatures, KOH (g) will be a thermodynamically favorable potassium species and it may condense on the probe. The condensed KOH may be further converted to K_2CO_3 due to the presence of CO_2 in the flue gas. A conversion from condensed KOH/K_2CO_3 to K_2SO_4 may also happen and contribute to the observed K_2SO_4 clusters.

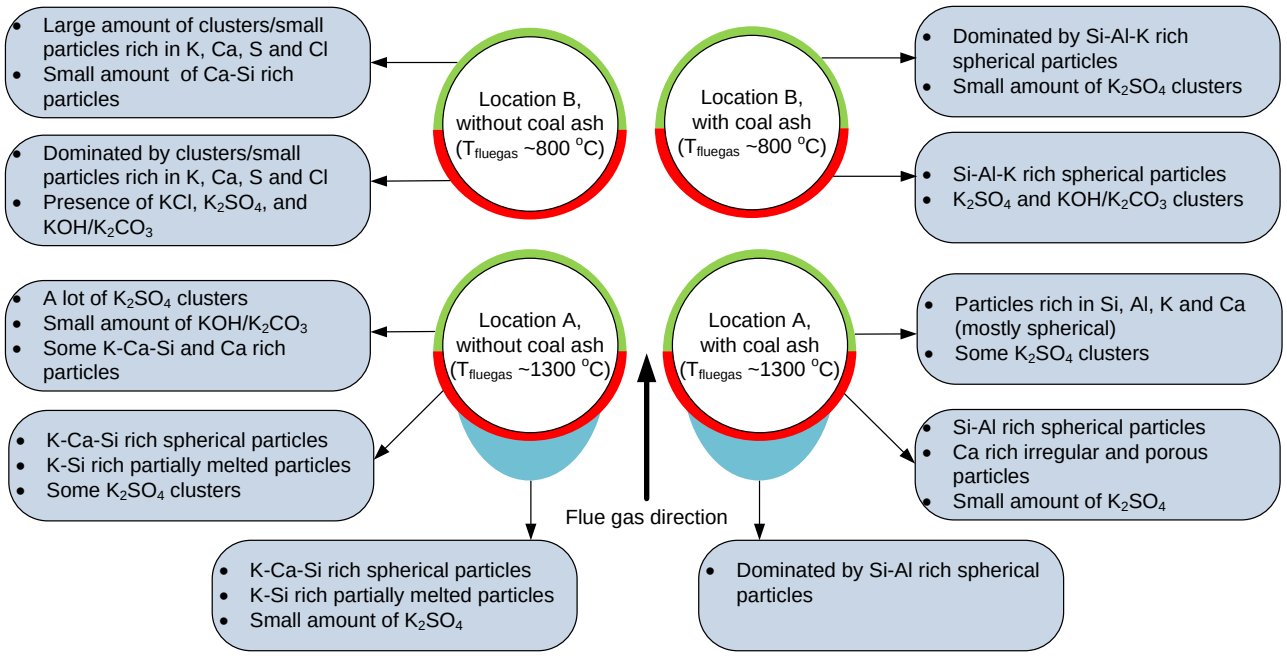

Figure 30 Summary of the deposit properties based on the SEM-EDS analyses.

With the addition of coal fly ash, the KCl, K_2SO_4, and KOH in the flue gas would be significant reduced or even become negligible [6]. Besides, the fly ash will be dominated by the added coal fly ash as the amount of added coal fly ash greatly exceeds that of wood ash (see Table 5). As a result, the deposits at Location A become dominated by Si-Al rich particles when coal fly ash is added. These Si-Al rich particles are typically in a size range of ~5-100 µm. Besides, the amount of K_2SO_4 in the deposits is significant decreased, although not completely removed. The presence of K_2SO_4 is probably because the added coal fly ash may not be able to fully remove the K_2SO_4, KCl and KOH in the flue gas. This is evident in the full-scale aerosol measurements, where only in some tests a complete removal of KCl and K_2SO_4 was seen [6].

Without coal ash addition, the properties of the deposits collected at Location B are quite different from those collected at Location A. The windward deposits at Location B are dominated by K, Ca, S and Cl species. Almost no particles containing Si are found in SEM-EDS analysis, implying that the inertial impaction of Si rich particles is not an important mechanism for the formation of windward deposits at Location B. This probably related to the low flue gas temperature at this location (~800 °C), which would lead to a low capture efficiency of the impacted particles. Moreover, even if some Si rich particles are captured, the gravity of these relatively large particles may exceed the adhesion strength between the particles and the deposits/tube, thereby causing gravity shedding of these particles. The majority of the windward deposits are found to be cluster of submicron particles rich in K, Ca, S and Cl. These particles are probably deposited via condensation or thermophoresis. The chorine found in the deposits is most likely KCl. The presence of KCl suggests that the degree of heterogeneous sulfation is not significant at Location B. This could be related to the relatively low flue gas temperature at this location, which may suppress the heterogeneous sulfation reaction. In addition, the SO_2 concentration may be very low at this location. According to thermodynamic calculations on woody fuels [12], SO_2 is found to be the only stable sulfur species at temperatures above 1200 °C. However, when the temperature is decreased from 1200 °C to 800 °C, the majority of the SO_2 would be converted to K_2SO_4. Such transformations may also happen in the boiler, and result in a very low SO_2 concentration at

Location B. This hypothesis is supported by the extremely low SO_2 concentration measured downstream of Location B during the tests without coal ash addition (see Table 5). The molar ratio of water soluble K/(Cl+2S) at windward deposits is about 2.44. This suggests that the condensation or thermophoresis of KOH/K_2CO_3 is probably also an important mechanism for the formation of windward deposits under this condition. Compared to the windward deposits, the leeward deposits generally have quite similar compositions, excepting that some large (e.g. >10 μm) Si-Ca rich particles are observed. This is probably because that it is more difficult for these particles to shed through gravity once they are deposited on the leeward of the probe.

The deposits collected at Location B during coal ash addition are quite different from those obtained without coal ash addition. Almost no chlorine is found in the deposits collected with coal ash addition. This could be linked to the reactions between the added coal fly ash and the KCl released from wood combustion, which can form K-aluminosilicates and gaseous HCl. In addition, the SO_2 concentration in the flue gas is much higher during coal ash addition (see Table 5). Therefore, even if small amount of KCl exist and form deposits, they may be converted to K_2SO_4 through heterogeneous sulfation reactions. This could be an explanation to the K_2SO_4 clusters found in the deposits. Besides, the K_2SO_4 clusters may also be from direct deposition of K_2SO_4 aerosols through thermophoresis. The windward deposits collected at this condition contain both small Si-Al-K rich particles (~2-3 μm) and K_2SO_4 clusters formed from submicron particles, whereas the leeward deposits seem to be dominated by relatively large Si-Al-K rich particles (~2-20 μm). Majority of these Si-Al-K rich particles are probably originated from the added coal fly ash. The enrichment of these particles in the leeward deposits is likely because these particles are more difficult to shed through gravity once they are deposited on the leeward of the probe.

The above results and discussions clearly show that the deposit compositions can be greatly changed when coal ash addition is not added to the boiler. For the deposits formed at high flue gas temperatures (e.g. ~1300 ^oC), the amount of K_2SO_4 will be considerably increased when coal ash is not added (especially at the leeside of the probe), and some KOH/K_2CO_3 may appear in the deposits. For the deposits formed at low flue gas temperatures (e.g. ~800 ^oC), the amount of KCl and KOH/K_2CO_3 will be significantly increased when coal ash addition is stopped. The change of the deposit compositions may lead to quite different corrosion behaviors. In order to evaluate the effect on corrosion, longer term tests are needed, which is outside the scope of this work.

4. Conclusions

In the present work, the formation of deposits during suspension-firing of wood at Avedøre Power Plant unit 2 (AVV2) was studied by using an advanced deposit probe system. The tests were conducted both with and without coal ash addition, and at two different locations with flue gas temperatures of 1250-1300 ^{o}C and 750-800 ^{o}C respectively.

At the location with a high flue gas temperature of 1250-1300 ^{o}C, when the coal fly ash is not added, the formed deposits are dominated by K-Ca-Si rich particles with a size range of ~5-100 µm and clusters of submicron K_2SO_4 particles. The differential deposit formation rate (DDF-rate) varies in a range of about 20-500 g/m^2/h, and the deposition propensity fluctuates in a range of ~0.1-4.5 %. The considerable variations of the DDF-rate and the deposition propensity are probably linked to the operational conditions of the boiler, particularly the wood properties. The calculated deposit removal frequencies on the probe are generally low (mostly<1 time/hr), and the mean mass drops are also small (<700 g/m^2). The recorded camera pictures and the boiler data suggest that the deposit removals on the probe as well as on the boiler walls are most likely induced by the operation of nearby soot blowers when coal fly ash is not added. With the addition of coal fly ash, the deposits at this location become dominated by Si-Al rich particles with a size range of ~5-100 µm, and the amount of K_2SO_4 is greatly reduced. In most cases, the DDF-rate is increased to above 2000 g/m^2/h, which is both related to the significantly larger ash load and the higher ash deposition propensity (about 5-15%) when coal ash is added. The deposit removal frequencies are also increased considerably to about 4-15 times/hr, and the mean mass drops become larger (about 500-3000 g/m^2). The major deposit removal mechanism during coal ash addition appears to be natural shedding, i.e. not caused by soot-blowing. The results imply that the high-temperature deposits are more easily removable when coal fly ash is added to the boiler.

At the location with a low flue gas temperature of 750-800 ^{o}C, the deposits formed without coal ash addition are dominated by small particles rich in K, Ca, S and Cl. A large fraction of K (>85%) in the deposits is water soluble, which is probably a mixture of KCl, K_2SO_4 and KOH/K_2CO_3.The DDF-rate under this condition is very small, which is only about 90 g/m^2/h. The deposit formation at this location is characterized by an initial slow build-up. After a few hours, the mass uptake of the deposit probe becomes almost constant, implying that the deposit buildup and shedding are close to equilibrium. With the addition of coal fly, it is evident that the chlorine disappears in the deposits collected at this location. The collected deposits are dominated by Si-Al-K rich particles, supplemented by a small amount of K_2SO_4 particles. The DDF-rate is still about 90 g/m^2/h, whereas the ash deposition propensity is decreased from about 0.8 % to 0.1 % when coal fly ash is added. The deposit formation at this condition is still characterized by a slow buildup followed by a constant deposit mass uptake after a few hours.

The results from the present work indicate that the addition of coal fly ash can significantly affect the ash deposition/shedding behaviors and the deposit properties. The effect is evident at both measurement locations. At the location with a flue gas temperature of 1250-1300 ^{o}C, although the addition of coal fly ash increases the DDF-rate and the ash deposition propensity, the deposits formed during coal ash addition appear to shed more frequently, suggesting that they are more easily removable. On the other hand, the amount of K_2SO_4 in the deposits is significantly reduced when coal ash is added, which is probably favorable in order to minimize corrosion. At the location with a flue gas temperature of 750-800 ^{o}C, the addition of coal fly ash reduces the ash deposition propensity and causes the formed deposits to becoming easily removable. Moreover, the KCl and

KOH/K_2CO_3 present in the deposits without coal ash addition disappear when coal ash is added, which is probably also favorable from a corrosion point of view.

Acknowledgements

The financial support by DONG Energy Power A/S and The Danish Strategic Research Council (GREEN) is gratefully acknowledged. We thank Bo Sander and Henrik Daniel Sørensen at DONG Energy Power A/S for their support and practical arrangement during the full-scale measurements. We are very grateful to Anders Tiedje and Jens Henry Poulsen at DTU Chemical Engineering for their practical support during the measurements. Bonnycroos Leanthian and Jens Peter Christensen at Rambøll Denmark A/S are acknowledged for providing the boiler data and the ash samples from the plant. Rolf Jensen at DTU Mechanical Engineering is appreciated for the helps in SEM-EDS analyses. Qiongxiao Wu at DTU Chemical Engineering is acknowledged for the assistances in XRD analyses.

References

[1] The Danish Government. Our Future Energy. , 2011.

[2] Skrifvars BJ, Laurén T, Hupa M, Korbee R, Ljung P. Ash behaviour in a pulverized wood fired boiler--a case study. Fuel 2004;83:1371-9.

[3] Jensen PA, Dall'ora M, Lin W, et al. Measurement on the 800 MWth Avdeøre oil, gas and wood co-fired suspension-boiler - Analysis of emission, burnout, deposit and FTIR measurements from April 2005. Department of Chemical and Biochemical Engineering, Technical University of Denmark, 2005.

[4] Bashir MS, Jensen PA, Frandsen FJ, et al. Suspension-firing of biomass. Part 1: Full-scale measurements of ash deposit build-up. Energy Fuels 2012;26:2317-30.

[5] Bashir MS, Jensen PA, Frandsen FJ, et al. Ash transformation and deposit build-up during biomass suspeinson and grate-firing: Full-scale experimental studies. Fuel Process Technol 2012;97:93-106.

[6] Damø AJ, Wu H. Full-scale aerosol measurements from tests with suspension firing of wood-pellects at AVV2. Department of Chemical and Biochemical Engineering, Technical University of Denmark, 2011.

[7] Sander B. Bioenergy for electricity and heat - experiences from biomass-fired CHP plants in Denmark. : DONG Energy, 2007.

[8] Bashir MS, Jensen PA, Frandsen FJ, Wedel S, Dam-Johansen K. Suspension-firing of wood with coal ash addition: Full-scale measurements of ash deposit build-up at Avedøre Power Plant (AVV2). Department of Chemical and Biochemical Engineering, Technical University of Denmark, 2011.

[9] International Flame Research Foundation. IFRF Suction Pyrometer, User Information Document.

[10] Bashir MS, Jensen PA, Frandsen FJ, Wedel S, Dam-Johansen K, Wadenback J. Suspension-firing of biomass. Part 2: Boiler measurementso f ash deposit shedding (in press). Energy Fuels 2012.

[11] Matsuda H, Ozawa S, Naruse K, Ito K, Kojima Y, Yanase T. Kinetics of HCl emission from inorganic chlorides in simulated municipal wastes incineration conditions. Chem Eng Sci 2005;60:545-52.

[12] van lith SC. Release of inorganic elements during wood-firing on a grate. PhD thesis, Department of Chemical Engineering, Technical University of Denmark, 2005.

Appendixes

Appendix A Method to determine derivative-based deposit formation rate (DDF-rate)

The method for calculating DDF-rate is developed by Bashir et al. [4]. Because the amount of deposit collected on the probe is a function of both the deposit formation process and shedding events, the true deposit formation rate ($g/m^2/h$) cannot be determined simply dividing the measured deposit mass increase by a given time, i.e. the integral deposit formation rate (IDF-rate). Therefore, the derivate-based deposit formation rate (DDF-rate), which is calculated by taking the time derivative of the deposit mass uptake in-between two macro shedding evens, is proposed to characterize the true deposit formation. Compared to IDF-rate, the DDF-rate should represent a fairly characteristic net-deposition rate for any plant, allowing general features of deposition and its dependence on operating conditions.

The deposit mass uptake signal is influenced by several processes: large shedding events, smaller shedding events (observed as a sudden deposit mass loss on the curve), a relatively slow deposit build-up process and some noise mainly caused by boiler fluctuations. Boiler fluctuations could be mechanical vibrations or large changes in boiler flow dynamics. Some fluctuations are observed when the boiler plant soot-blowers were used. Even though the plant soot-blowers very near to the probe were shutdown, the rest of the soot-blowers to some extent were effective in causing both minor and larger shedding events.

In order to analyze data systematically under these conditions where noise, small and large shedding events are present, a deposit mass uptake signal treatment method is developed. The method allows us to identify shedding events and can quantify the deposit formation rate between major shedding events. The idea is to average out the noise in the deposit mass uptake signals and to identify the larger shedding events.

The steps involved in the deposit mass signal treatment are based on Matlab procedures and are:

Step A: The deposit mass uptake signals are filtered using a 10 point resampling method implemented in Matlab. This effectively smoothes the data over 10 points, returning one resampled data point for further use.

Step B: Slope calculations are done using a moderately low order polynomial (3rd order, current case) that is fitted to the data in a sliding window (5 data points) and finally differentiation of the model is performed.

Step C: Cut off of negative slope values is made at different levels to remove major shedding events. The cut off level is adjusted to determine the number of major shedding events accurately while still giving a satisfactory prediction of apparent rates. A high cut off level e.g. -200 g/m2/h can result in a higher deposit formation rate and a low cut off e.g. -6,000 g/m2/h may result in a lower deposit formation rate before and after the shedding event. The selected cut off level was -3,800 g/m2/h for all the tests. This represents a subjective judgment that strikes a balance between keeping the effect of smaller, intrinsic deposit removal processes in the analysis and removing the larger shedding events from the analysis.

Step D: Smoothing of the raw slope calculations is made using a moving average filter over 31 points. Our choice of 15 data points on each side of the ith data point represents a subjective judgment that balances effective smoothing against undesired removal of minor, but significant variations in the deposit formation rate. The result of the smoothed data is the DDF-rate.

This complete procedure was validated. It should be kept in mind that our aim is to treat all data systematically once the subjective judgments of steps C and D have been made, thus avoiding the pitfall of seeing or not seeing trends from case to case based on incomparable criteria. A comparison the approximate manually calculated slopes of the 0-8 h interval during test 1 of these slopes and the calculated DDF-rates using the procedure described above is shown in Figure A1. It is clear that the DDF-rates calculated by steps A through D are in good agreement with manually calculated average deposition rates.

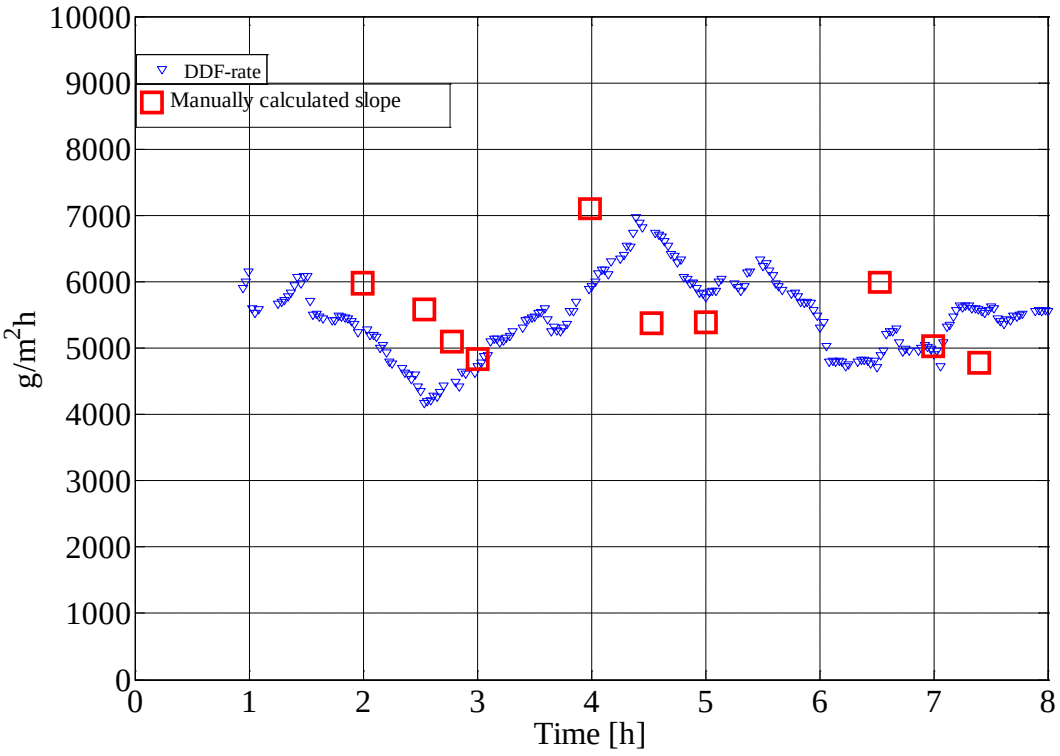

Figure A1 Comparison of manually calculated slopes and slopes calculated by the mathematical procedure (DDF-rate) for the initial 8 hours of test 1.

Appendix B Detailed measurement data

Appendix B.1 Data from Test 1

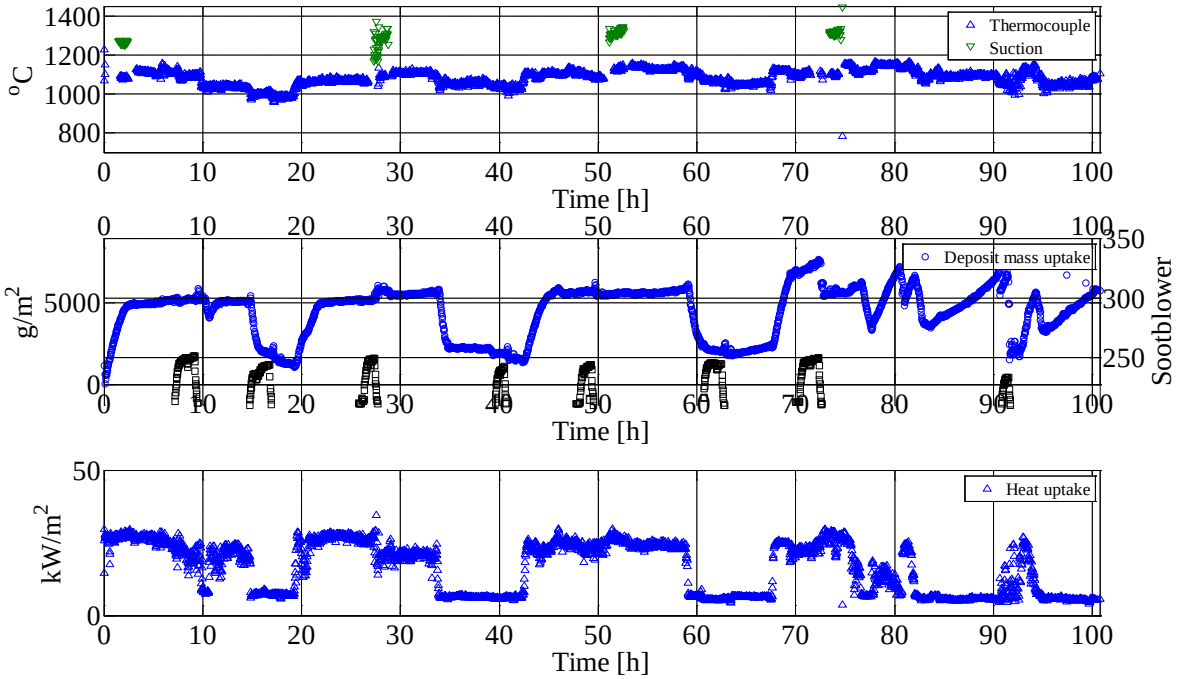

Figure B1 Flue gas temperature, deposit mass uptake, soot-blowing events and probe heat uptake during Test 1. The plant soot blower is active when the back-wall temperature is greater than the normal value, i.e. a peak/plateau observed in the figure.

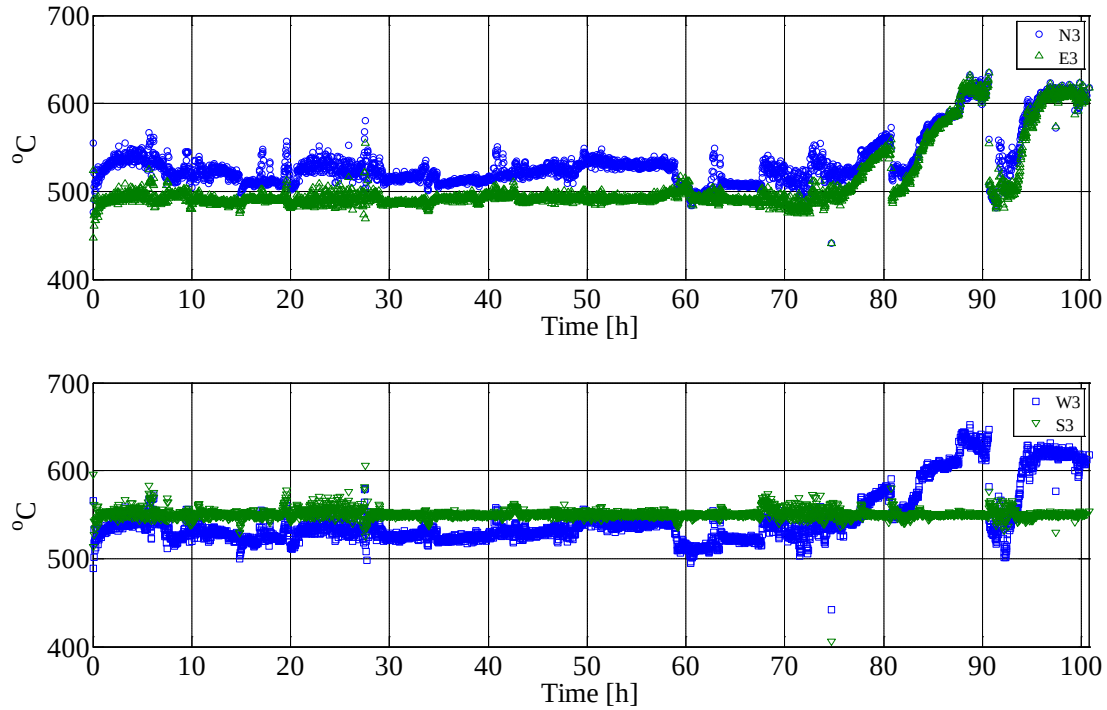

Figure B2 Measured probe surface temperature during Test 1.

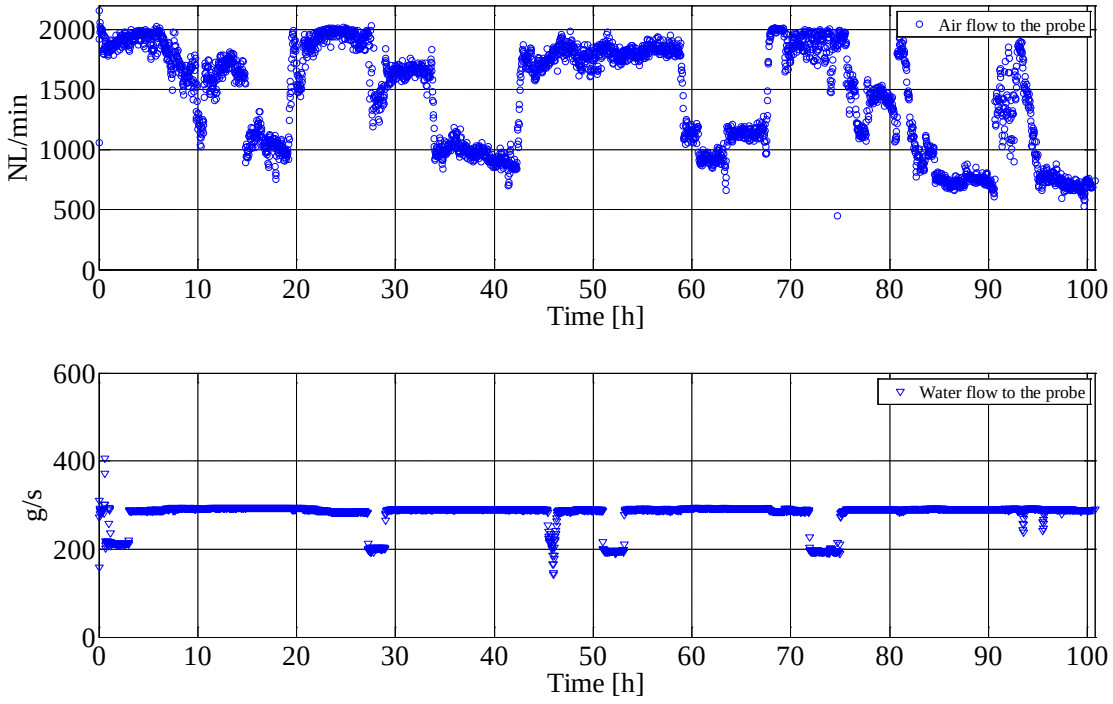

Figure B3 Measured air and water flow to the probe during Test 1.

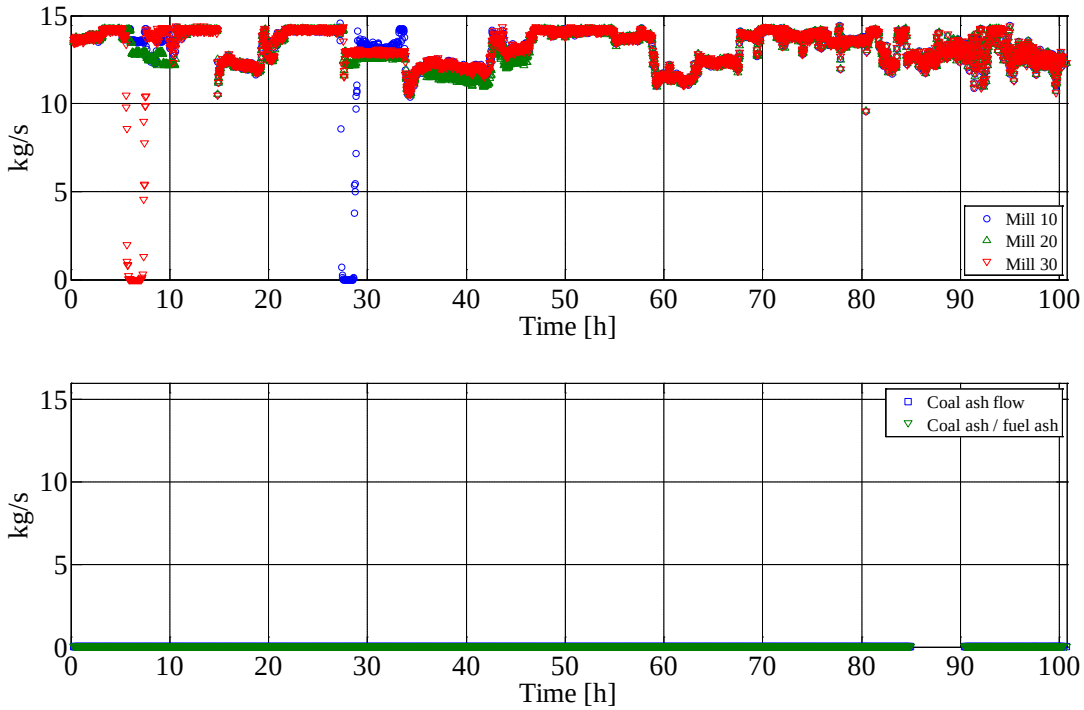

Figure B4 Measured wood flow through each mill, coal ash flow (kg/s) and ratio between coal ash and wood ash during Test 1.

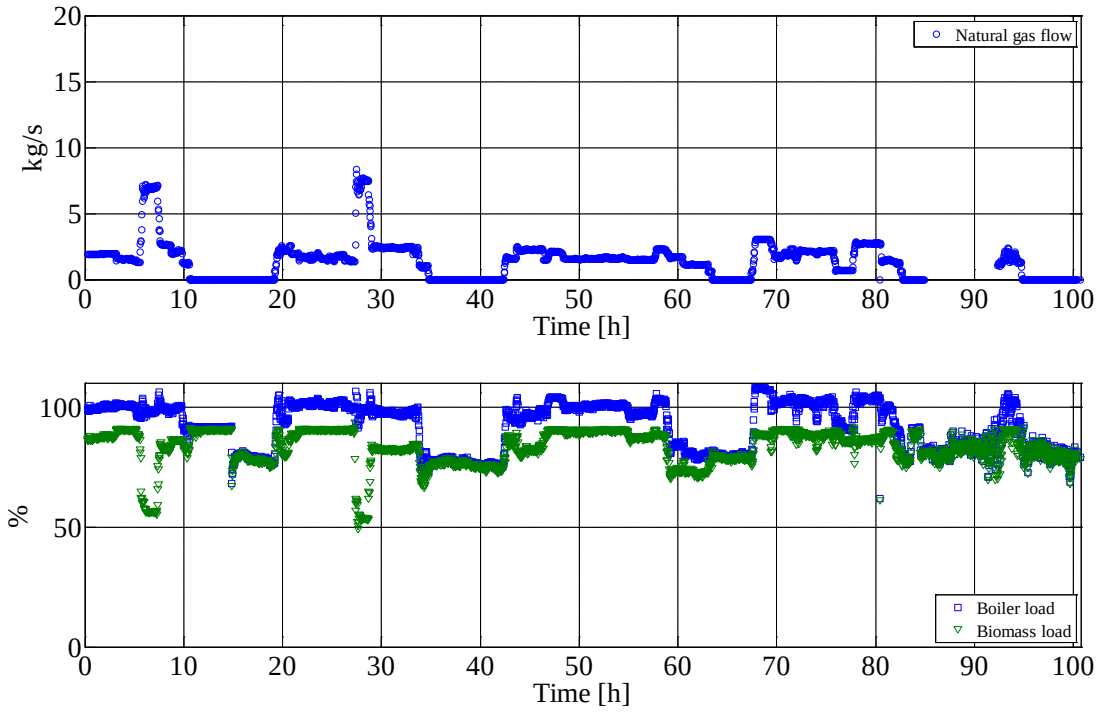

Figure B5 Natural gas flow, overall boiler load and biomass load during Test 1.

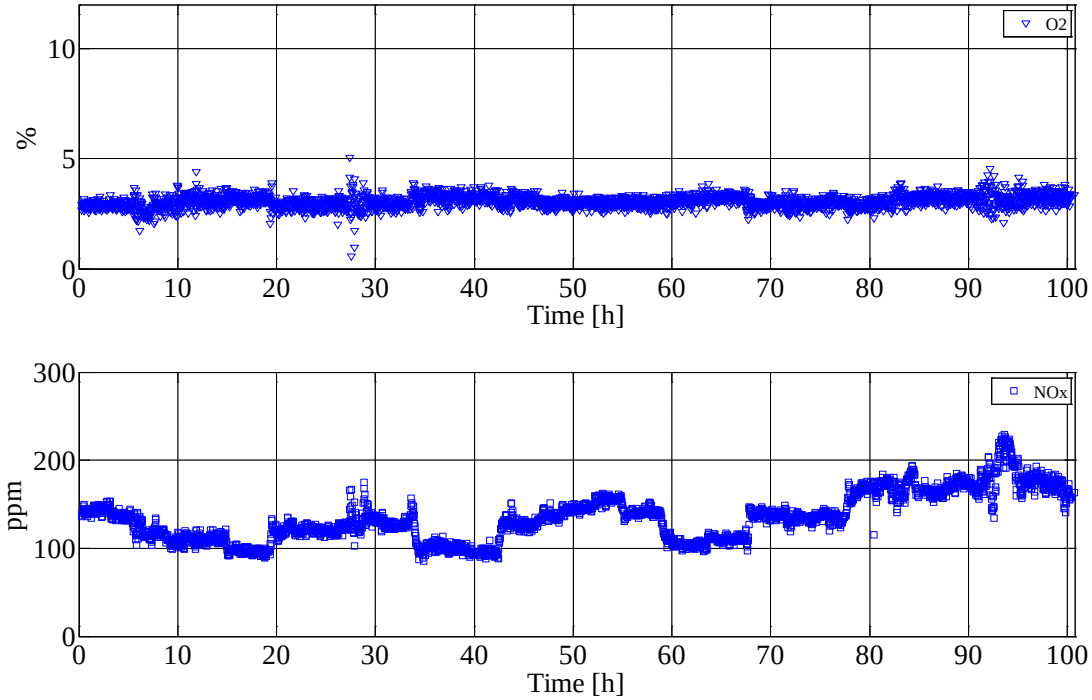

Figure B6 O_2 and NO_x (before SCR) concentrations in the flue gas during Test 1.

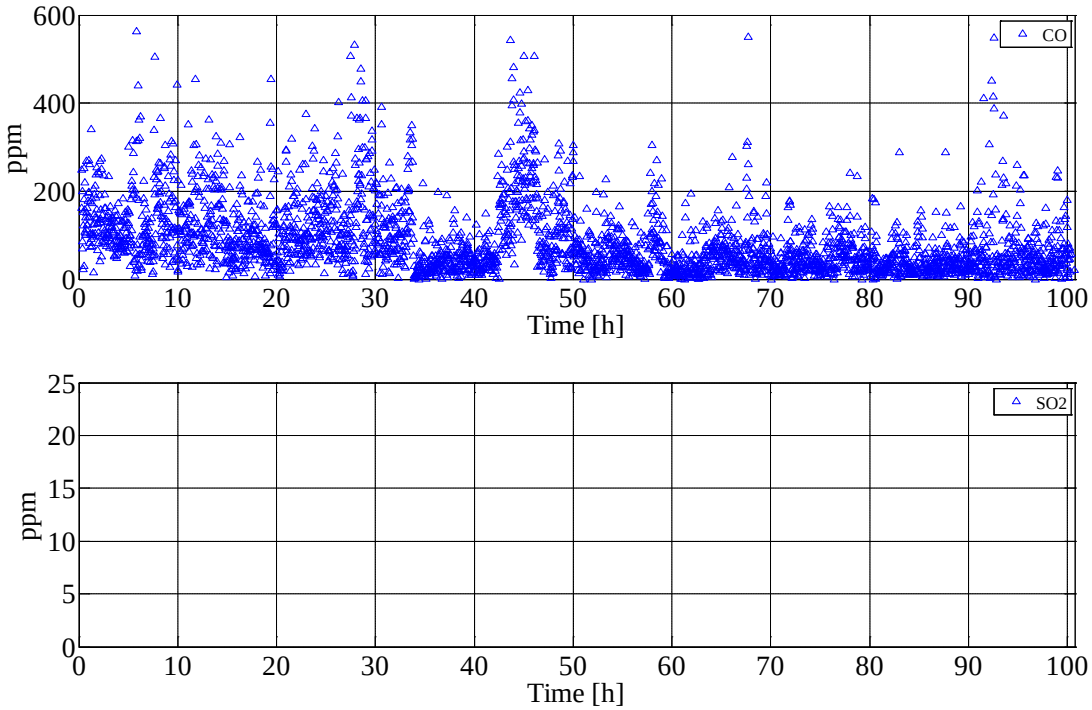

Figure B7 CO and SO_2 concentrations in the flue gas during Test 1 (only values larger than zero are shown).

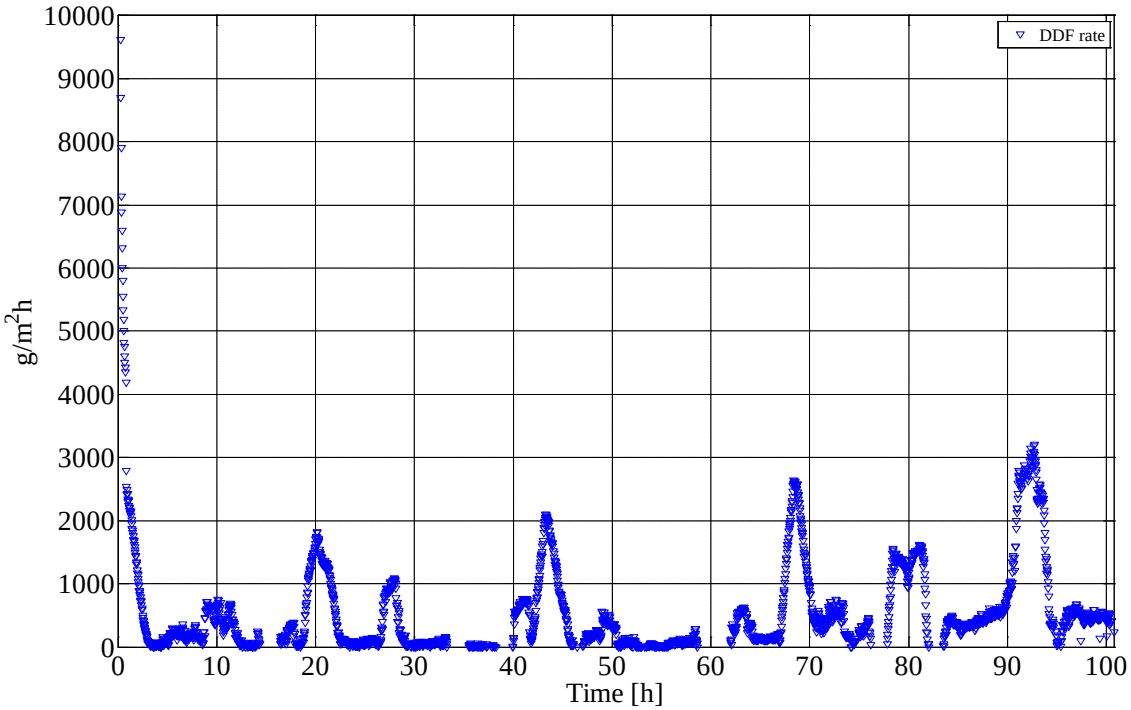

Figure B8 Calculated derivative-based deposit formation (DDF) rate during test 1.

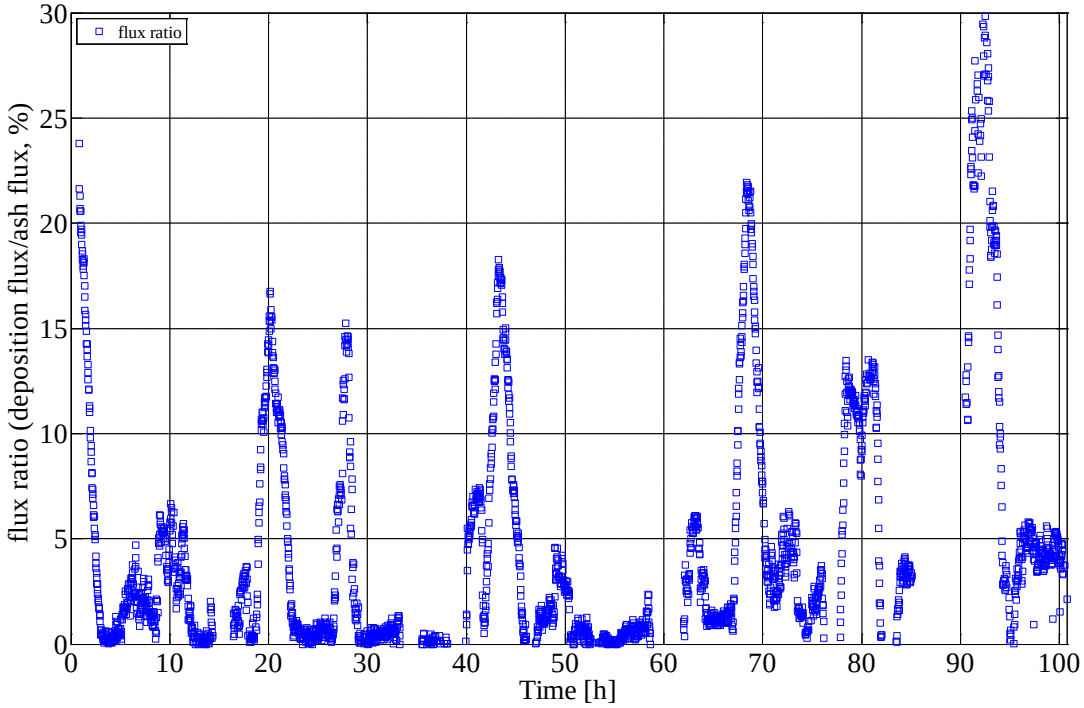

Figure B9 Calculated ash deposition propensity during test 1.

Appendix B.2 Data from Test 2

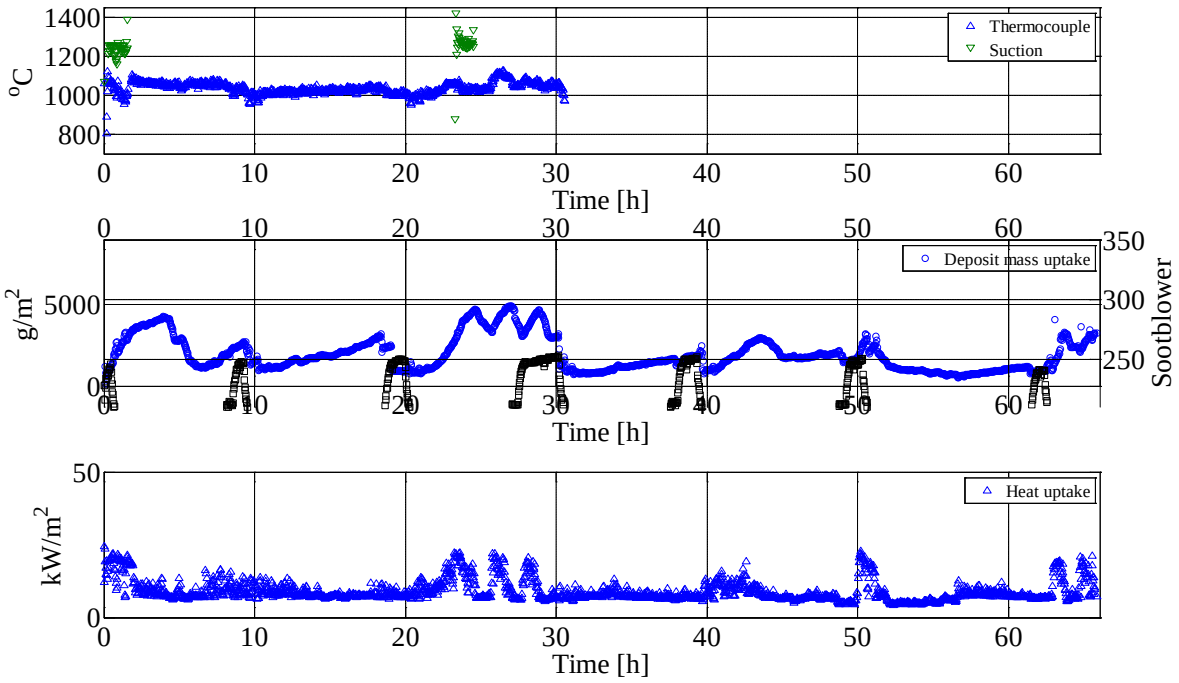

Figure B10 Flue gas temperature, deposit mass uptake, soot-blowing events and probe heat uptake during Test 2. The plant soot blower is active when the back-wall temperature is greater than the normal value, i.e. a peak/plateau observed in the figure.

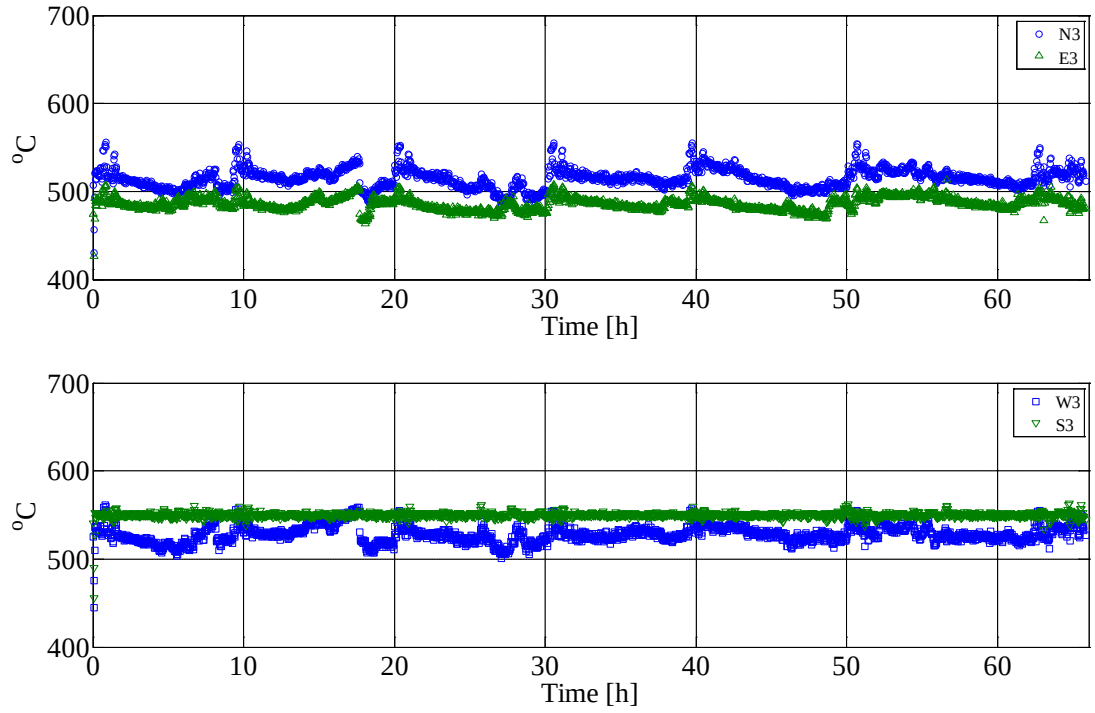

Figure B11 Measured probe surface temperature during Test 2.

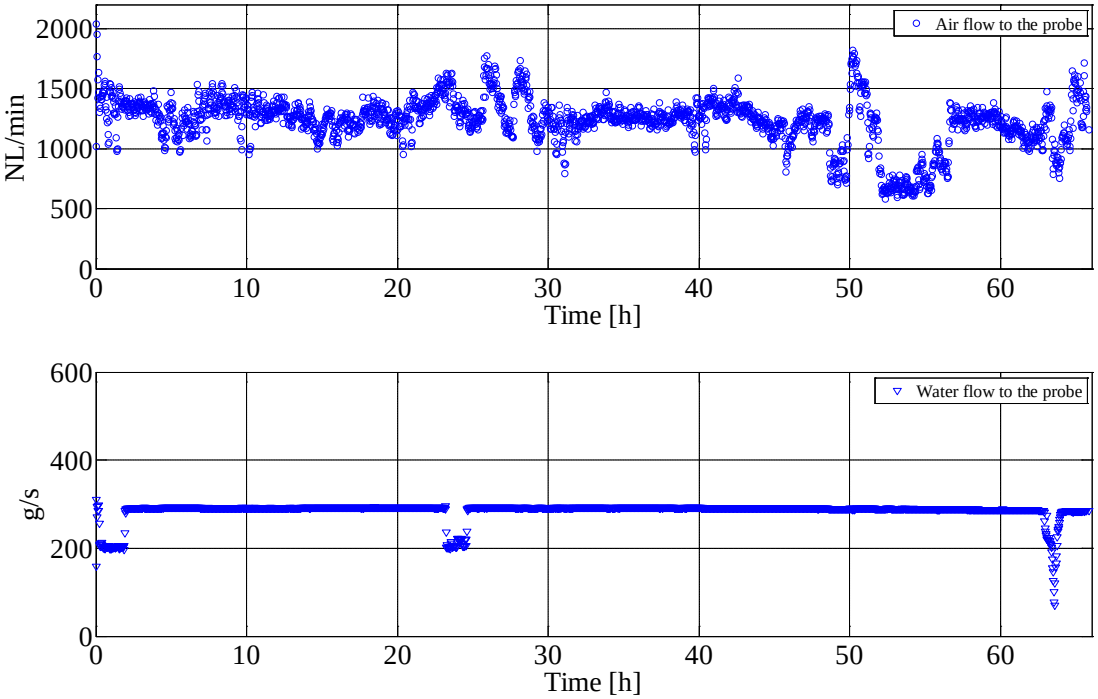

Figure B12 Measured air and water flow to the probe during Test 2.

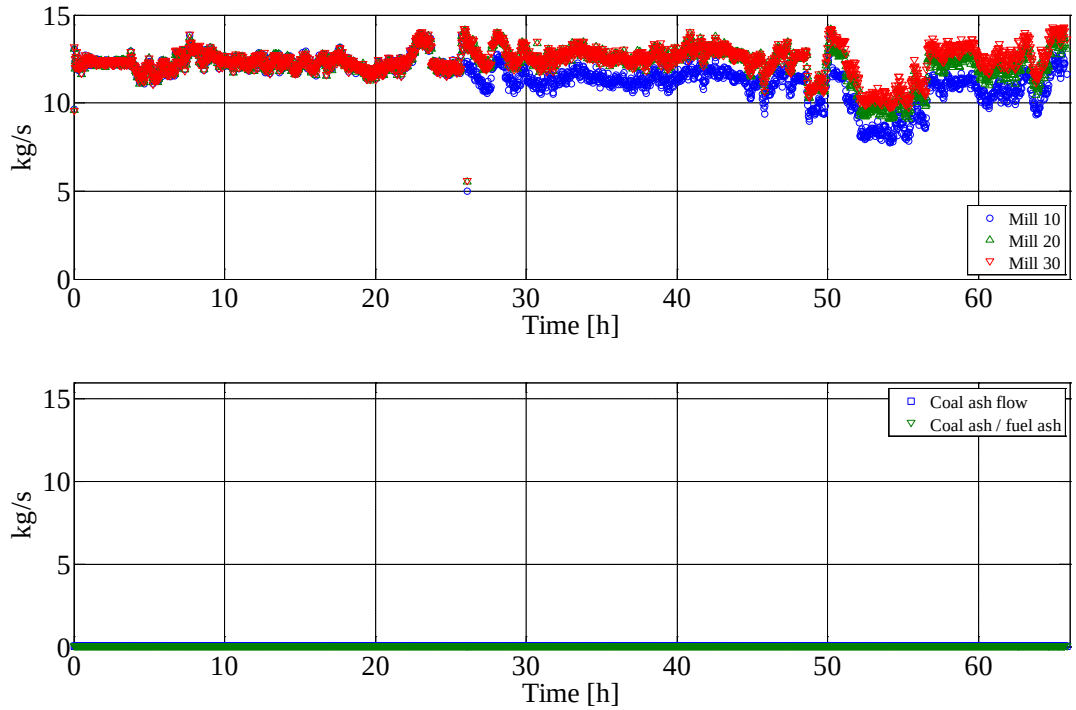

Figure B13 Measured wood flow through each mill, coal ash flow (kg/s) and ratio between coal ash and wood ash during Test 2.

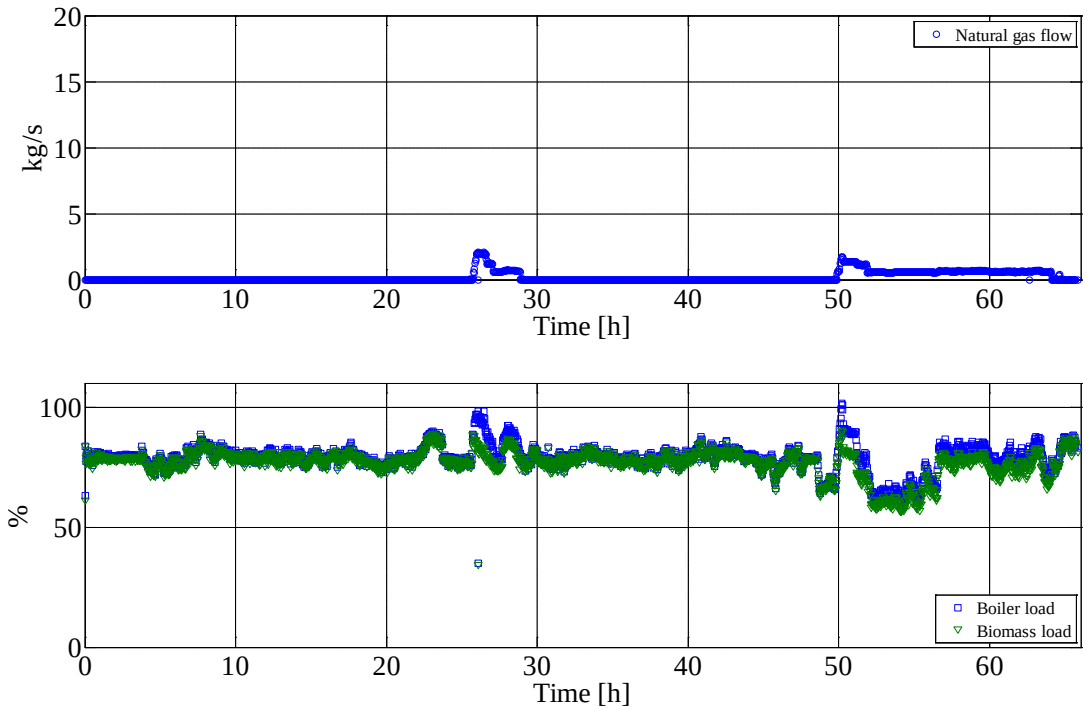

Figure B14 Natural gas flow, overall boiler load and biomass load during Test 2.

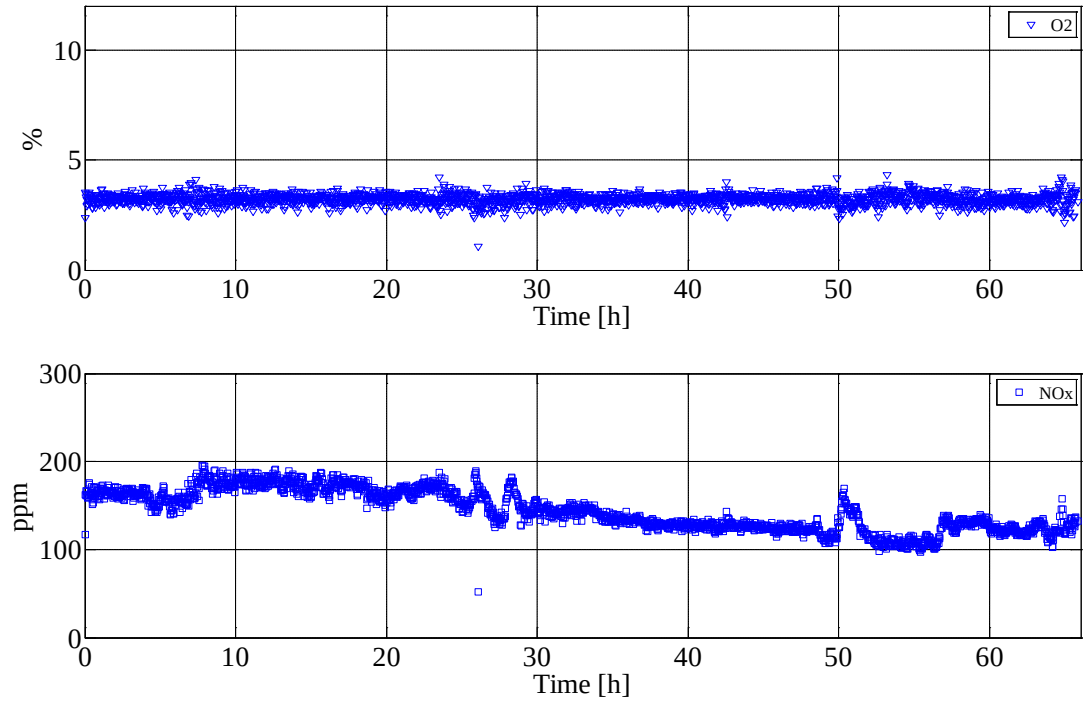

Figure B15 O_2 and NO_x (before SCR) concentrations in the flue gas during Test 2.

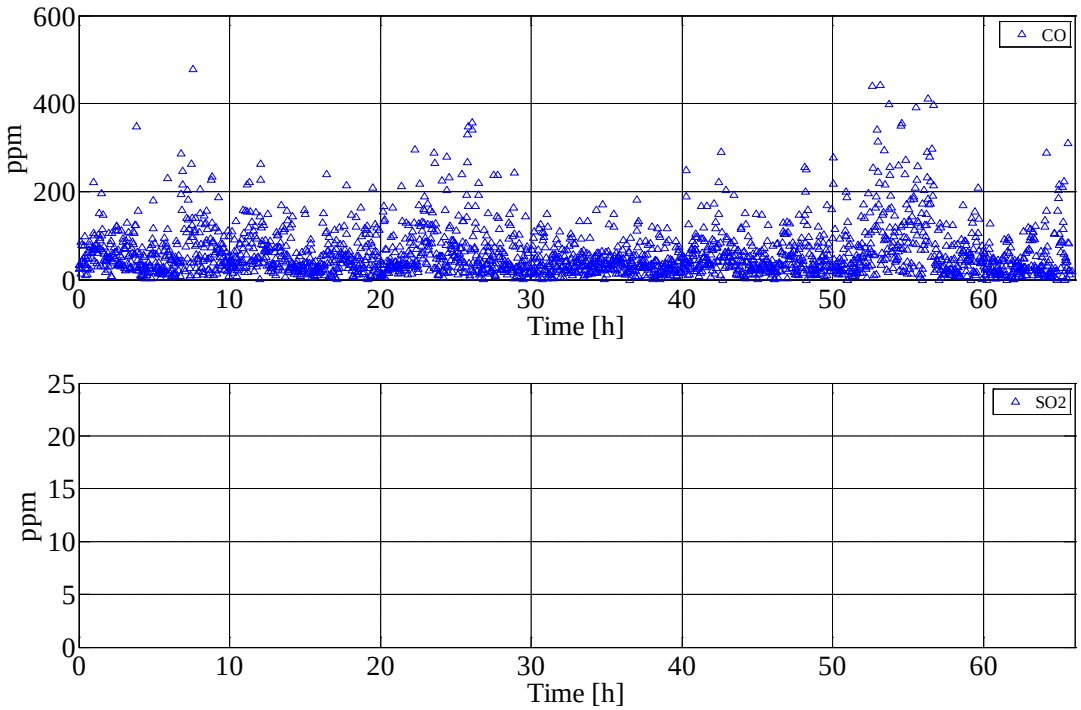

Figure B16 CO and SO_2 concentrations in the flue gas during Test 2 (only values larger than zero are shown).

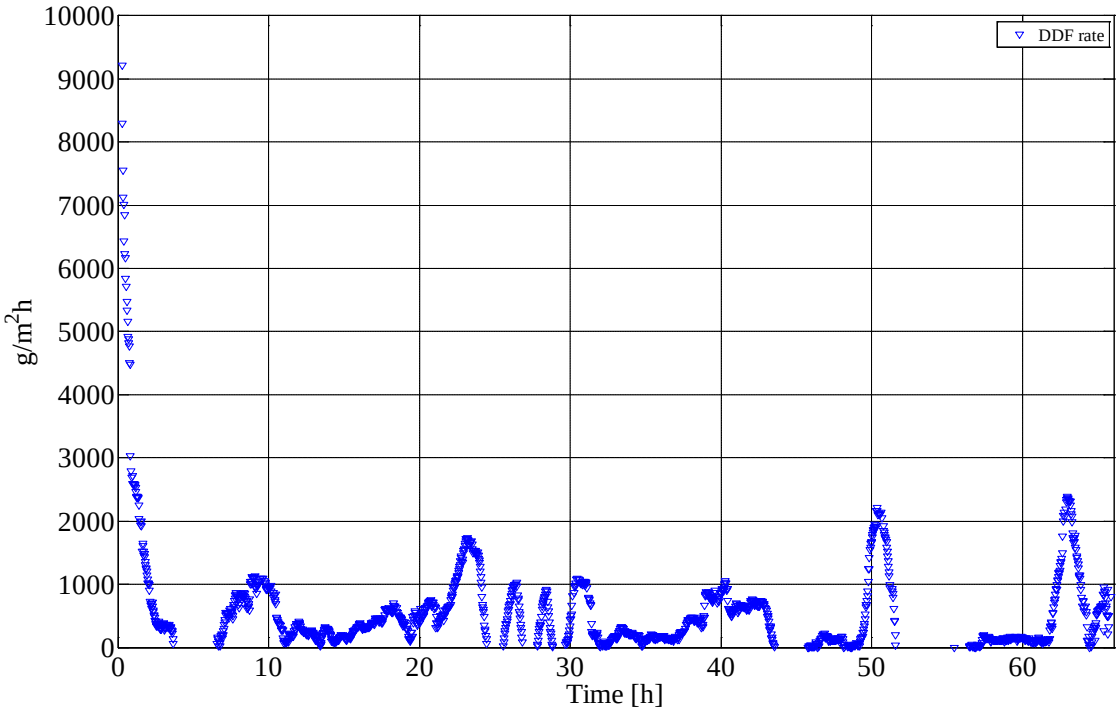

Figure B17 Calculated derivative-based deposit formation (DDF) rate during Test 2.

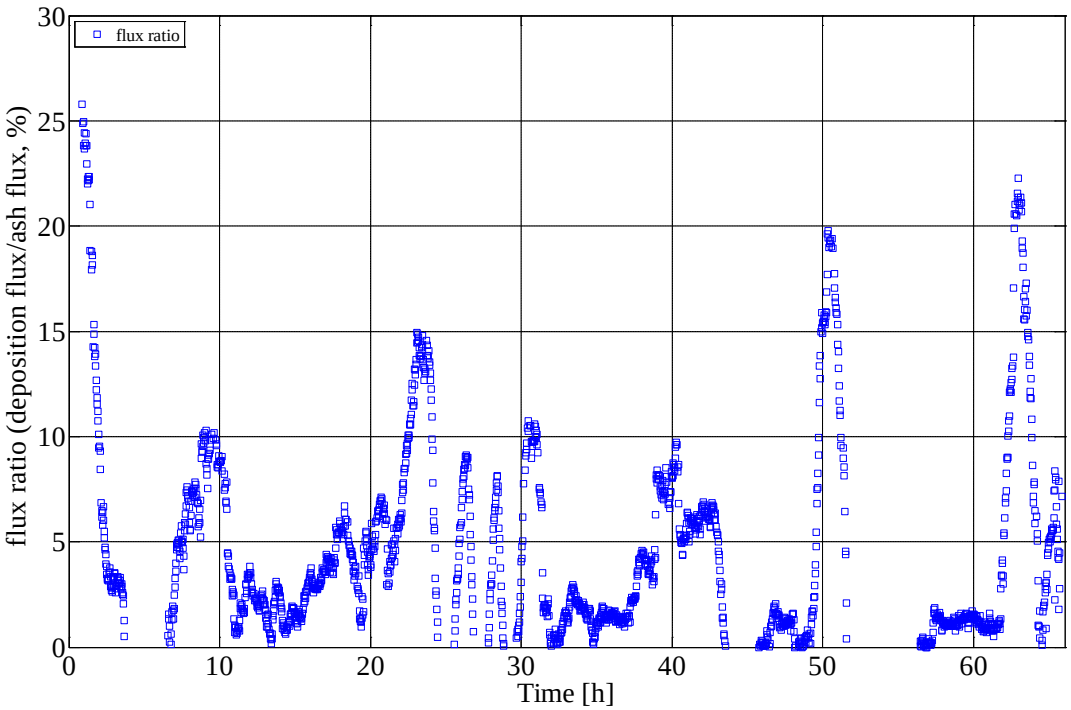

Figure B18 Calculated ash deposition propensity during Test 2.

Appendix B.3 Data from Test 3

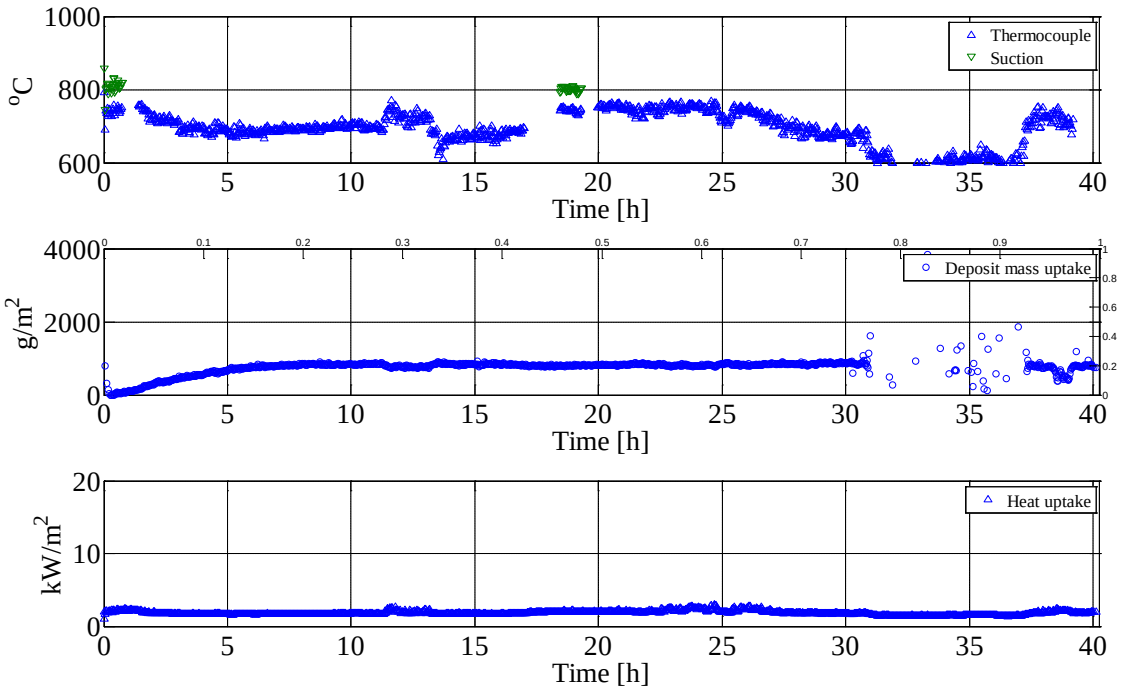

Figure B19 Flue gas temperature, deposit mass uptake, soot-blowing events and probe heat uptake during Test 3. The plant soot blower is active when the back-wall temperature is greater than the normal value, i.e. a peak/plateau observed in the figure.

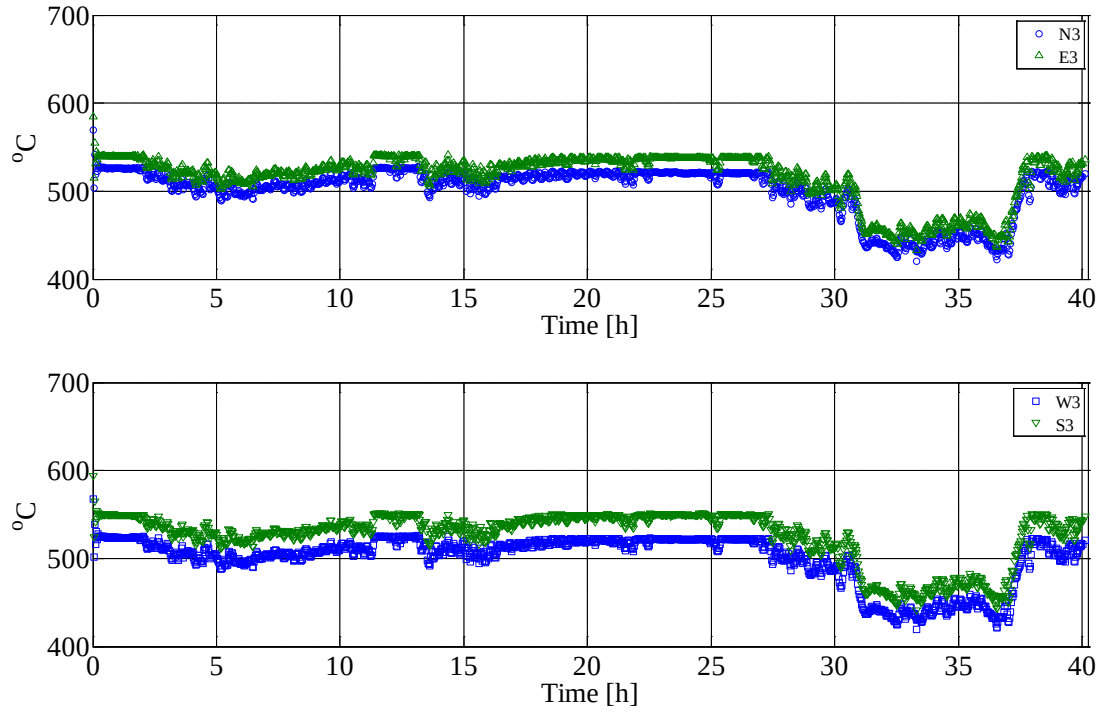

Figure B20 Measured probe surface temperature during Test 3.

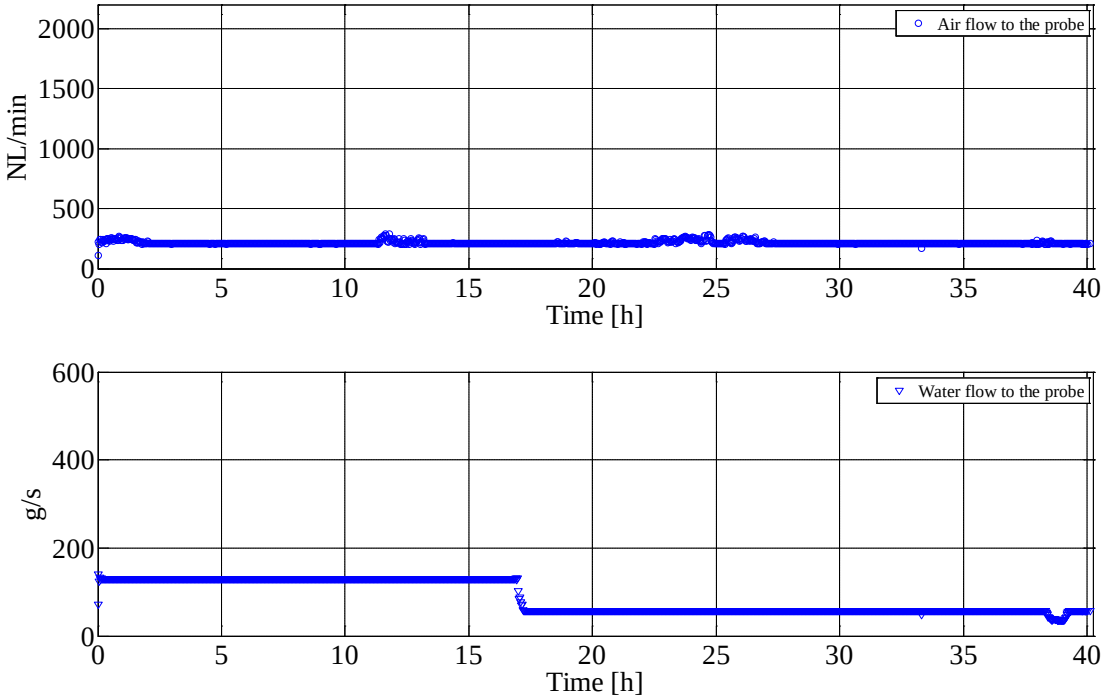

Figure B21 Measured air and water flow to the probe during Test 3.

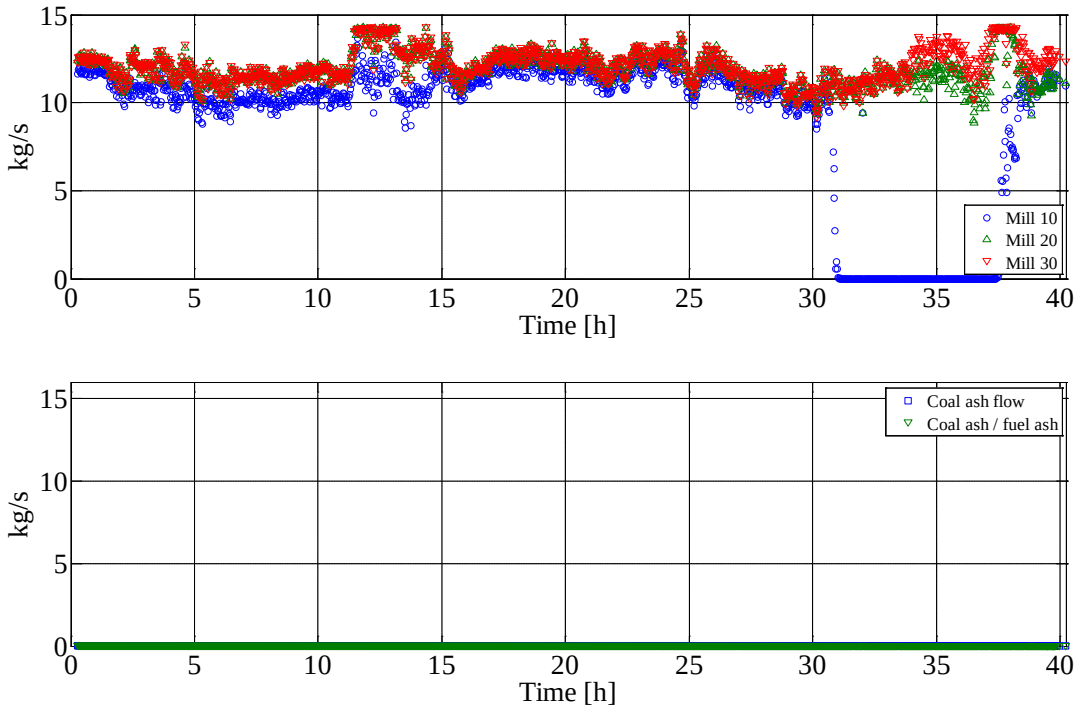

Figure B22 Measured wood flow through each mill, coal ash flow (kg/s) and ratio between coal ash and wood ash during Test 3.

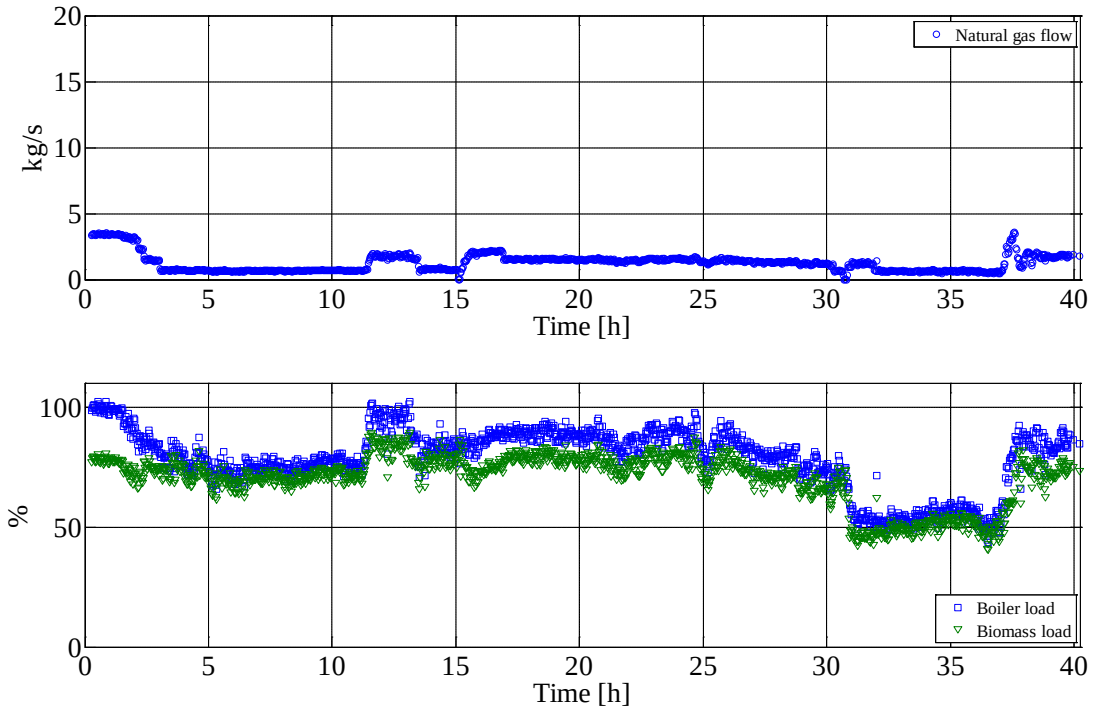

Figure B23 Natural gas flow, overall boiler load and biomass load during Test 3.

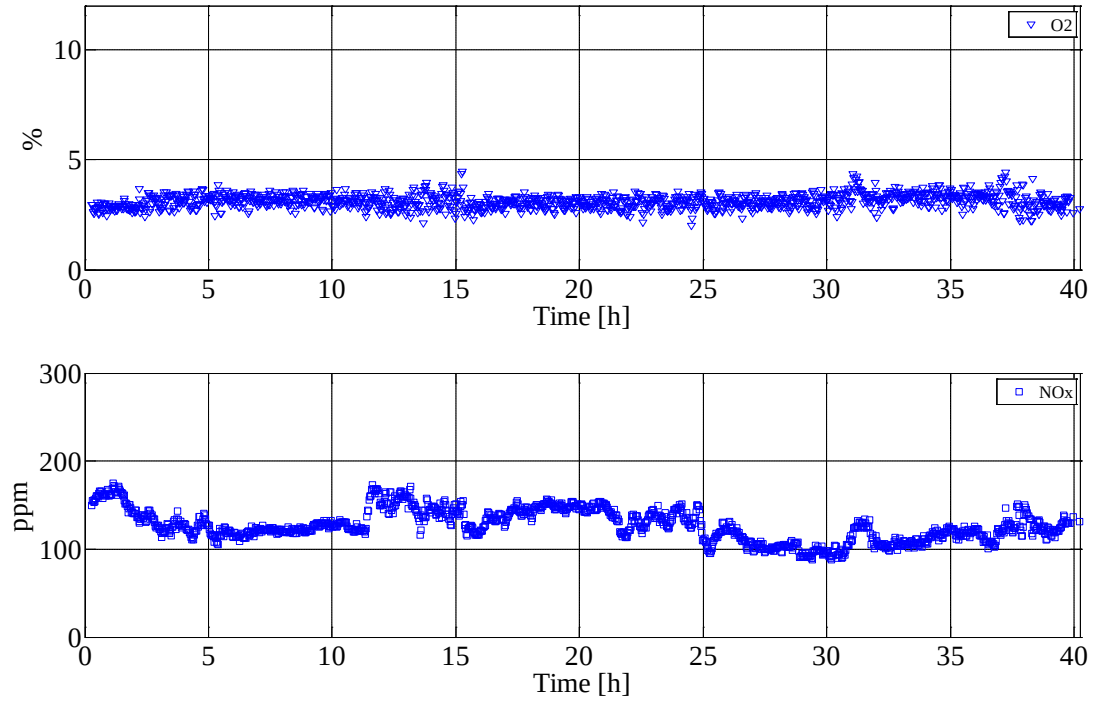

Figure B24 O_2 and NO_x (before SCR) concentrations in the flue gas during Test 3.

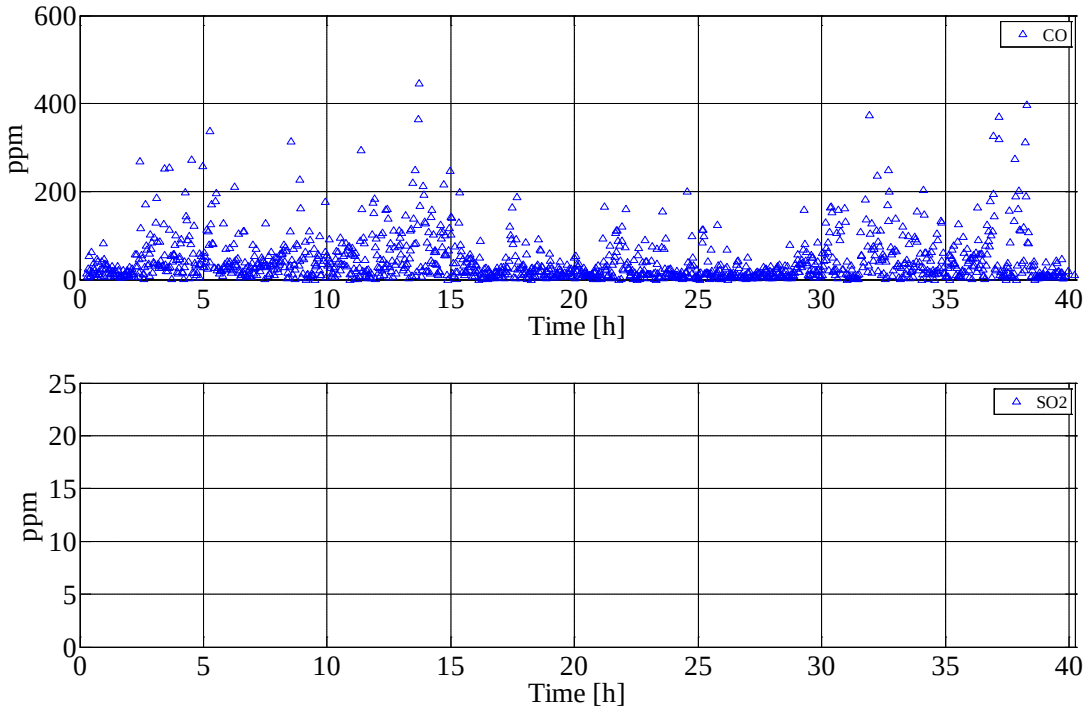

Figure B25 CO and SO_2 concentrations in the flue gas during Test 3 (only values larger than zero are shown).

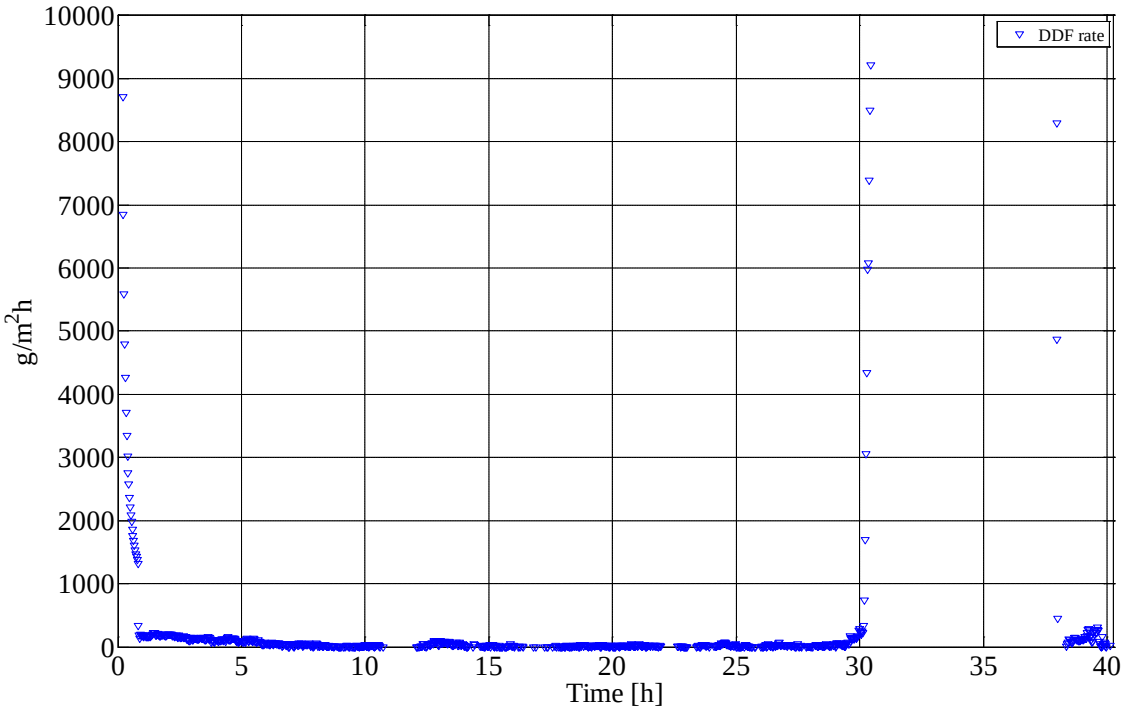

Figure B26 Calculated derivative-based deposit formation (DDF) rate during Test 3.

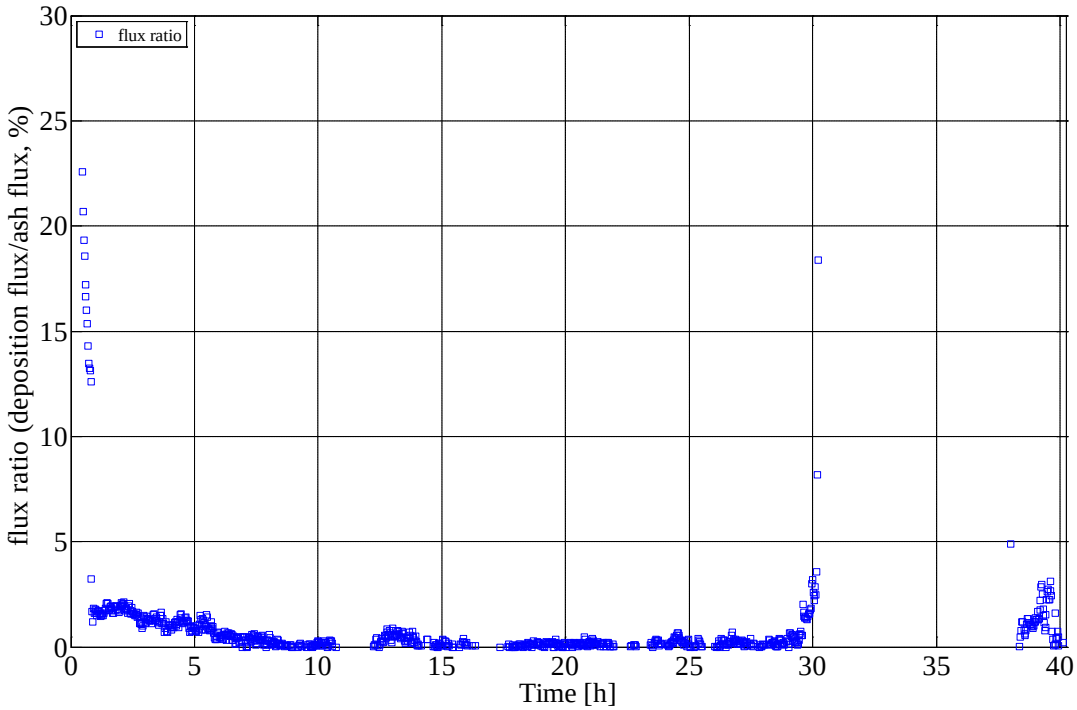

Figure B27 Calculated ash deposition propensity during Test 3.

Appendix B.4 Data from Test 4

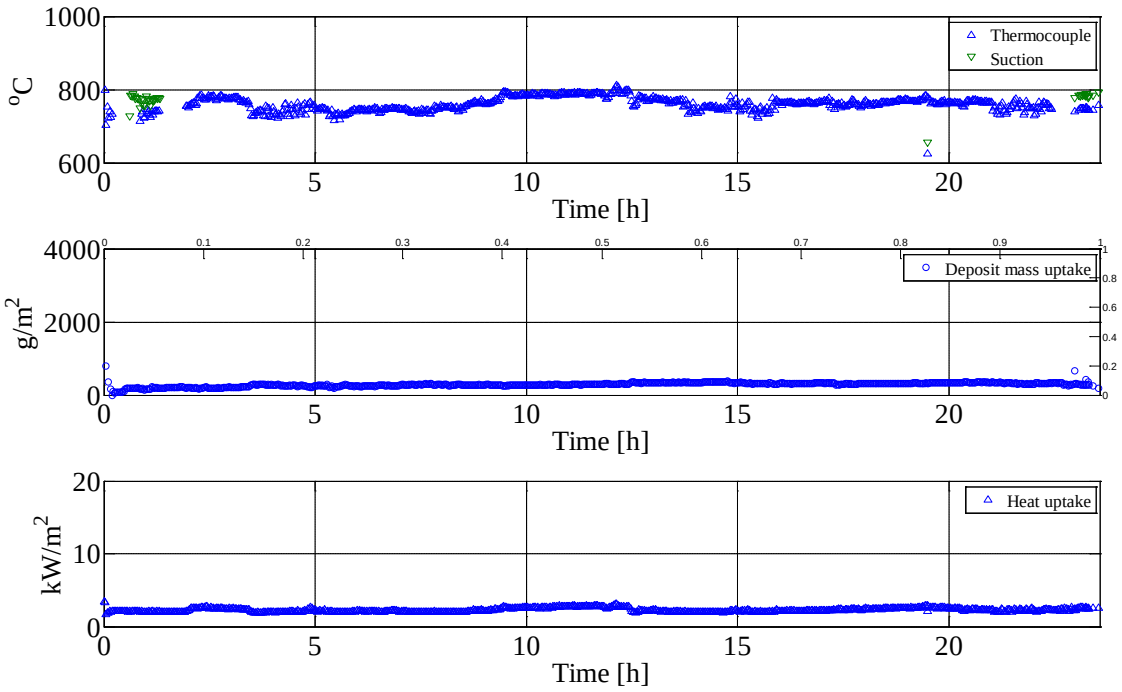

Figure B28 Flue gas temperature, deposit mass uptake, soot-blowing events and probe heat uptake during Test 4. The plant soot blower is active when the back-wall temperature is greater than the normal value, i.e. a peak/plateau observed in the figure.

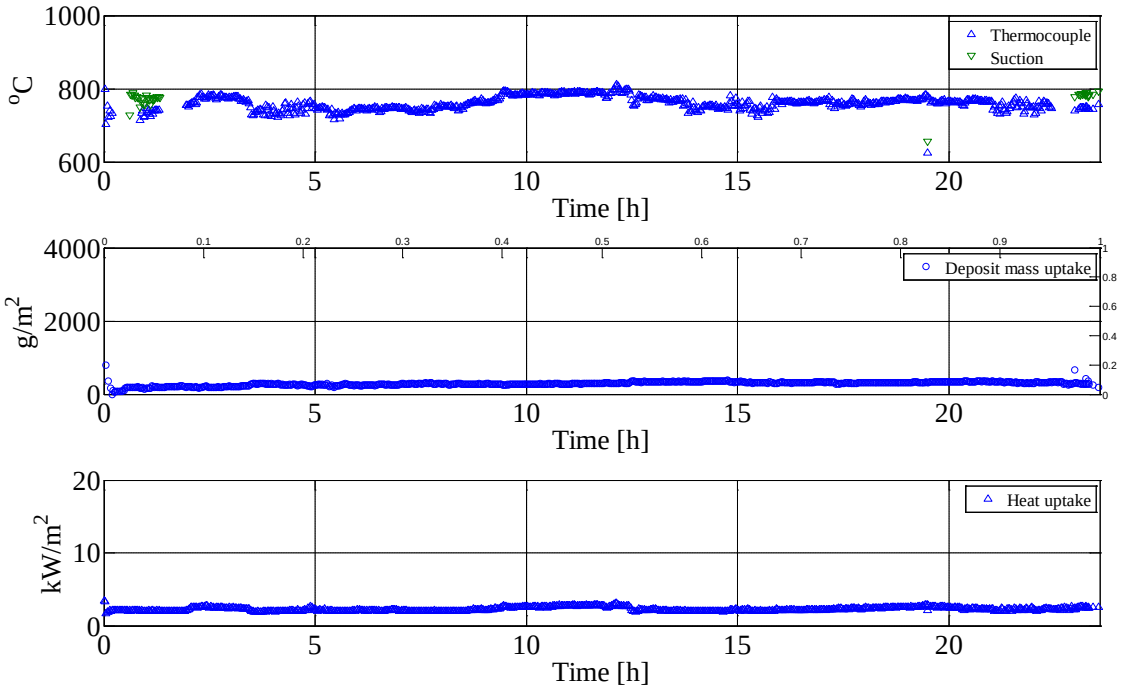

Figure B29 Measured probe surface temperature during Test 4.

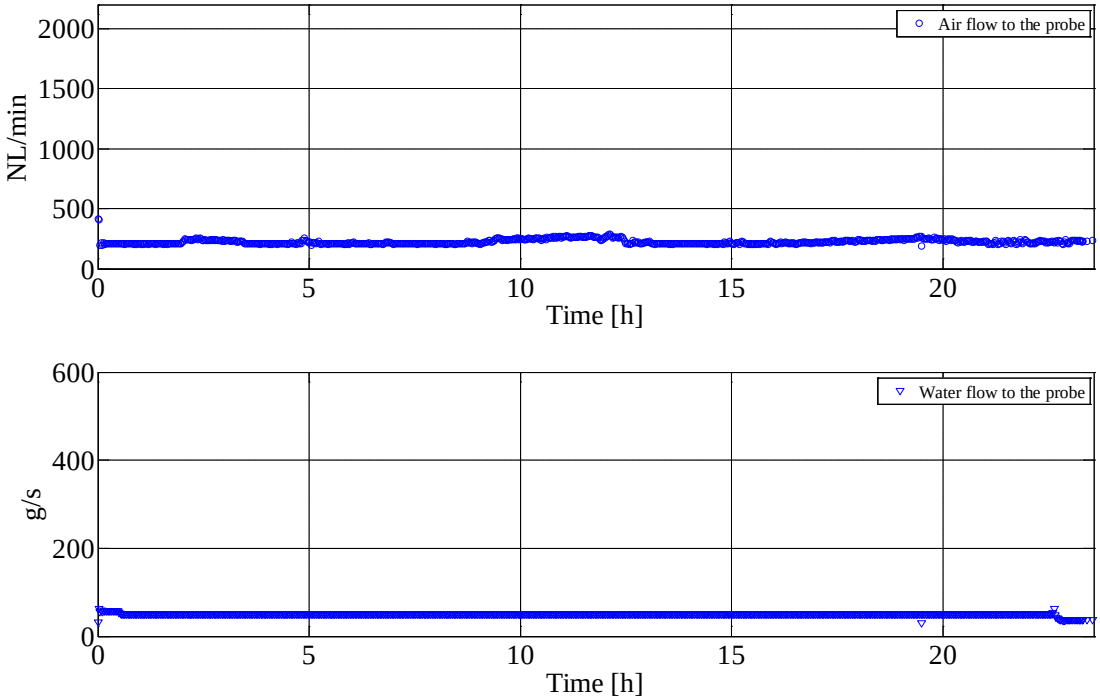

Figure B30 Measured air and water flow to the probe during Test 4.

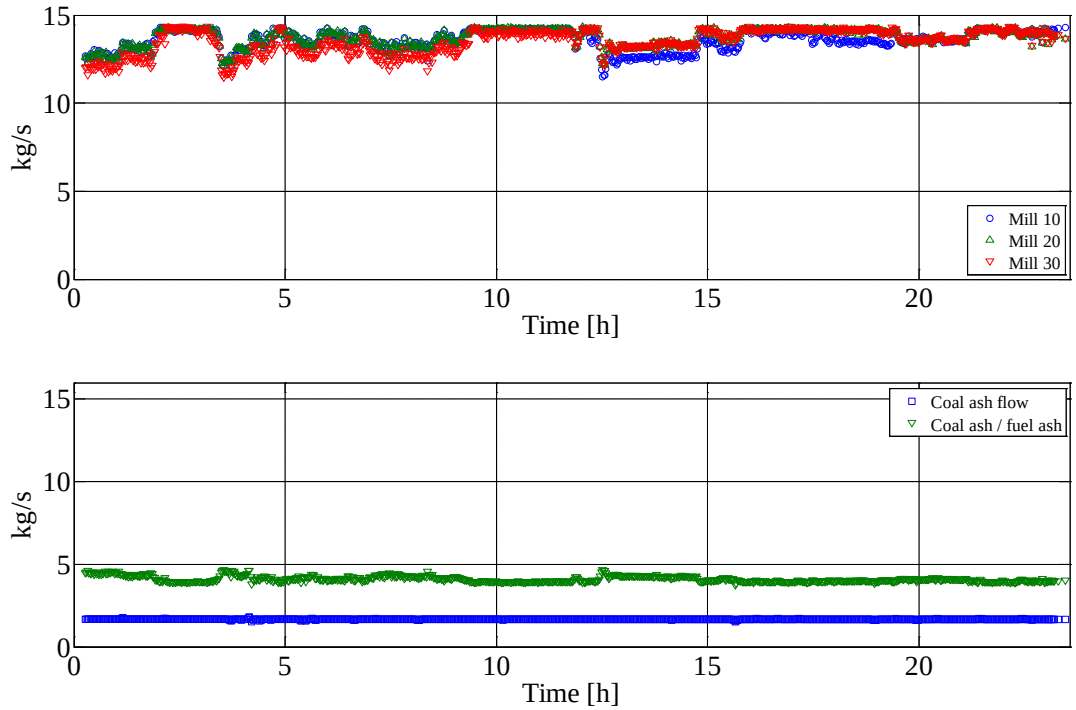

Figure B31 Measured wood flow through each mill, coal ash flow (kg/s) and ratio between coal ash and wood ash during Test 4.

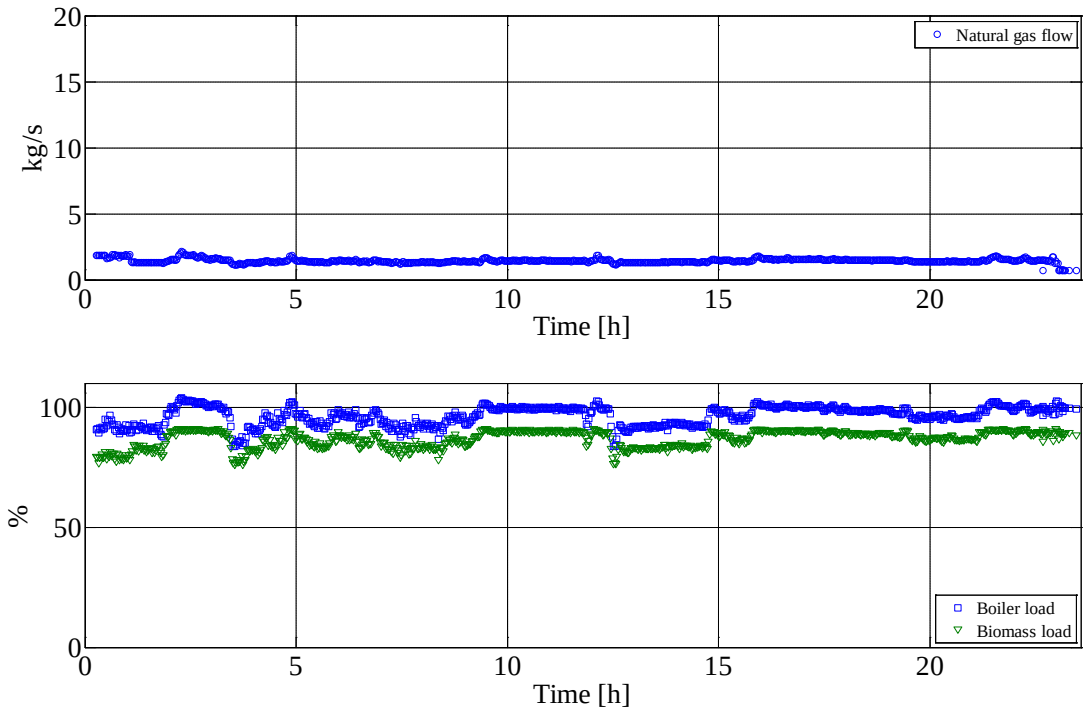

Figure B32 Natural gas flow, overall boiler load and biomass load during Test 4.

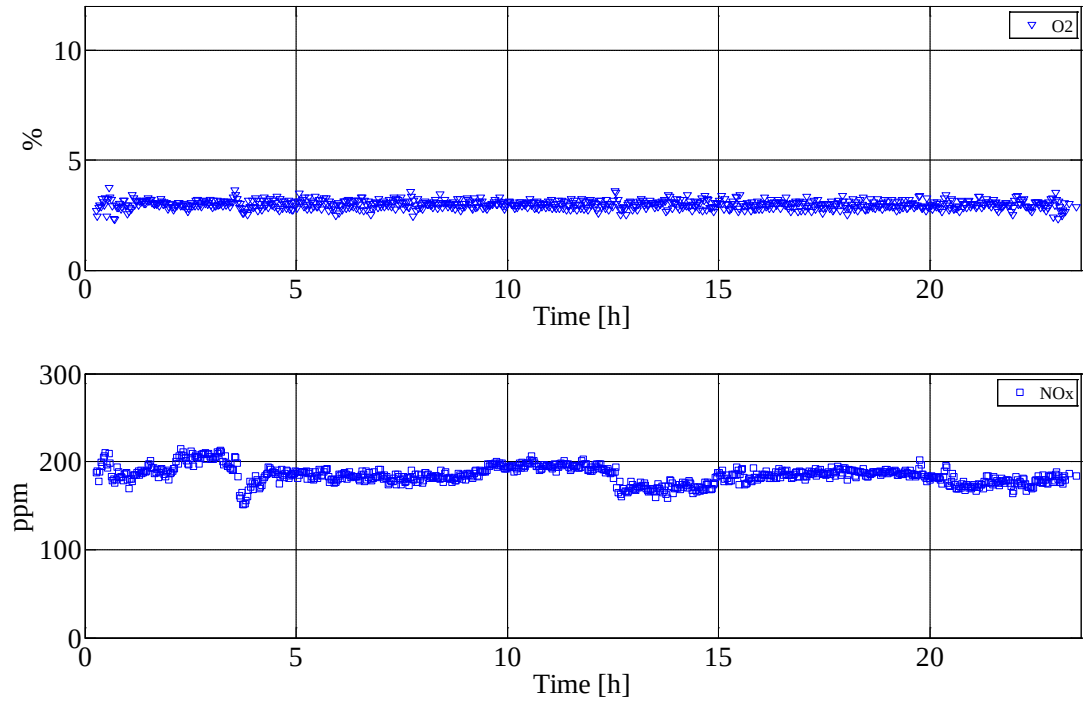

Figure B33 O_2 and NO_x (before SCR) concentrations in the flue gas during Test 4.

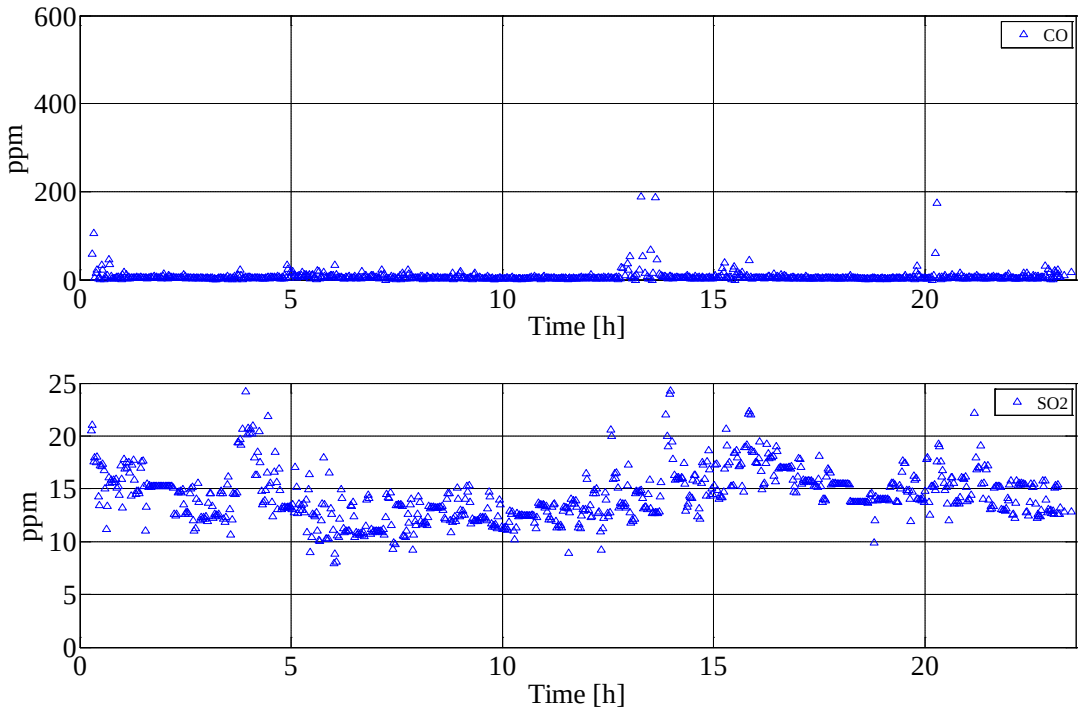

Figure B34 CO and SO_2 concentrations in the flue gas during Test 4 (only values larger than zero are shown).

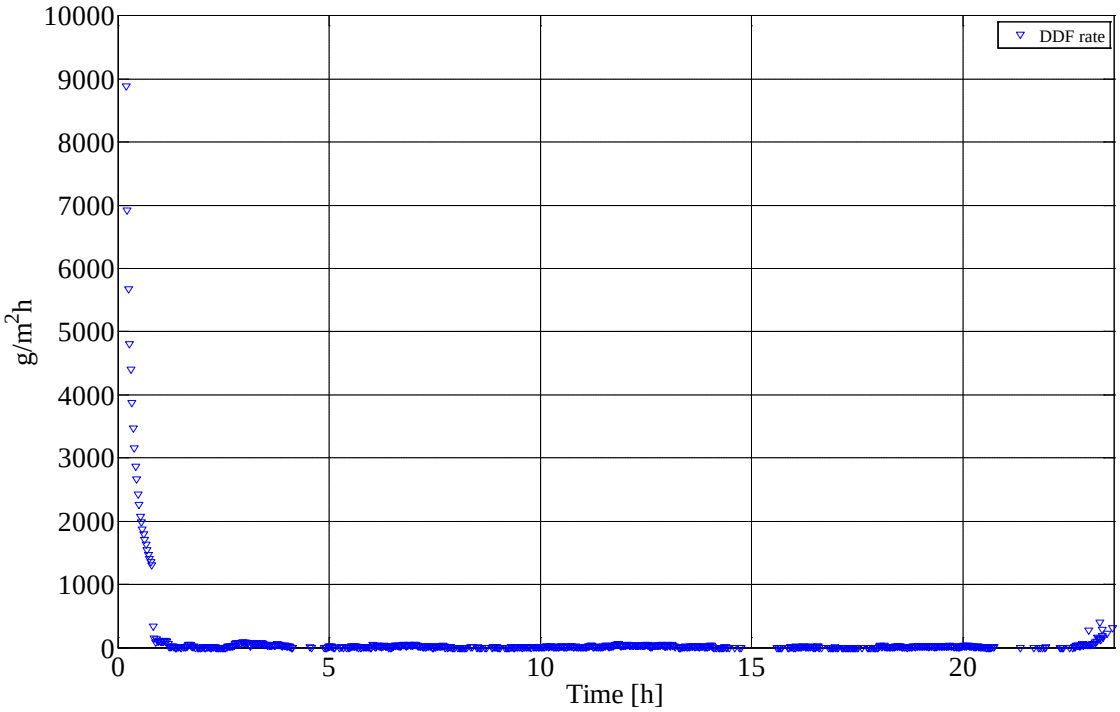

Figure B35 Calculated derivative-based deposit formation (DDF) rate during Test 4.

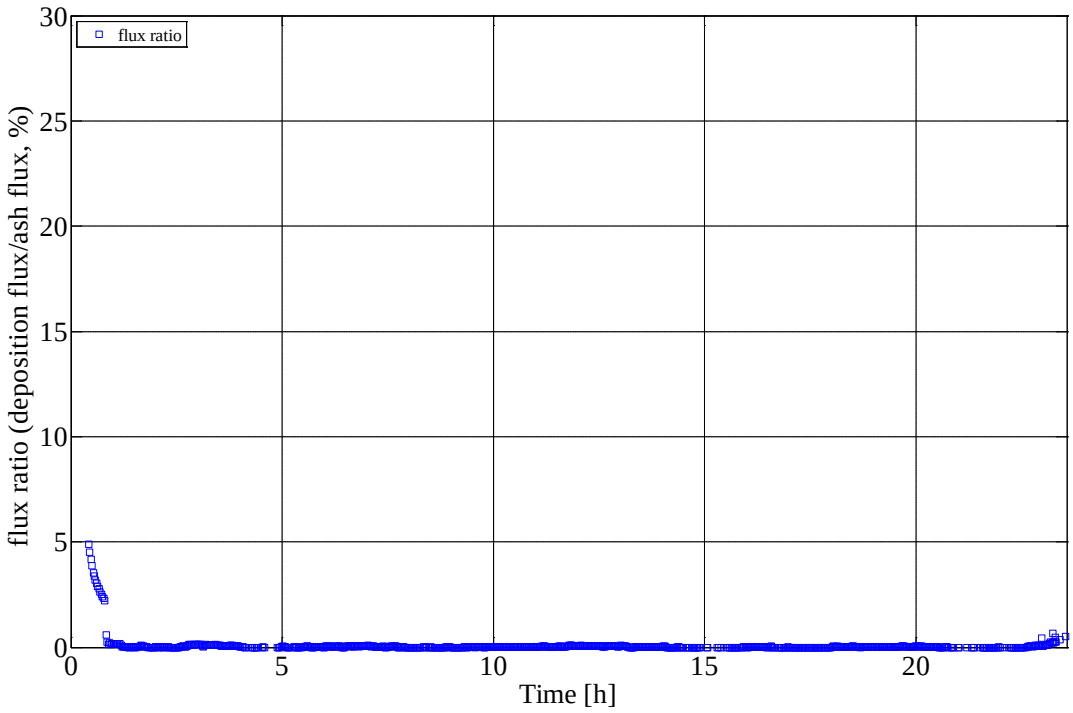

Figure B36 Calculated ash deposition propensity during Test 4.

Appendix B.5 Data from Test 5

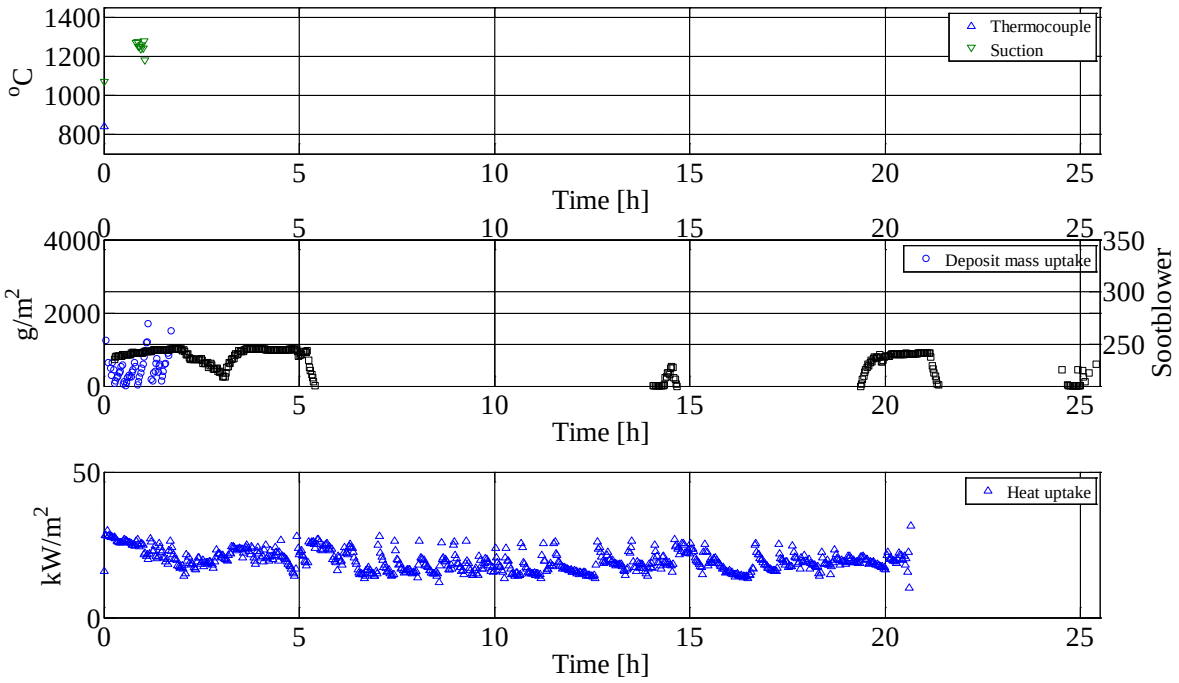

Figure B37 Flue gas temperature, deposit mass uptake, soot-blowing events and probe heat uptake during Test 5. The plant soot blower is active when the back-wall temperature is greater than the normal value, i.e. a peak/plateau observed in the figure.

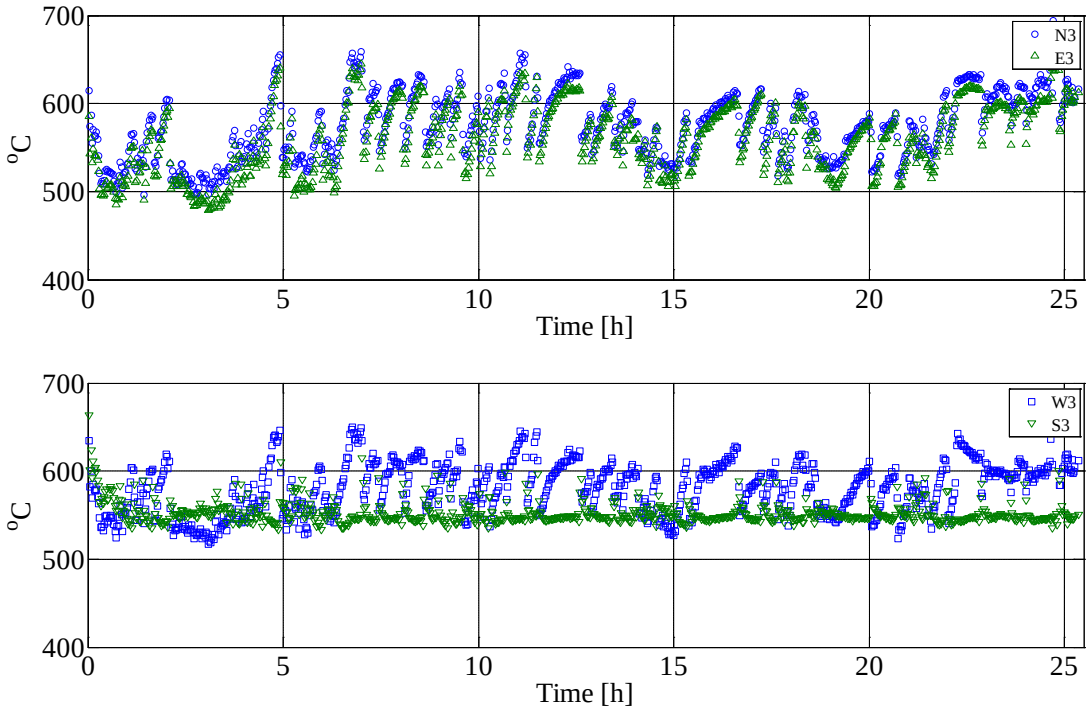

Figure B38 Measured probe surface temperature during Test 5.

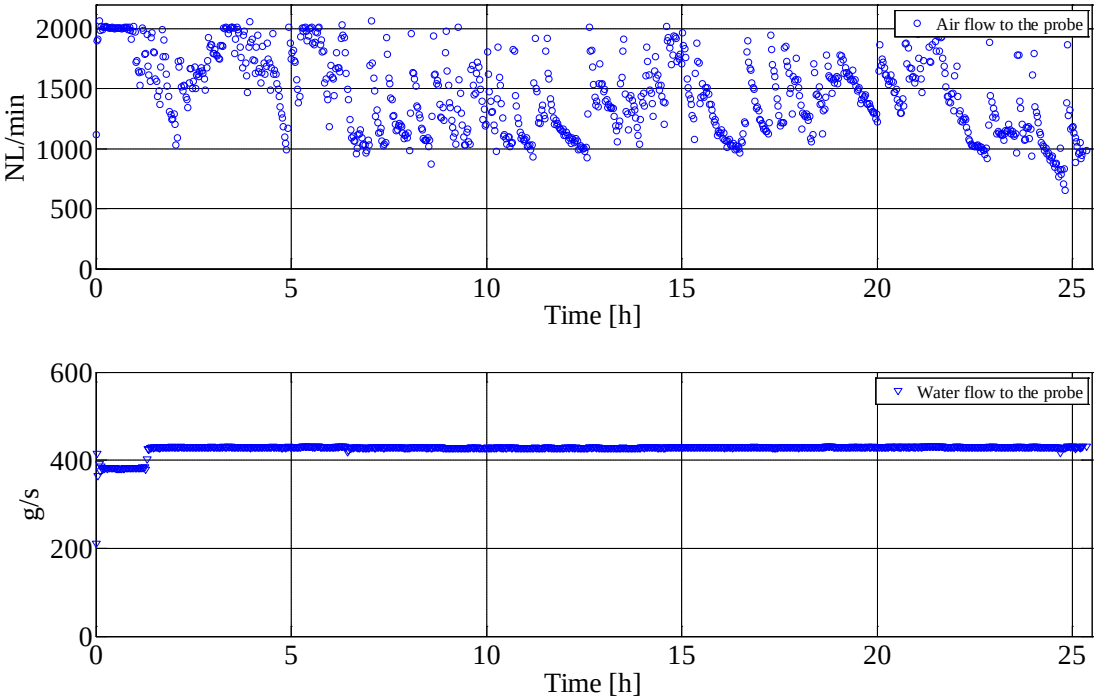

Figure B39 Measured air and water flow to the probe during Test 5.

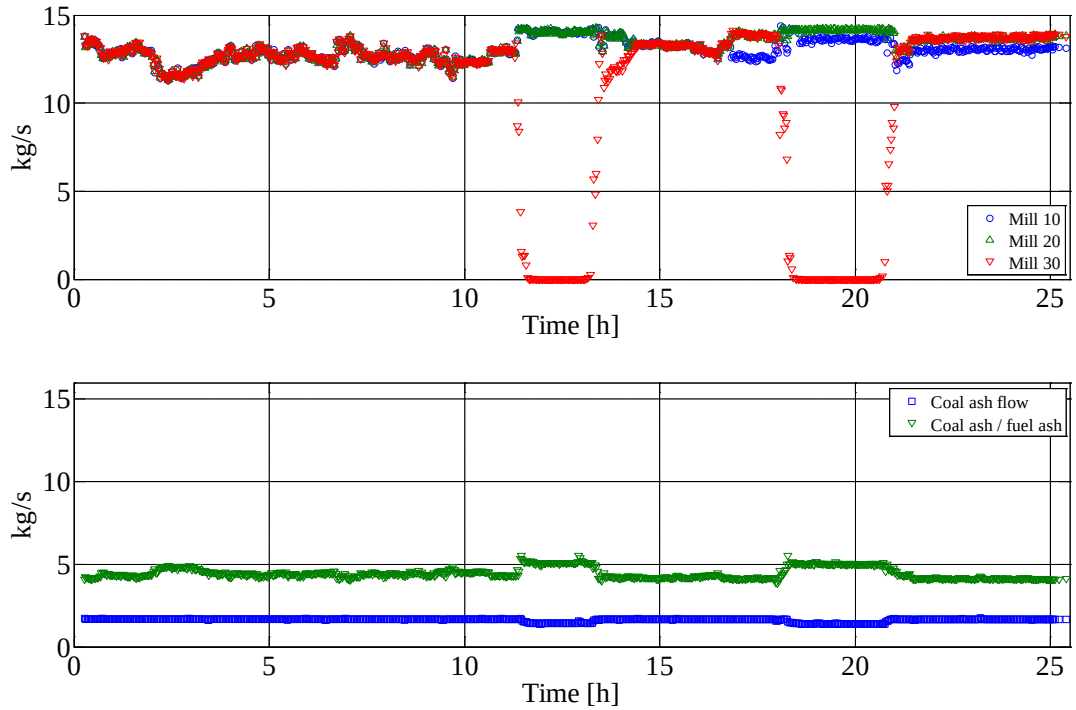

Figure B40 Measured wood flow through each mill, coal ash flow (kg/s) and ratio between coal ash and wood ash during Test 5.

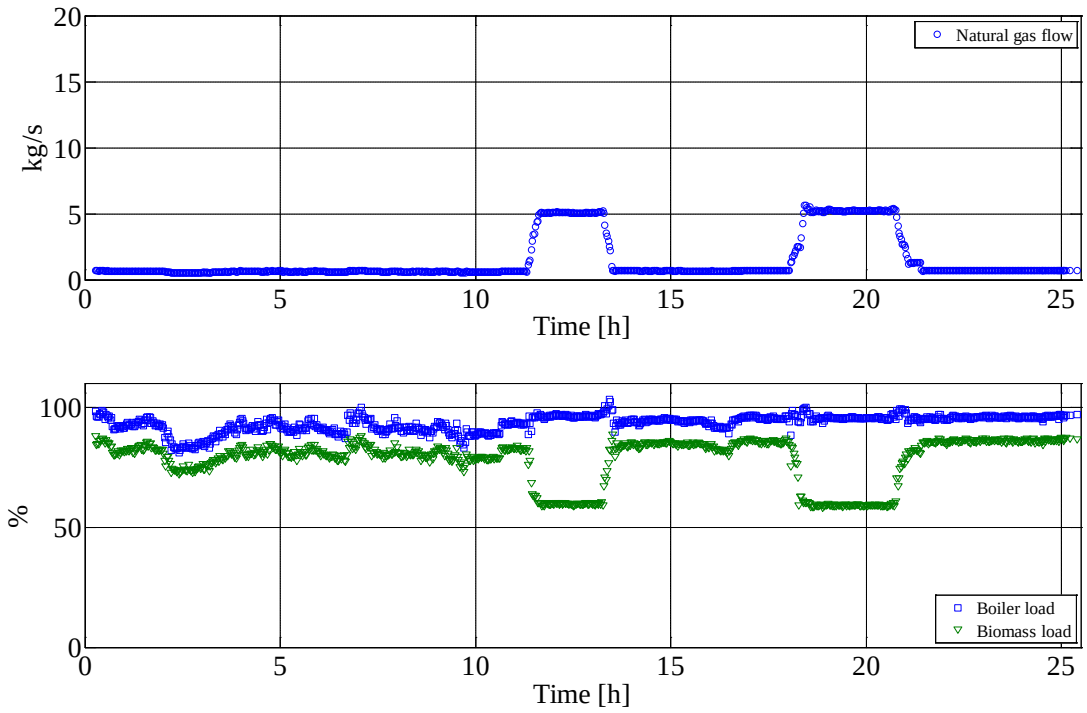

Figure B41 Natural gas flow, overall boiler load and biomass load during Test 5.

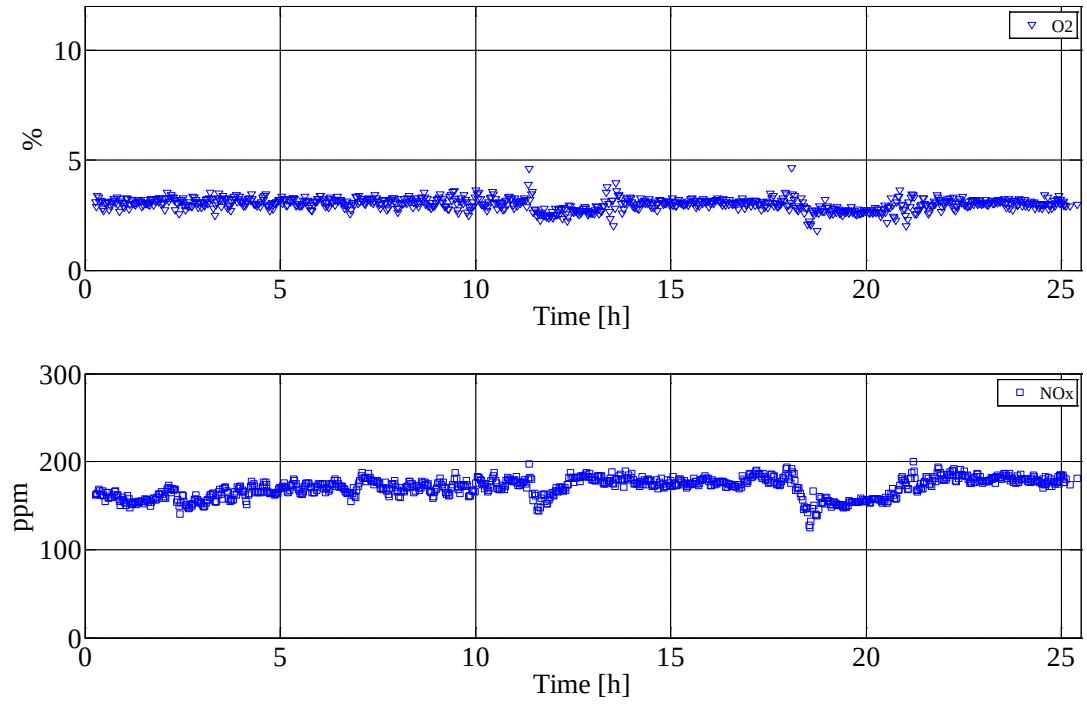

Figure B42 O_2 and NO_x (before SCR) concentrations in the flue gas during Test 5.

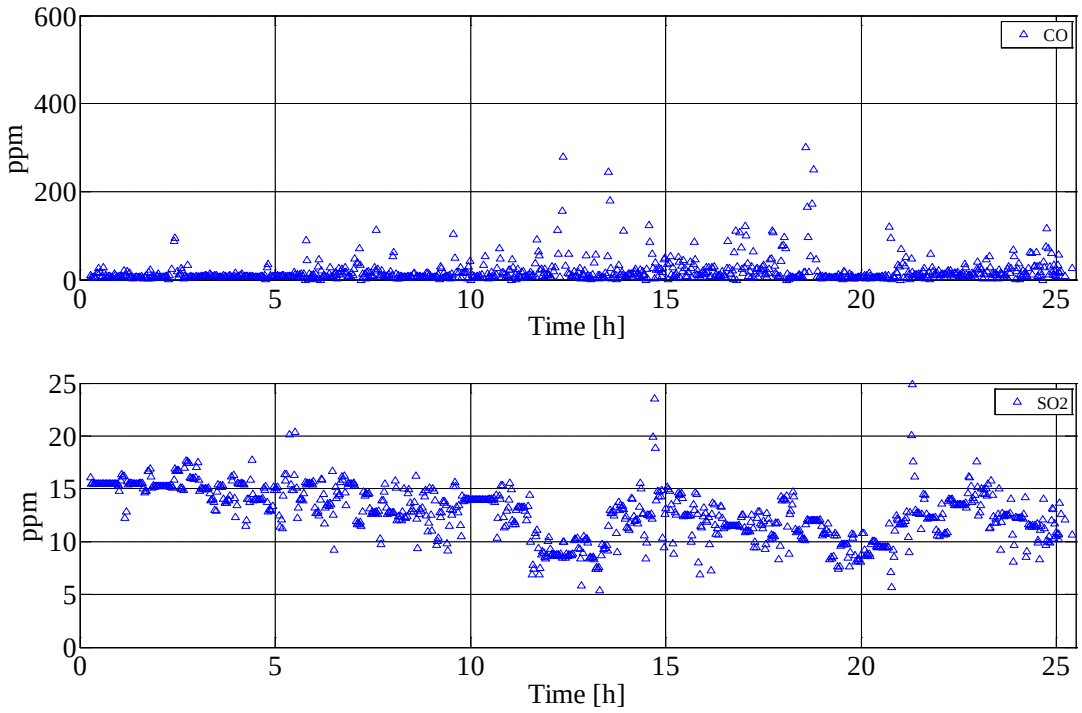

Figure B43 CO and SO_2 concentrations in the flue gas during Test 5 (only values larger than zero are shown).

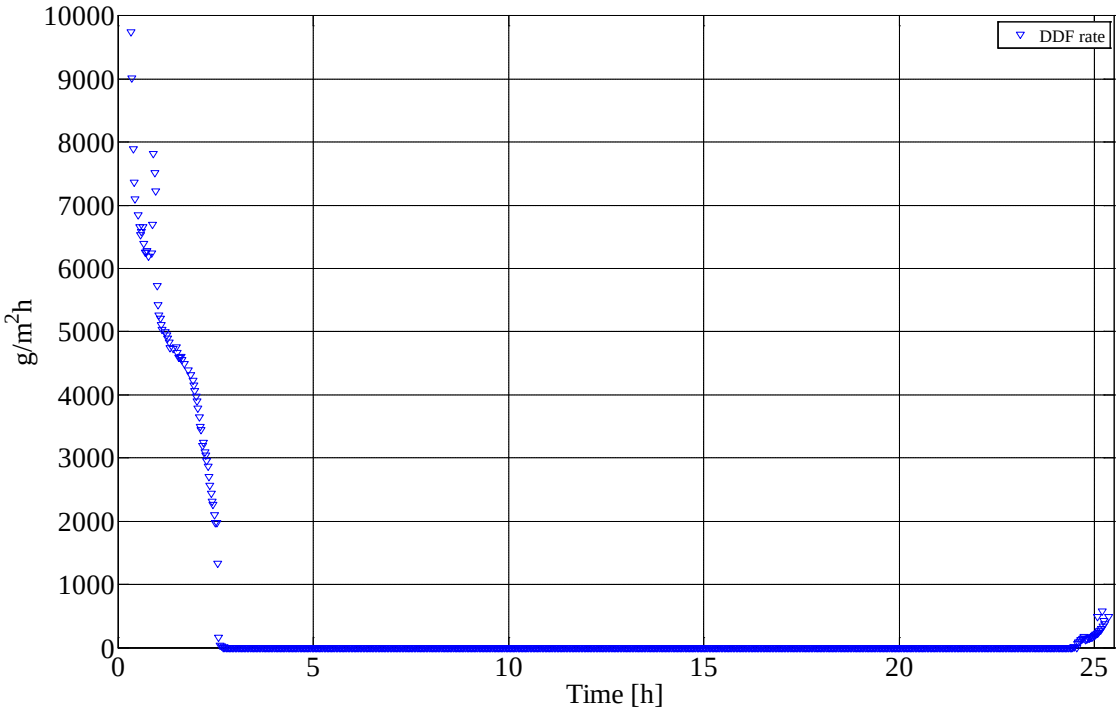

Figure B44 Calculated derivative-based deposit formation (DDF) rate during Test 5.

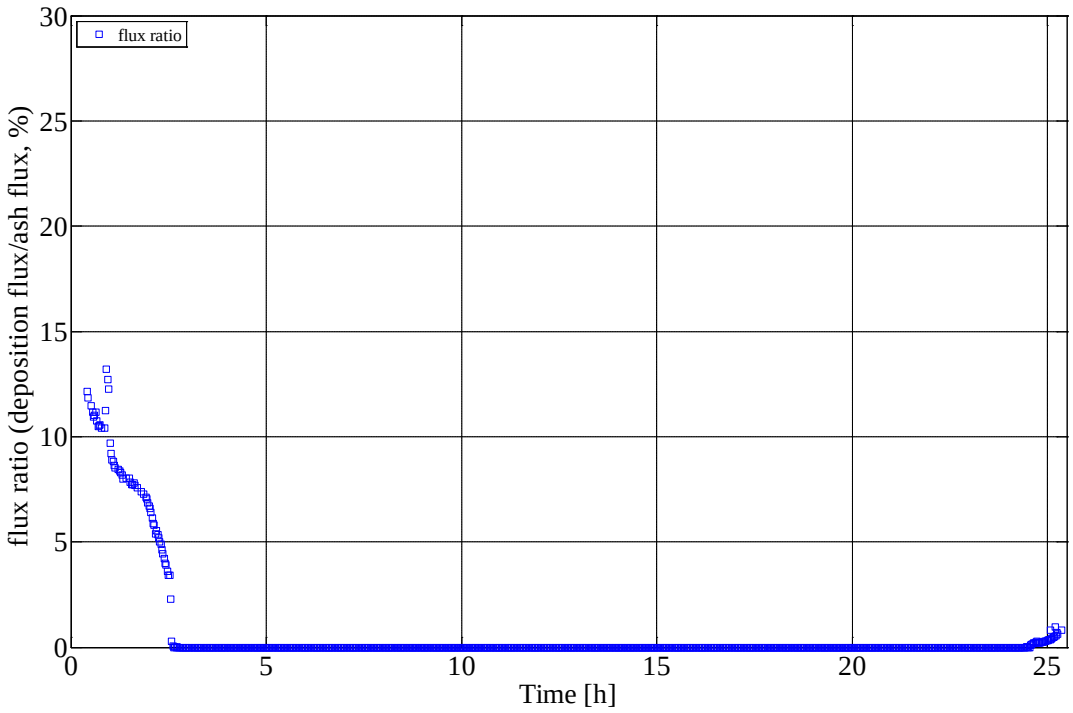

Figure B45 Calculated ash deposition propensity during Test 5.

Appendix B.6 Data from Test 6

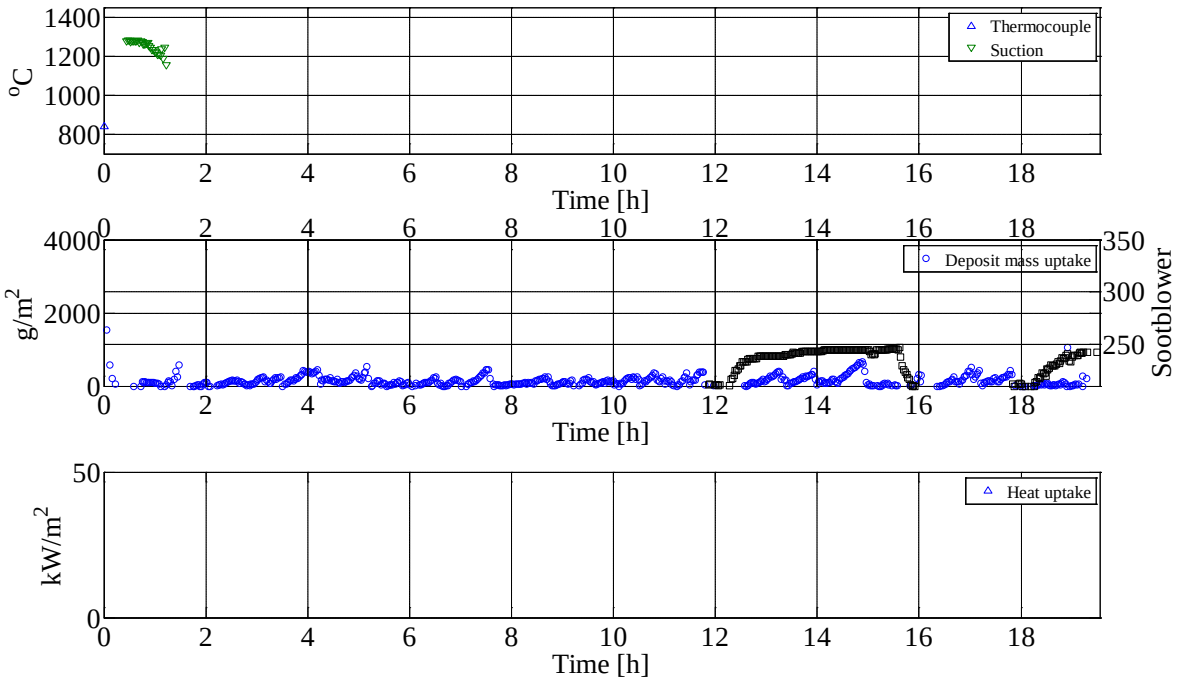

Figure B46 Flue gas temperature, deposit mass uptake, soot-blowing events and probe heat uptake during Test 6. The plant soot blower is active when the back-wall temperature is greater than the normal value, i.e. a peak/plateau observed in the figure.

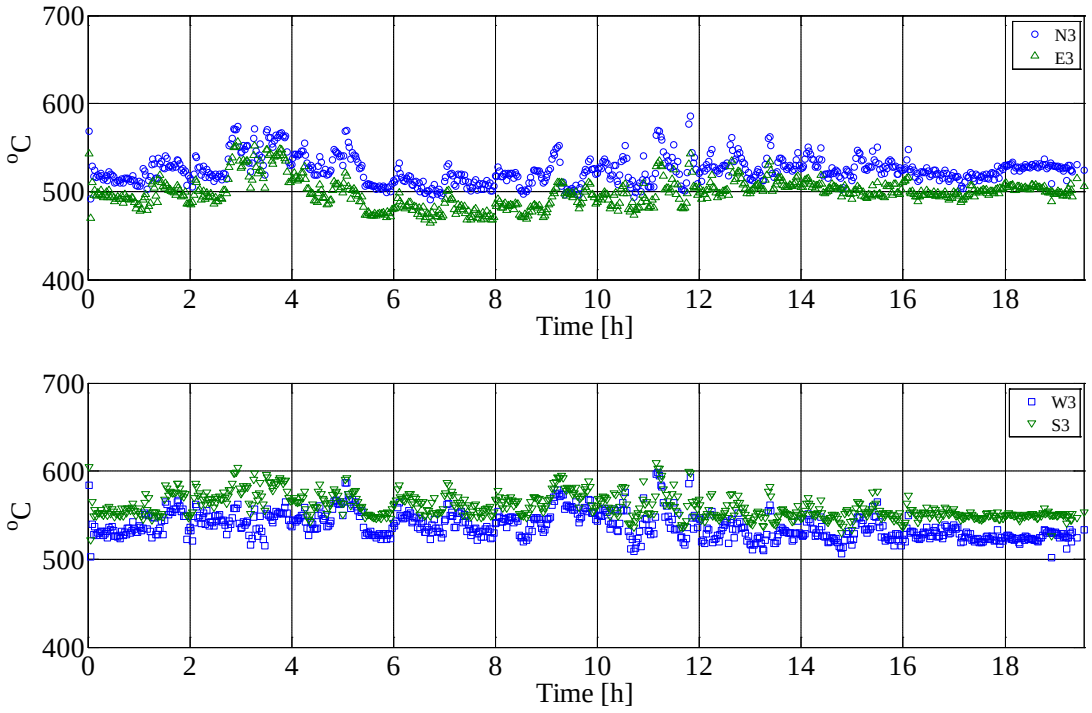

Figure B47 Measured probe surface temperature during Test 6.

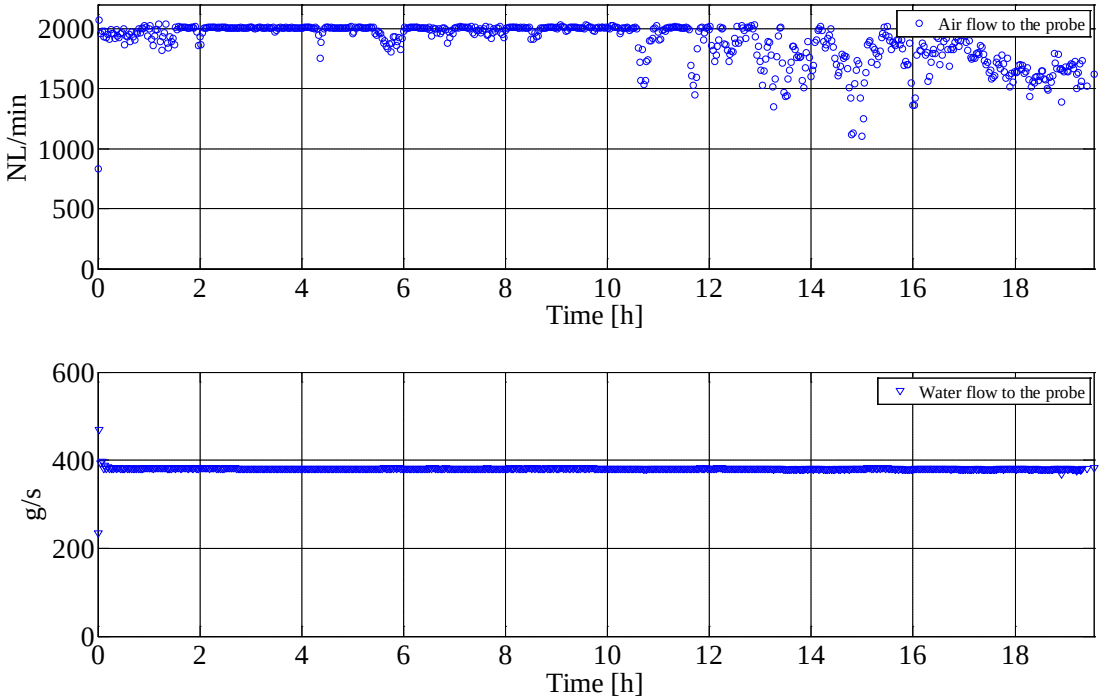

Figure B48 Measured air and water flow to the probe during Test 6.

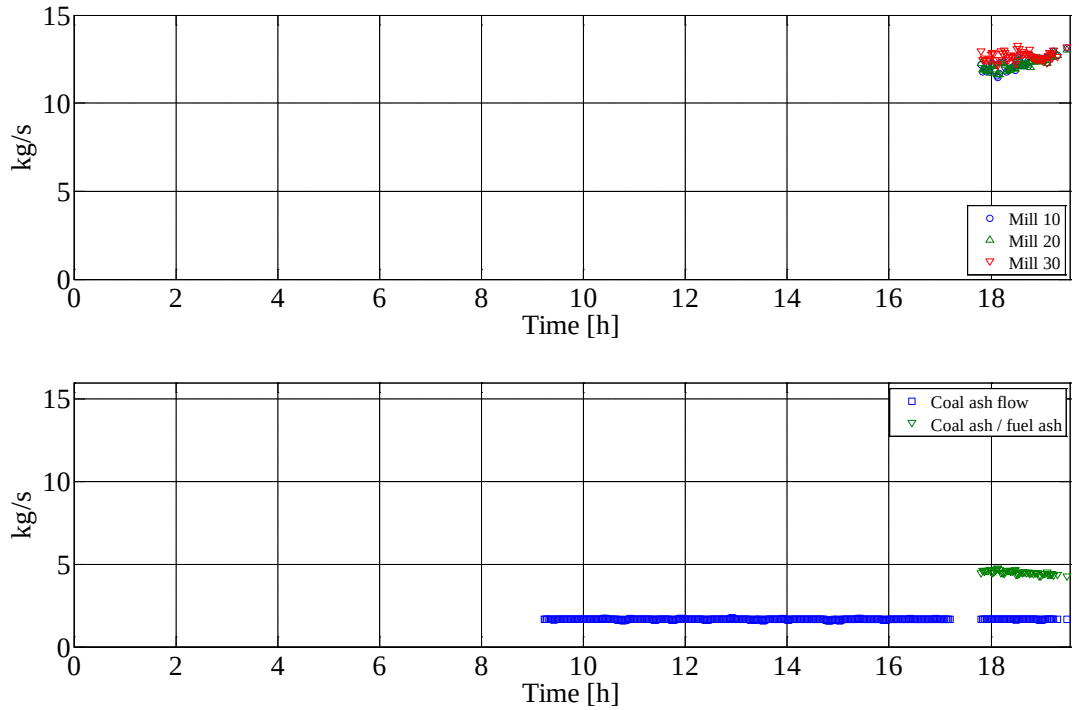

Figure B49 Measured wood flow through each mill, coal ash flow (kg/s) and ratio between coal ash and wood ash during Test 6.

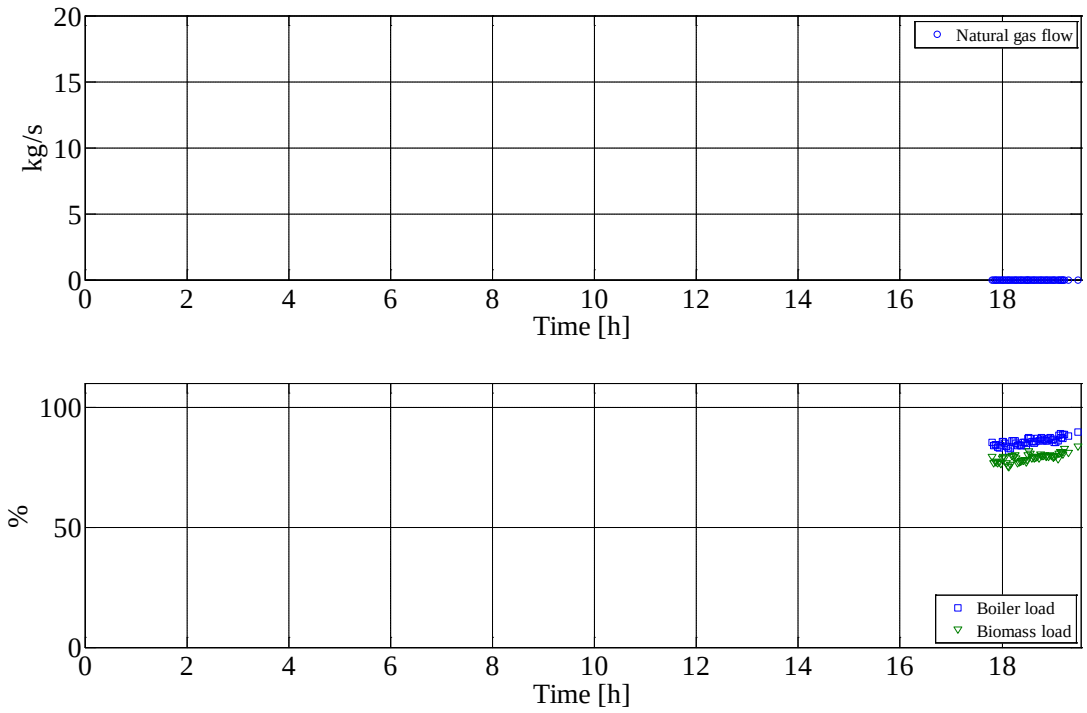

Figure B50 Natural gas flow, overall boiler load and biomass load during Test 6.

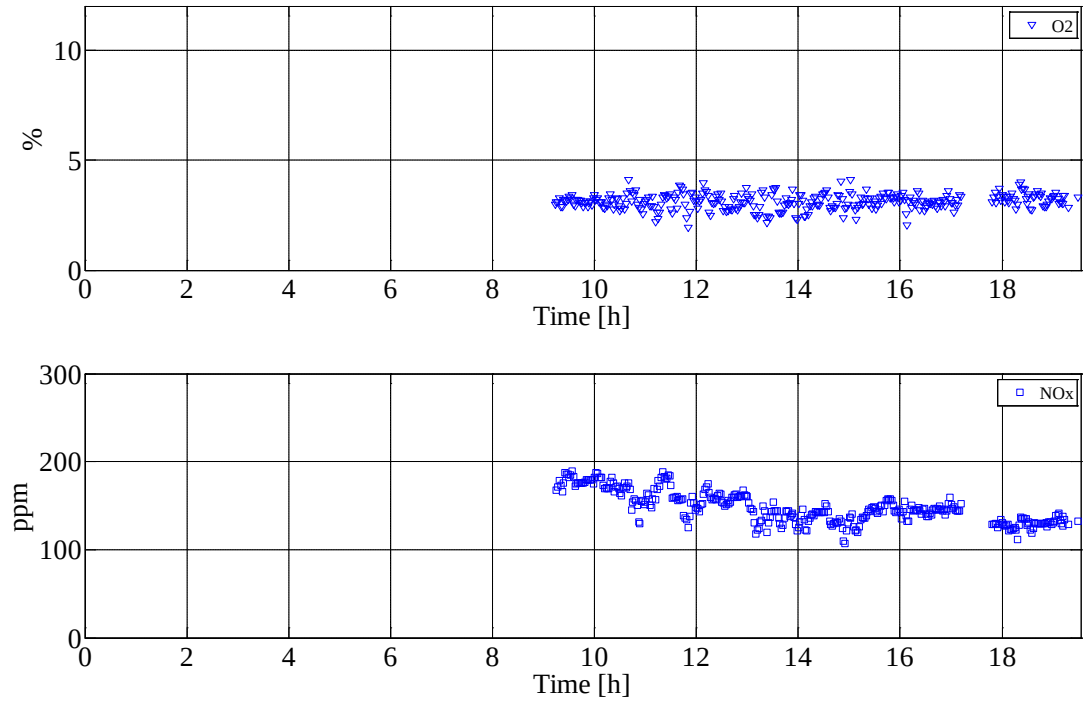

Figure B51 O_2 and NO_x (before SCR) concentrations in the flue gas during Test 6.

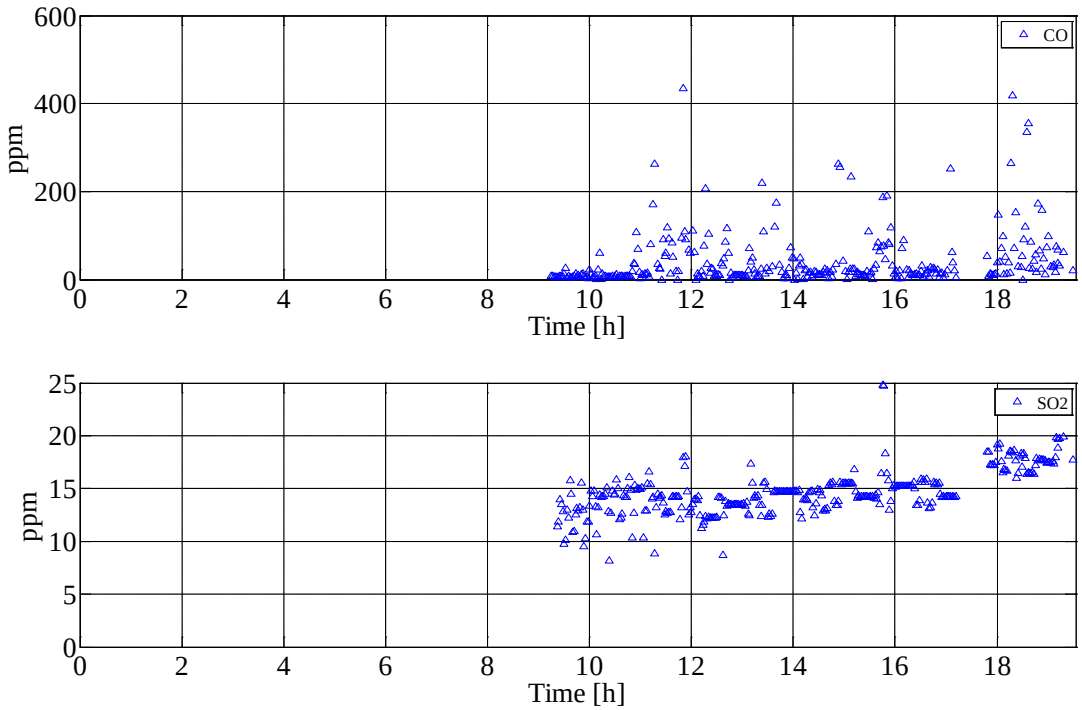

Figure B52 CO and SO_2 concentrations in the flue gas during Test 6 (only values larger than zero are shown).

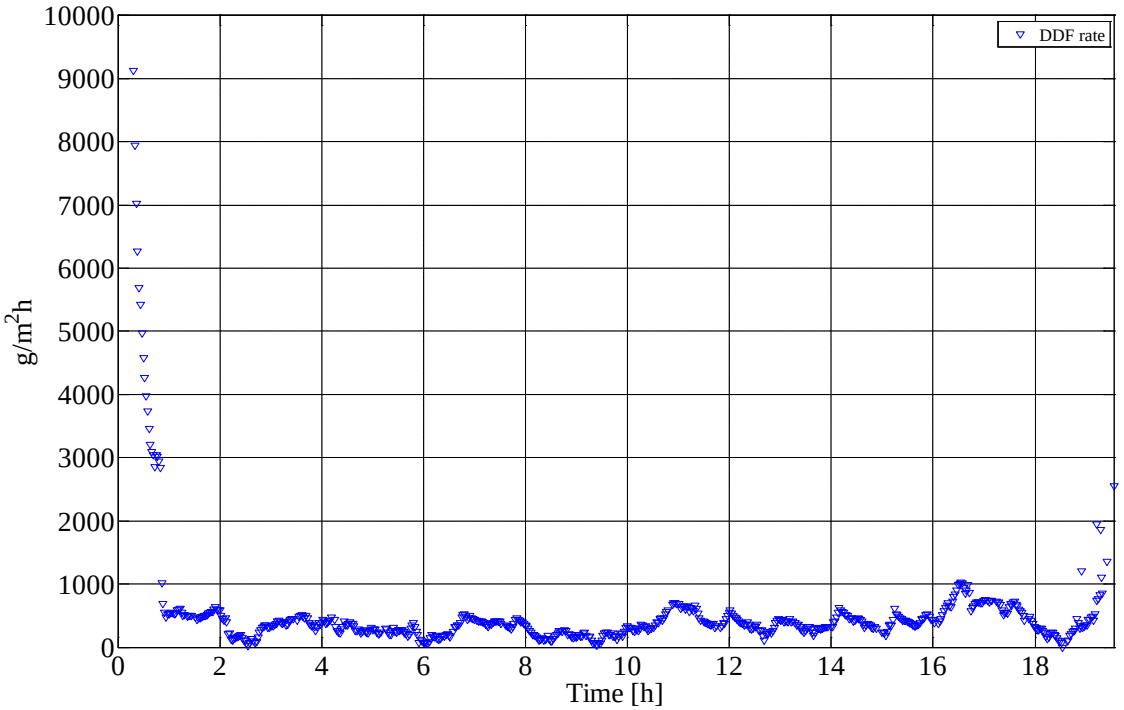

Figure B53 Calculated derivative-based deposit formation (DDF) rate during Test 6.

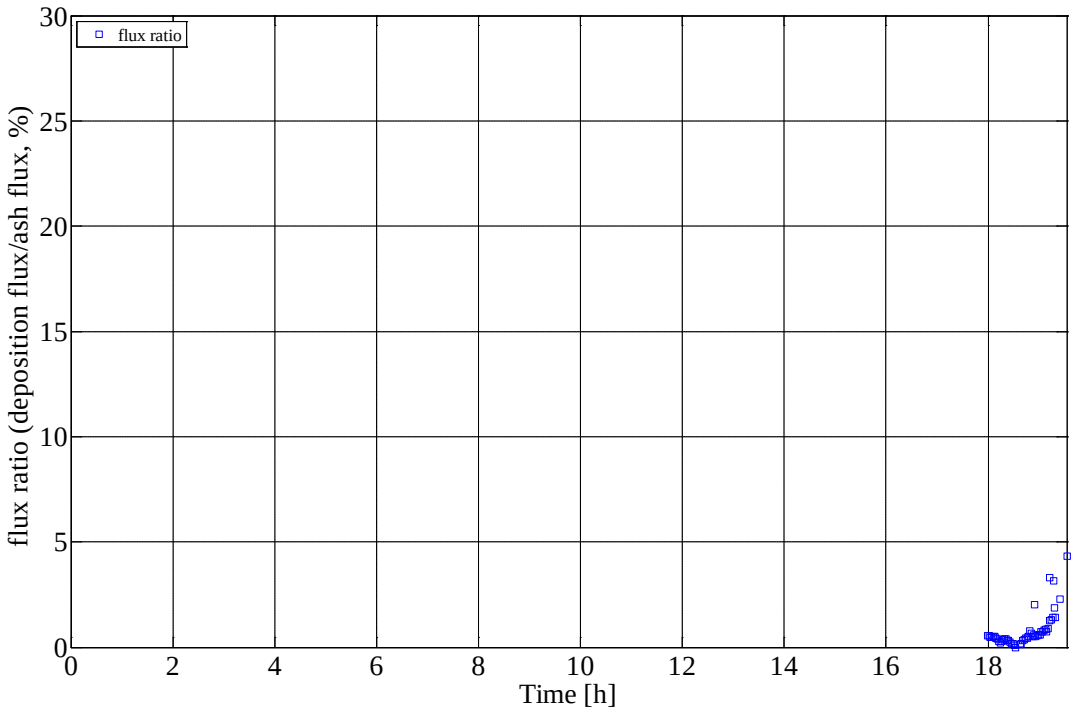

Figure B54 Calculated ash deposition propensity during Test 6.

Appendix B.7 Data from Test 7

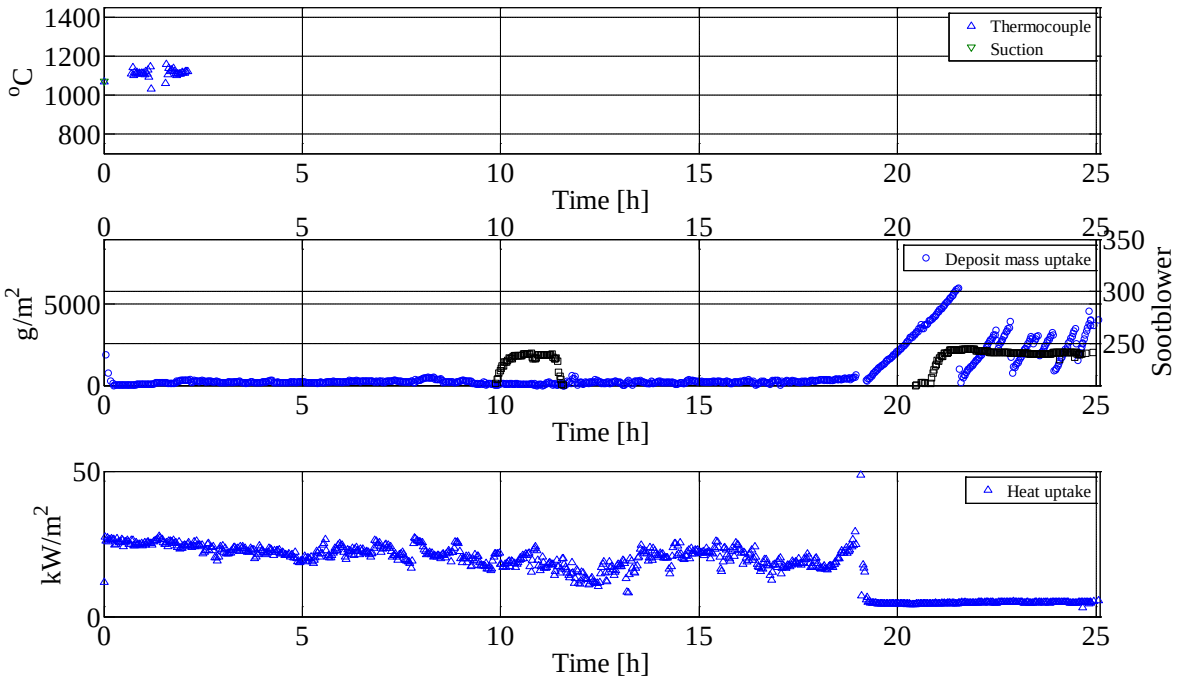

Figure B55 Flue gas temperature, deposit mass uptake, soot-blowing events and probe heat uptake during Test 7. The plant soot blower is active when the back-wall temperature is greater than the normal value, i.e. a peak/plateau observed in the figure.

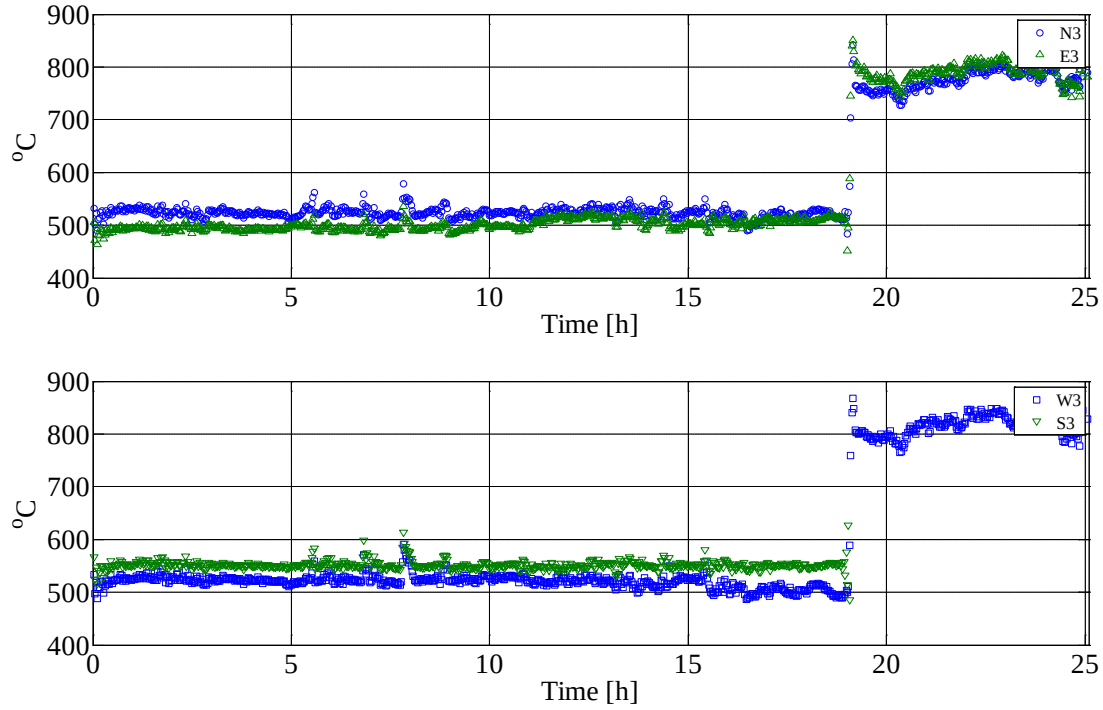

Figure B56 Measured probe surface temperature during Test 7.

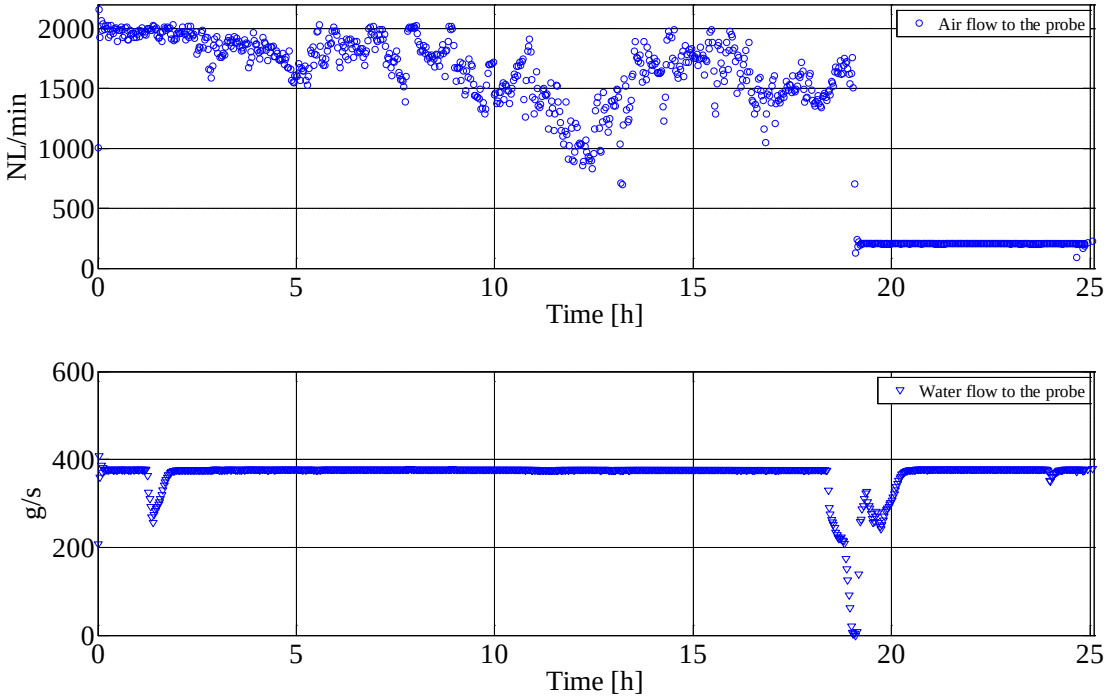

Figure B57 Measured air and water flow to the probe during Test 7.

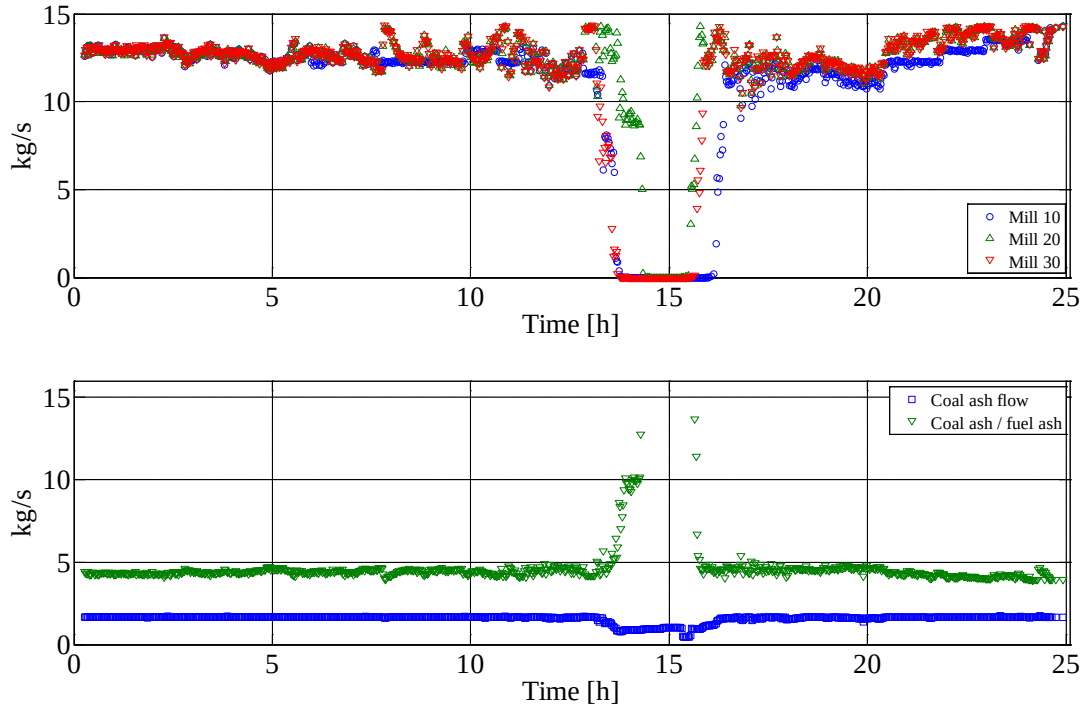

Figure B58 Measured wood flow through each mill, coal ash flow (kg/s) and ratio between coal ash and wood ash during Test 7.

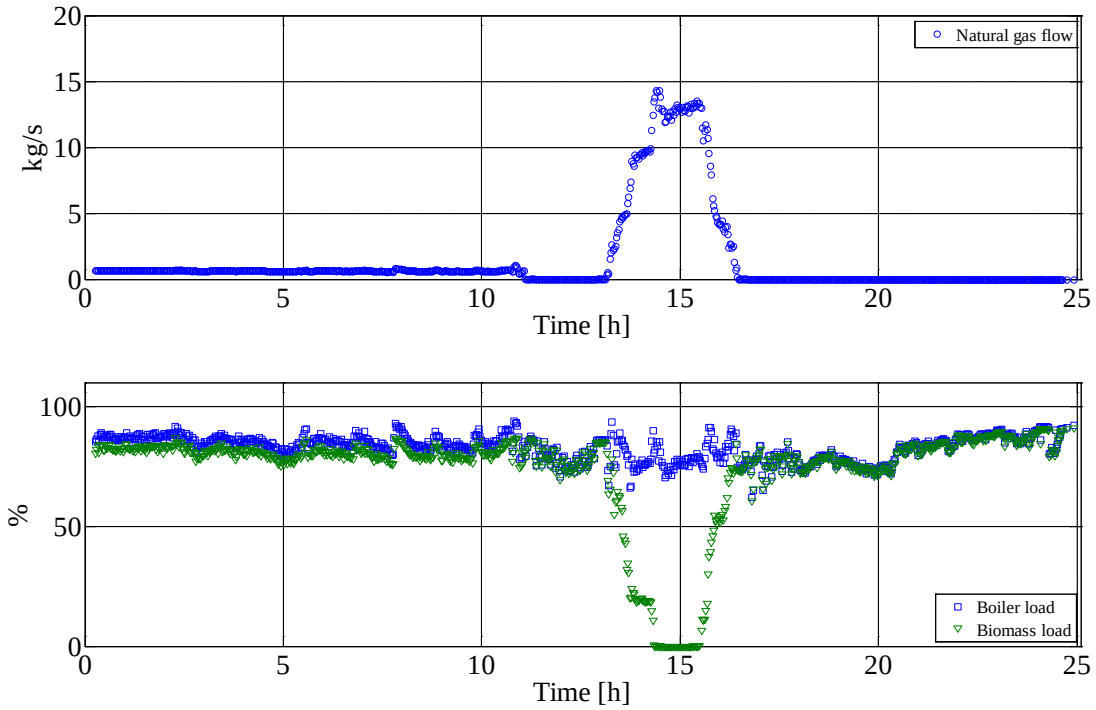

Figure B59 Natural gas flow, overall boiler load and biomass load during Test 7.

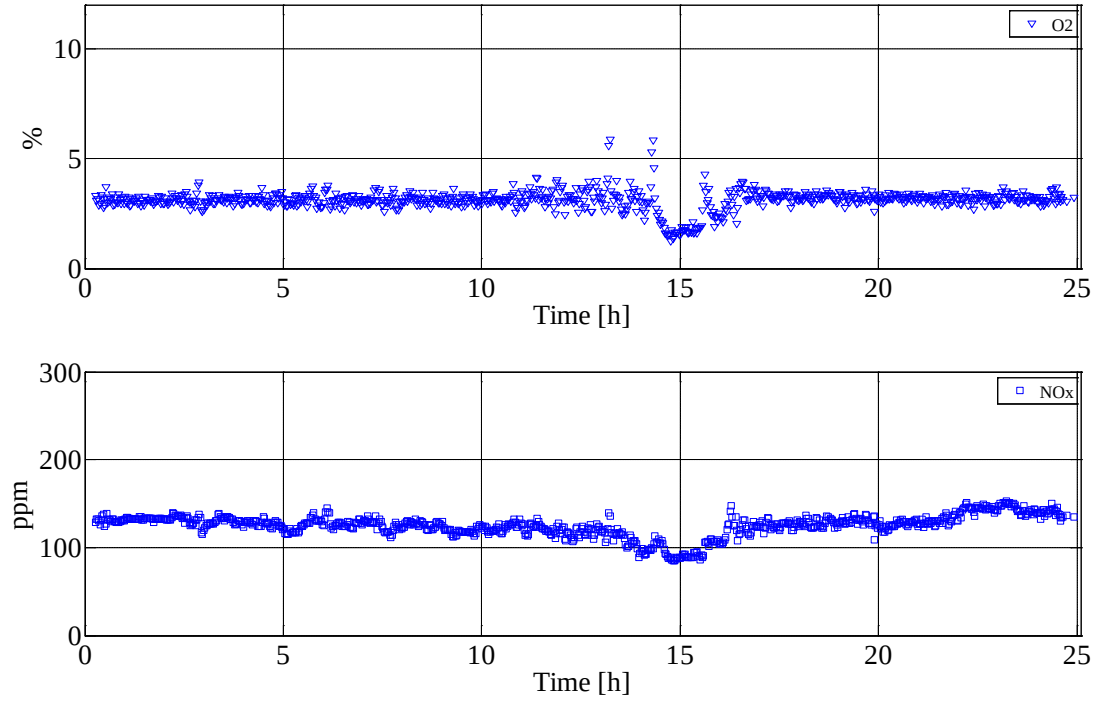

Figure B60 O_2 and NO_x (before SCR) concentrations in the flue gas during Test 7.

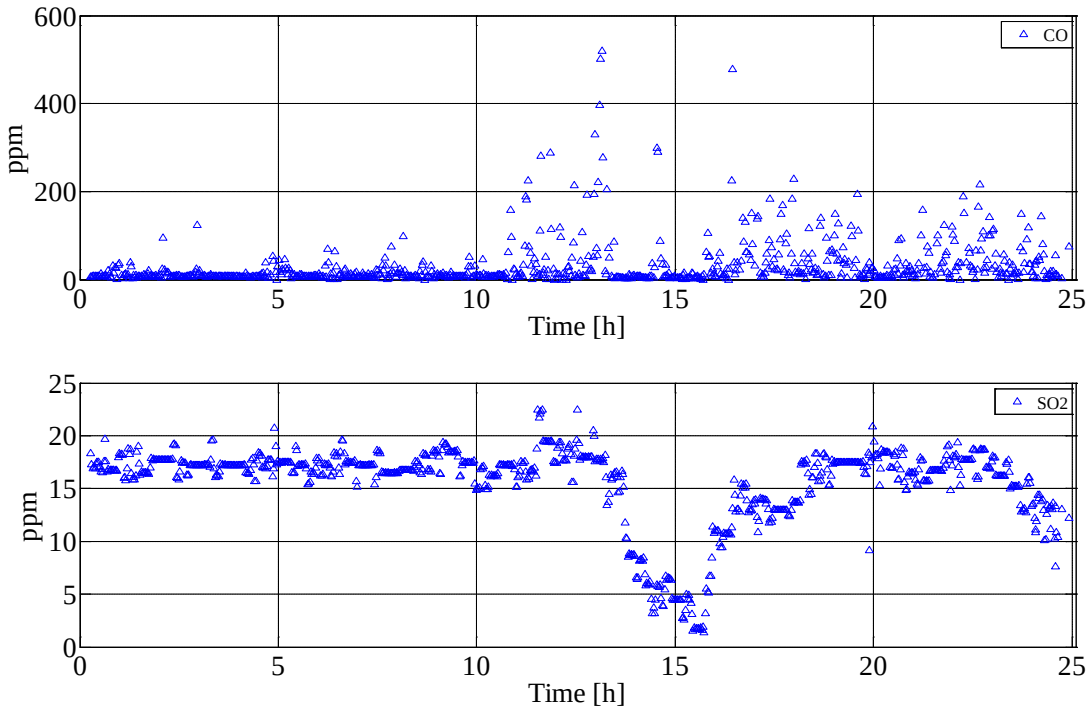

Figure B61 CO and SO_2 concentrations in the flue gas during Test 7 (only values larger than zero are shown).

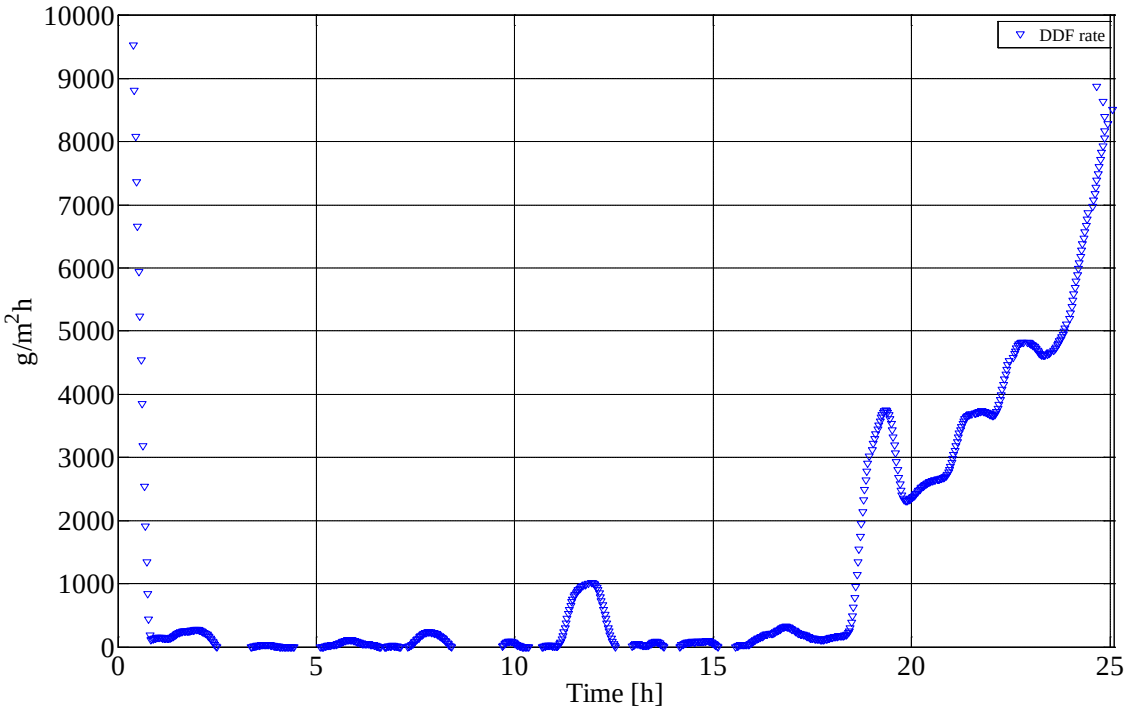

Figure B62 Calculated derivative-based deposit formation (DDF) rate during Test 7.

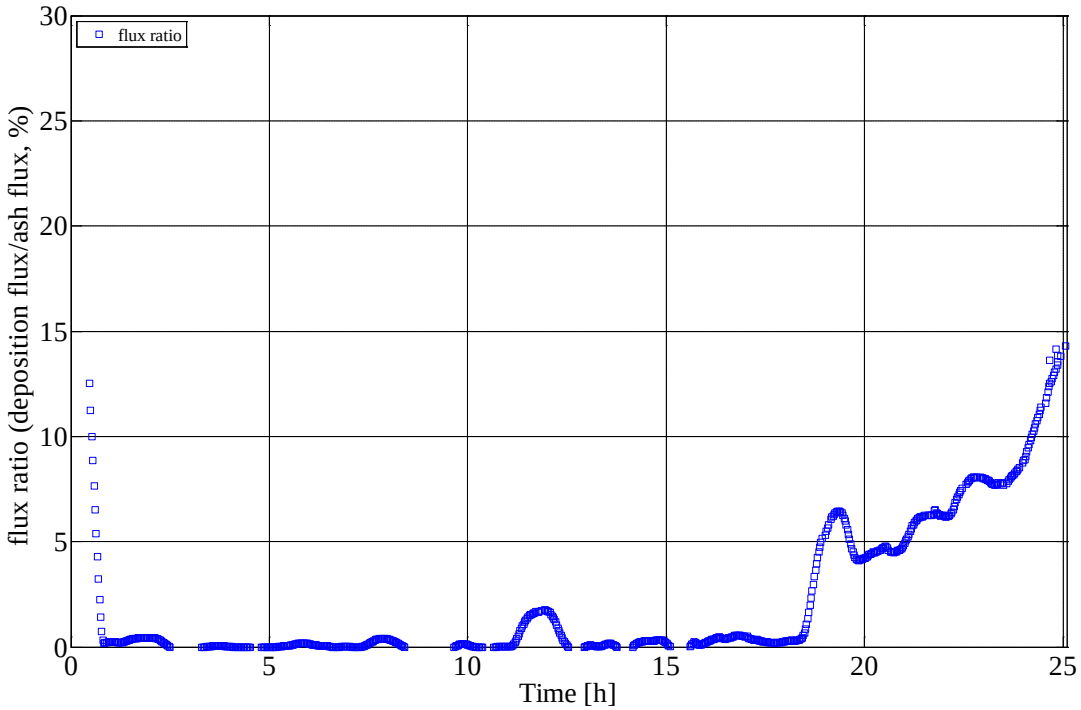

Figure B63 Calculated ash deposition propensity during Test 7.

Appendix B.8 Data from Test 8

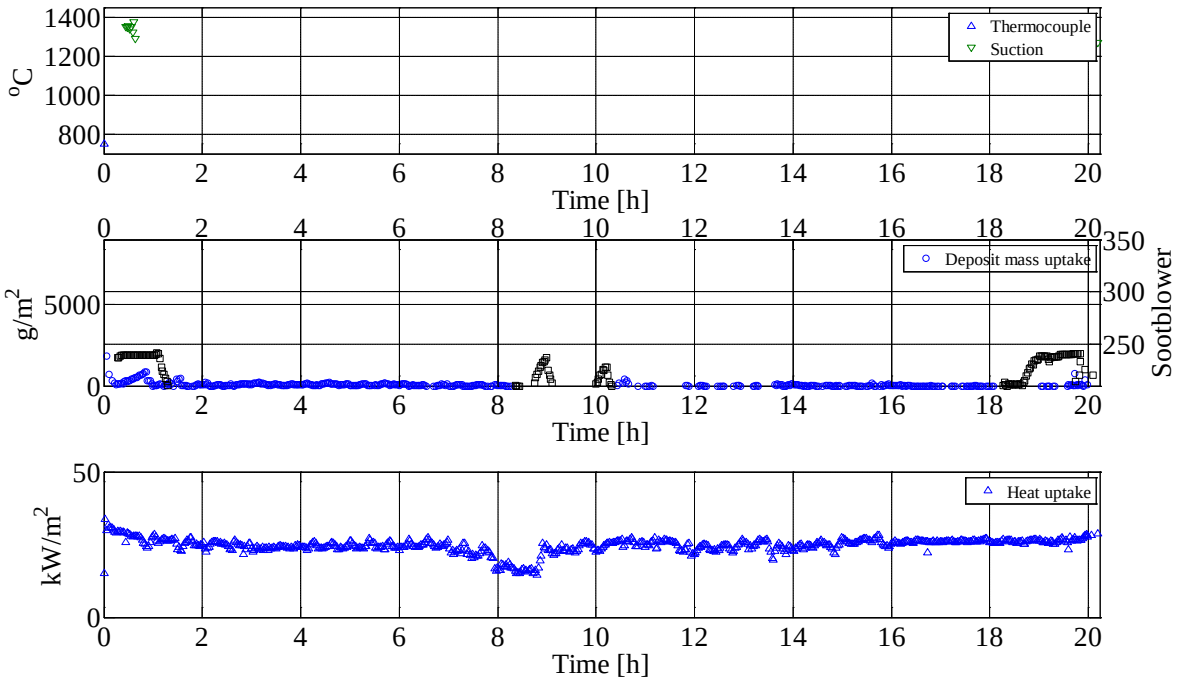

Figure B64 Flue gas temperature, deposit mass uptake, soot-blowing events and probe heat uptake during Test 8. The plant soot blower is active when the back-wall temperature is greater than the normal value, i.e. a peak/plateau observed in the figure.

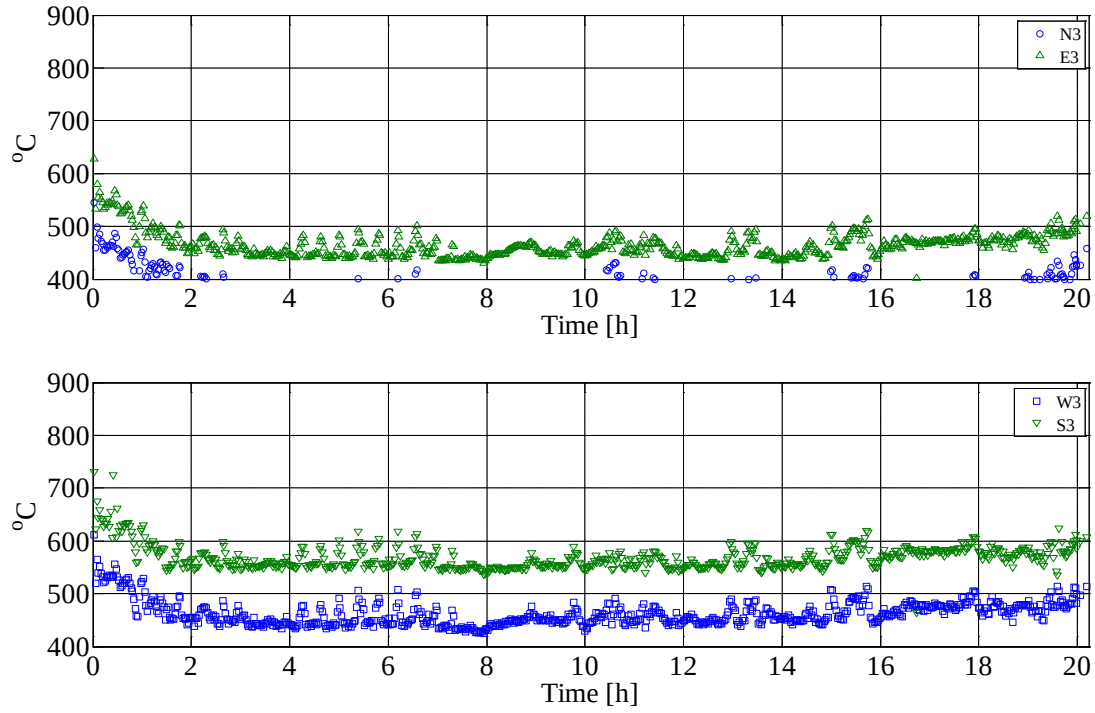

Figure B65 Measured probe surface temperature during Test 8.

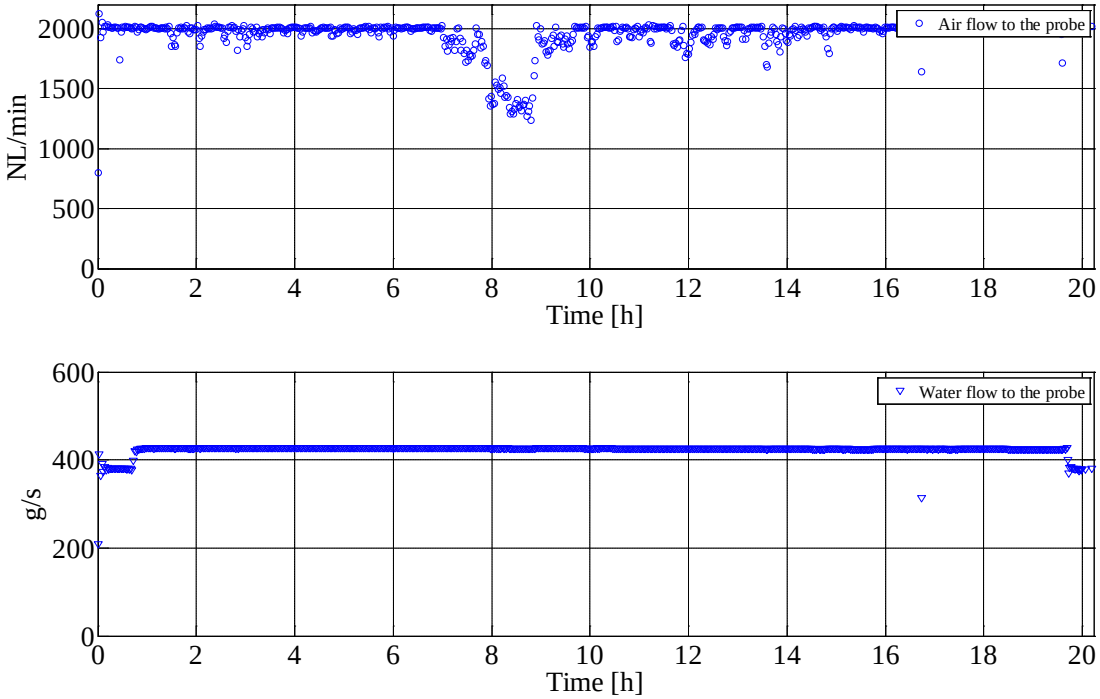

Figure B66 Measured air and water flow to the probe during Test 8.

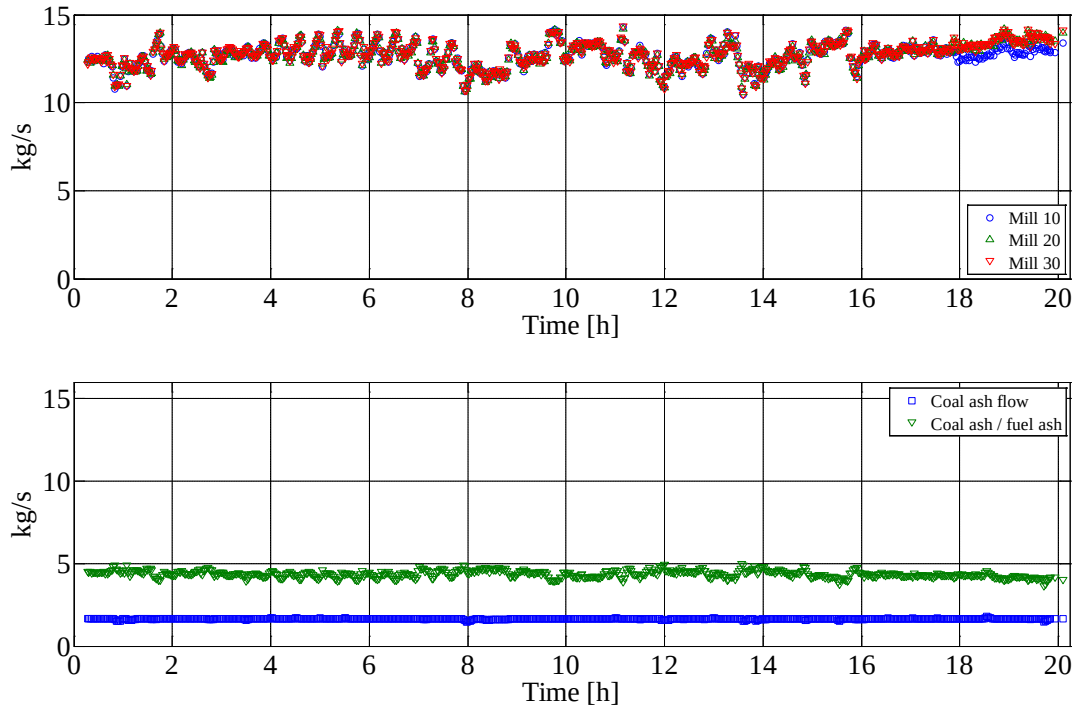

Figure B67 Measured wood flow through each mill, coal ash flow (kg/s) and ratio between coal ash and wood ash during Test 8.

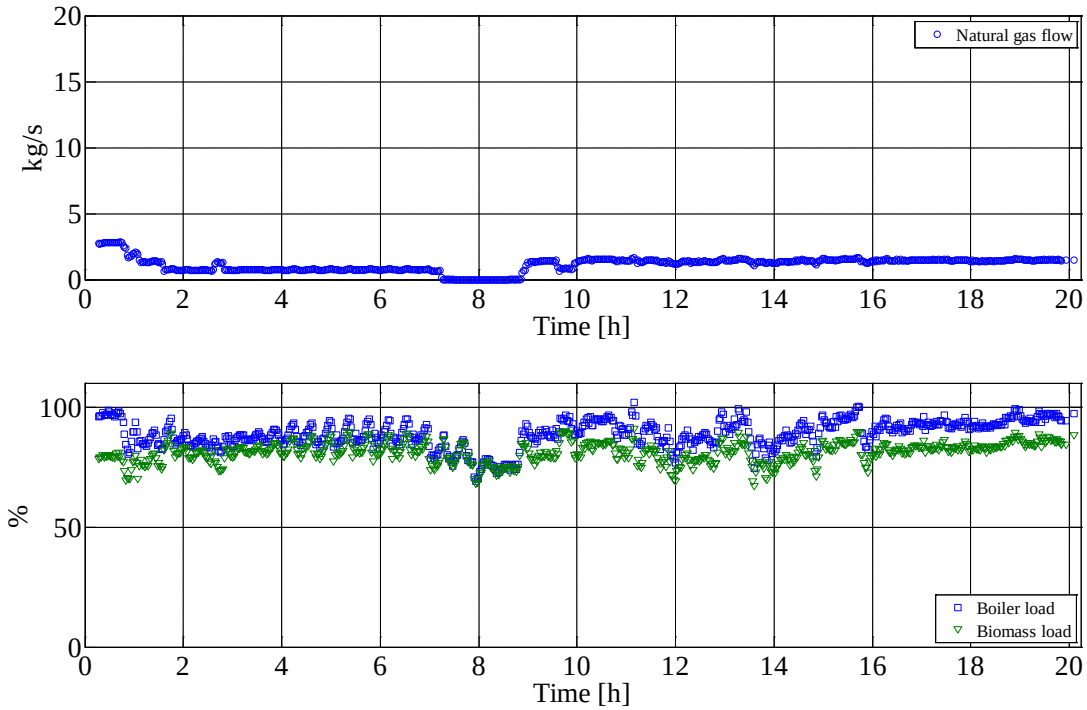

Figure B68 Natural gas flow, overall boiler load and biomass load during Test 8.

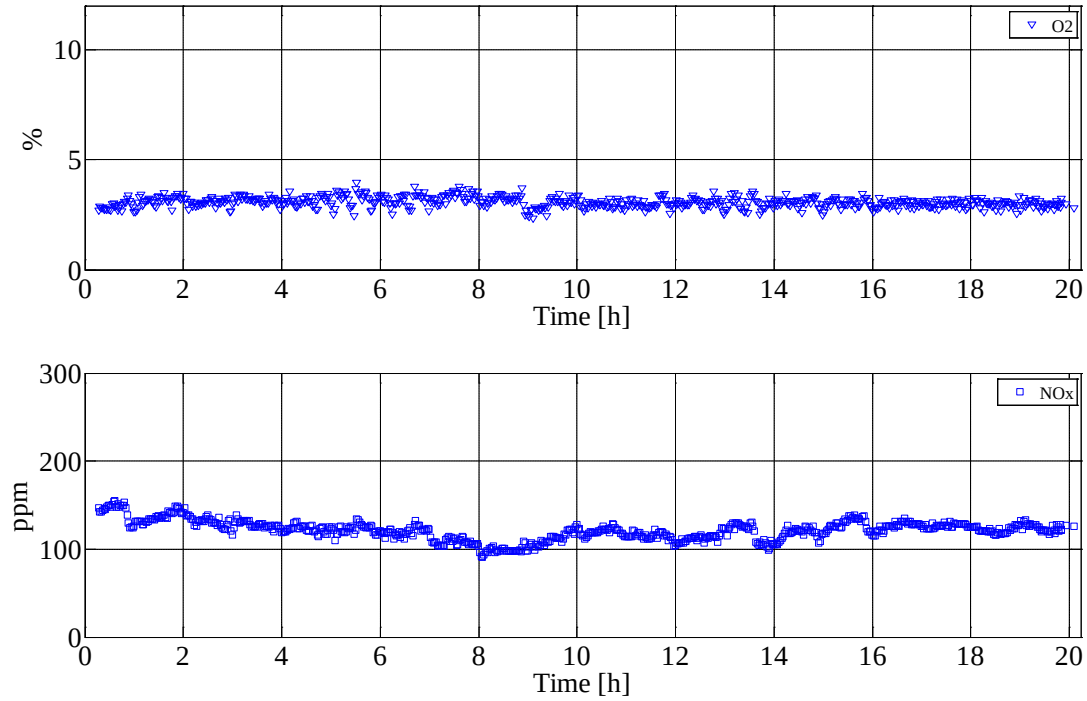

Figure B69 O_2 and NO_x (before SCR) concentrations in the flue gas during Test 8.

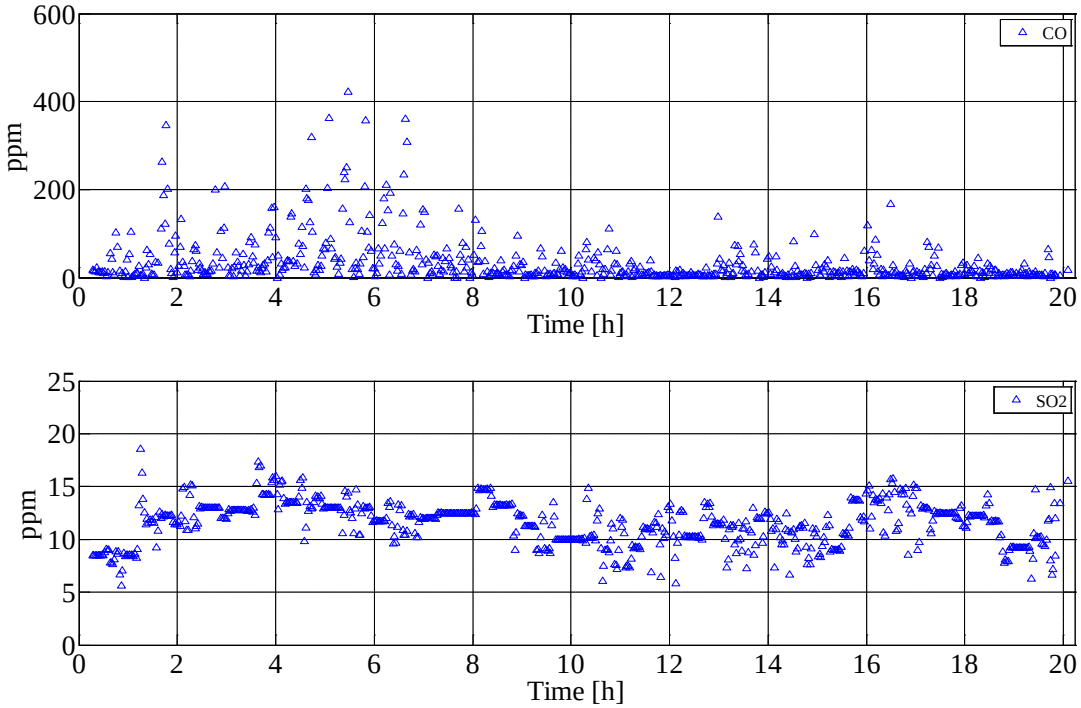

Figure B70 CO and SO_2 concentrations in the flue gas during Test 8 (only values larger than zero are shown).

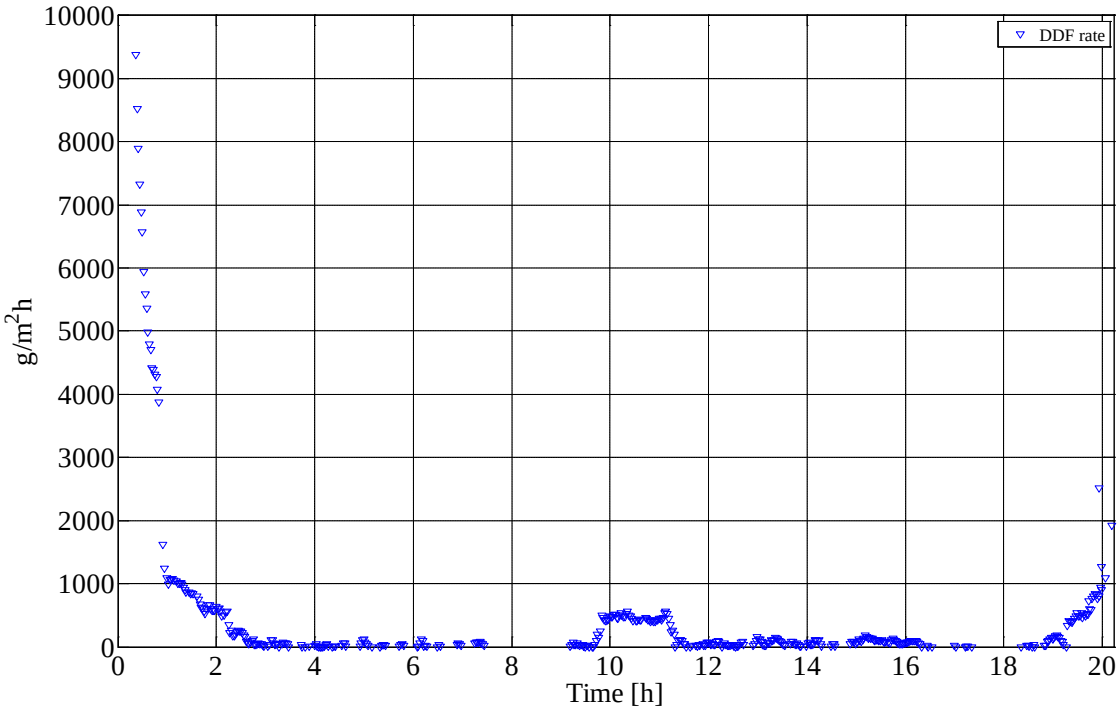

Figure B71 Calculated derivative-based deposit formation (DDF) rate during Test 8.

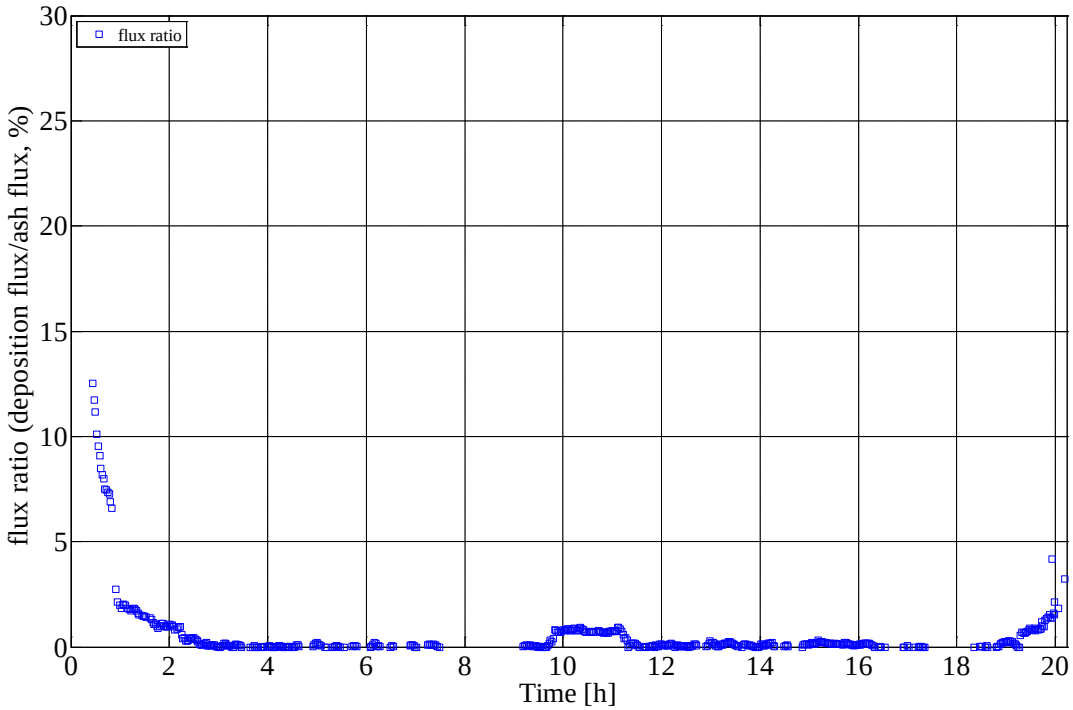

Figure B72 Calculated ash deposition propensity during Test 8.